Structure and Dynamics of Alamethicin Dimers by High-Resolution ^{1}H and ^{15}N NMR Spectroscopy

By

Xing Li

A thesis submitted to the Faculty of Graduate Studies

In partial fulfillment of the requirements for the degree of

Master of Science

Department of Chemistry
University of Manitoba
Winnipeg, Manitoba

THE UNIVERSITY OF MANITOBA

FACULTY OF GRADUATE STUDIES

*****

COPYRIGHT PERMISSION PAGE

Structure and Dynamics of Alamethicin Dimers by High-Resolution ^{1}H and ^{15}N NMR Spectroscopy

BY

Xing Li

A Thesis/Practicum submitted to the Faculty of Graduate Studies of The University of Manitoba in partial fulfillment of the requirements of the degree of Master of Science

ACKOWLEDGEMENTS

I would like to express my deepest appreciation to my supervisor Dr J. O'Neil for his thoughtful guidance, helpful discussions, encouragement, patience, enthusiasm and his financial assistance during the course of this study. I would like to thank Dr. Jim Peeling for reading my thesis, and Dr. H. Perreaul for reading my thesis, for running the mass spectra, and for her helpful advice on mass spectra.

I would like to thank Terry Wolowiec and Kirk Marat for running the NMR spectra, helping me with the use of NMR spectrometers, and assistance in using NMR processing software. I thank Dr. F. E. Hultin for allowing me to work in his laboratory during the synthesis of my product and Dr. A. Chow for allowing me to use his HPLC.

I would also like to thank all the members of Dr. O'Neil's laboratory, especially Gillian for discussions on my research, personal advice, and her valuable comments on my thesis.

Finally, I thank my parents, my husband, and my daughter for their love and support throughout the years.

ABSTRACT

Alamethicin is an α-aminoisobutyric acid-containing antibiotic produced by the soil fungus *Trichoderma viride*. It forms voltage-dependent ion channels in lipid with multiple conductance levels. The multiple conductance levels are thought to correspond to oligomer barrels with varying numbers of monomers. Woolley has suggested that oligomer association and conductance states can be stabilized by formation of covalent alamethicin dimers [Shaochun You *et al. Biochemistry* 1996, 35, 6225-6232]. Unlabeled and ^{15}N labeled alamethicin dimers were synthesized in which two monomers are linked at their C-terminal ends by a flexible linker. Electrospray ionization mass spectrometry confirmed the identity of the dimers purified by high-performance liquid chromatography.

The structure and dynamics of alamethicin dimers were studied by carrying out extensive nuclear magnetic resonance spectroscopy and circular dichroism experiments. The ^{1}H and ^{15}N resonances of the dimers were assigned using one- and two-dimensional NMR spectra with the help of previous ^{1}H and ^{15}N assignments of alamethicin monomer. We have conducted chemical shift analysis, scalar coupling constant analysis, measured internuclear distances from NOE, and conducted temperature-dependent studies of the backbone resonances. The results suggest that the entire peptide exists in a helical conformation, the N-terminus (Aib_1-Aib_{10}) has a more stable helical structure than the C-terminus (Val_{15}-Pho_{20}) and a flexible structure in the middle (Gly_{11}-Pro_{14}) connects the helices. The data from ^{15}N-labeled alamethicin dimer suggest little differences in conformation between the dimer and monomer in the Aib_1-Pro_{14} region. Significant difference in the conformation of the C-terminus are manifest in the NH chemical shifts in the Val_{15}-Pho_{20} region. The C-terminus appears slightly more stable in the dimer than the monomer. The results suggest that the C-terminal helices associate but the N-termini do not and support a gating mechanism that undergoes a voltage-dependent conformational rearrangement of the peptide with respect to the bilayer.

CONTENTS

Chapter 4

Discussion

Lists of Abbreviations

Ac: acetyl

Ala: Alanine

Aib: α-aminoiosobutyric acid

Alm: Alamethicin

aq: acquisition time

BAPHDA: bis(N-3-aminopropyl)-1,7-heptanediamide

CD: circular dichroism spectroscopy

CPD: composite-pulse decoupling

dw_i: dwell time

d_{NN}, $d_{\alpha N}$, $d_{\beta N}$: NOE connectivity between the NH, αH and βH, respectively.

DS: number of dummy scan

DSS: 4-dimethyl-4-silapentance-1-sulfonate

DQF-COSY: double quantum filter-correlated spectroscopy

ESI-MS: Electrospray Ionization Mass Spectrometry

E-COSY: extensive correlated spectroscopy

EM: exponential multiplication with LB

FID: free induction decay

GB: the processing parameter (between 0 to 1) determines the Gaussian function

Gln: glutamine

Gly: glycine

GM: Gaussian multiplication with LB and GB

HSQC: heteronuclear single-quantum correlation

HPLC: high-performance liquid chromatography

$^3J_{\alpha N}$: the NH-$C^{\alpha}H$ coupling constant

$^3J_{\alpha\beta}$: the $C^{\alpha}H$-$C^{\beta}H$ coupling constant

k: the exchange rate

LB (in Hertz): the processing parameter determines the line broadening

Leu: leucine

MW: molecular weight

m/z: mass to charge ratios

n: the number of positive charge in mass spectra

NMR: nuclear magnetic resonance

NOE: nuclear Overhauser enhancements

NOESY: nuclear Overhauser and exchange spectroscopy

NS: number of scans

PAPDA: pimelic acid piperazine diamide

Pro: proline

Pho: phenylalaninol

ppm: parts per million

ppb: parts per billion

qseq: sequential alternate sampling mode

qsim: simultaneous sampling mode

Qsine: multiplication with a sine-squared filter

ROE: rotating frame nuclear Overhauser enhancements

ROESY: rotating frame Overhouser enhancement spectroscopy

r_{ij}: the distance between the *i* and *j* nuclei

SI: number of real data points

SW: sweep width

THF: tetrahydrofuran

TPPI: time proportional phase increment

TD: time domain data size

TOCSY: Total correlated spectroscopy

T_1, T_2: the relaxation times

T_m: the mixing time

Val: valine

W_0, W_1 and W_2: zero-, single- and double-quantum transition

ϕ, φ: dihedral angles

α_{ij}: the intensity of cross peak between *i* and *j* nuclei in ROESY

τ_c: the correlation time

σ: the cross-relaxation rate

$\Delta\delta$: the changes in chemical shift

$\eta_i(s)$: the NOE of *i* spin while the *s* spin is saturated

List of Figures

List of Tables

Chapter 1

Introduction

1.1. Alamethicin Monomer and Dimer

Alamethicin is an antibiotic peptide produced by the soil fungus *Trichoderma viride*. The peptide is rich in α-aminoisobutyric acid (Aib), has an alcoholic C-terminus, and is sometime called a peptaibol [1-2]. Alamethicin is synthesized by a non-template-directed enzyme complex [3] as a family of approximately 12 molecules [4]. The most abundant forms of alamethicin are designated as Alm-R_f30 (Glu_{18}) and Alm-R_f50 (Gln_{18}) where the residue at position six may be either Aib (Alm_1) or Ala (Alm_2). Other primary sequence variants may occur in minor amounts depending on *Trichoderma viride* culture conditions. Fig. 1-1 shows the sequences of the two molecules used in this study.

Alm1 or 2: Ac-B_1-P_2-B_3-A_4-B_5- B_6(or A_6)-Q_7-B_8-V_9-B_{10}-G_{11}-L_{12}-B_{13}-P_{14}-V_{15}-B_{16}-B_{17}-Q_{18}-Q_{19}-O_{20}

Fig. 1-1. Primary sequences of the two alamethicin peptides used in this study. Abbreviations for the amino acid residues are as follows: B, Aib; P, Pro; A, Ala; Q, Gln; V, Val; G, Gly; L, Leu; O, Phenylalaninol (Pho). Ac is an N-terminal acetyl. Aib is α-aminoisobutyric acid.

The high-resolution (1.5Å) crystal structure of alamethicin [5] revealed that three individual alamethicin molecules exist in the asymmetric unit and each helix is bent slightly near Pro_{14}. The peptide mainly adopts an α-helical conformation, with small deviations in the form of short 3_{10}-helix segments (Fig.1-2a). Spectroscopic and NMR studies [6-8] provided information on the alamethicin structure and dynamics in solution which suggested that the N-terminal half of the molecule is α-helical and the C-terminal region is more extended, with a kink induced by Pro at position 14.

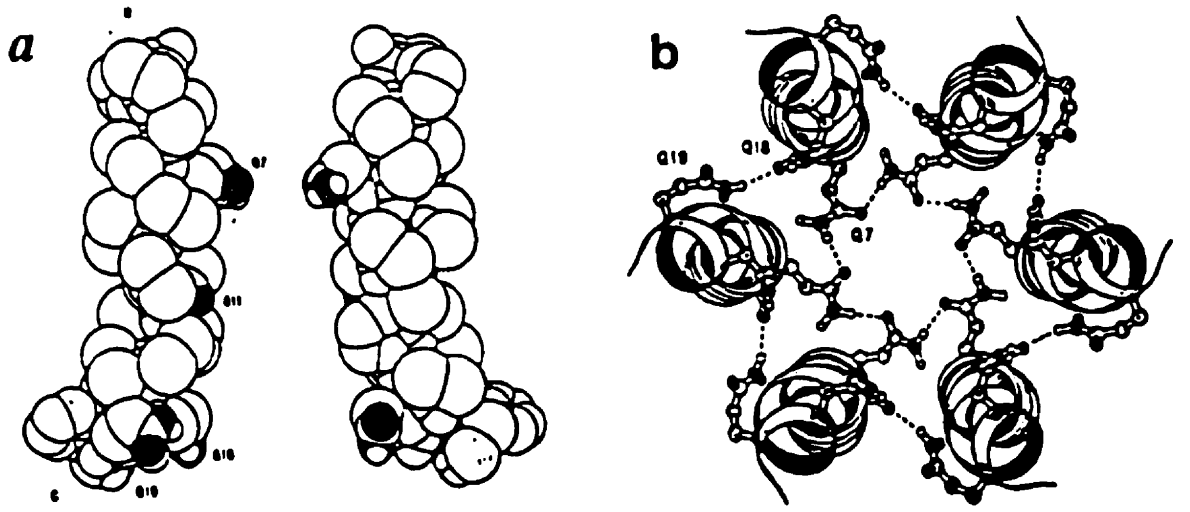

Fig. 1-2. The models of alamethicin monomers and pore (a) A space-filling model of two opposing alamethicin monomers. (b) A view down a proposed pore (six monomers) from the C-terminal end (Taken with permission from M.S.P. Sansom, 1993 [12]).

Alamethicin is one of many membrane-active antibiotic peptides found in nature. It forms voltage-dependent ion channels in lipid bilayers and was found to lyse different biological cells. In addition, it has been found to uncouple oxidative phosphorylation in mitochondria [reviewed in 9 and 10]. Studies of alamethicin may help improve our understanding of the ion channel activity, voltage-gating mechanism and of the molecular mechanisms of other channel-forming peptides [reviewed in 11].

A single helical polypeptide cannot accommodate the passage of ions though the interior of individual helices. To form functional membrane channels, alamethicin monomers presumably self-assemble forming a macromolecular pore in the bilayer. There are many models proposed which suggest aggregates of 6-12 monomers, i.e., "barrel" or "bundle" models [reviewed in 12-14]. In one proposed pore model (Fig.1-2b) [13], the N-terminal helices are packed parallel to one another so as to form a funnel-shaped pore with the wider mouth at the C-terminal. The N-terminal helix-helix separation is 9.5 Å and the convex faces are

directed inwards. The bundles are stabilized by side chain H-bonds between Gln_7 residues of adjacent monomers and also by Gln_{18}-Gln_{19} H-bonds. The narrowest region of the pore is lined by the side chains of Gln_7, and by the exposed carbonyl oxygen of Gly_{11}. Channels formed by bundles of alamethicin helices contain aqueous pores through which ions can pass across the lipid bilayer.

A wide range of electrical studies on alamethicin have been conducted to understand the ion channel properties. The conductance of alamethicin is strongly voltage-, concentration- and ionic strength-dependent [reviewed in 15]. The mechanism of voltage activation of channels was revealed by applying a slowly changing voltage difference across a lipid bilayer which was exposed to 0.5 μM Alm-R_f50 in the *cis* compartment [12]. Alamethicin induces a macroscopic current in the bilayer which is strongly voltage dependent. An average current-voltage *(I-V)* relationship is obtained which exhibits a marked asymmetry, with voltage-activation occurring mainly at *cis* positive potentials (Fig.1-3). The sign of the potential is given for the alamethicin side of the membrane. The degree of asymmetry depends on the lipid composition of the membrane and peptide structure.

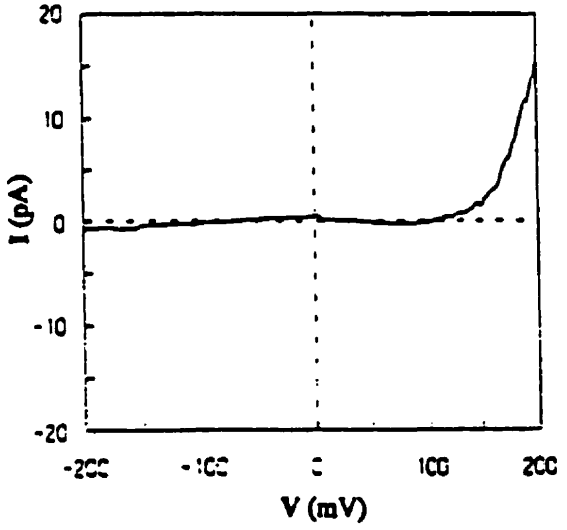

Fig.1-3. The current-voltage relationship. Alamethicin channel activation occurs principally at *cis* positive potentials. Any current observed at elevated negative potentials is thought to be due to leakage of alamethicin through the bilayer. (Taken with permission from Sansom, 1991[10])

The high dependence of the conductance on alamethicin concentration has been attributed to a change in the number of gated channels rather than a change in the properties of a single channel at high peptide concentrations. At low concentrations, conductance fluctuations are observed which have been attributed to single-channel gating events [16]. Gordon and Sansom [17-18] demonstrated that individual alamethicin channels exhibit multi-level opening with prolonged closed periods under an applied transmembrane potential, providing strong evidence for the helix bundle model of alamethicin channel formation. One example of a single-channel record [13] of alamethicin monomer (R_f50) in a diphytanoyl-phosphatidycholine membrane with 0.5M KCl as the electrolyte and at a membrane potential of 125 mV, revealed that the alamethicin channel opens as multi-level bursts containing five or more well-defined conductance states (Fig.1-4a). The different levels represent conductance substates of one channel. The lifetimes of the individual substates are in the millisecond range and the open state of the channel as a whole may last for seconds. Another single-channel record of alamethicin [19] in a diphytanoyl-phosphatidycholine/decane membrane (1 M KCl, pH 5.8, 160 mV) also exhibited multiple conductance level channel activity with three predominant conductance states and the lifetime of each substate was about 1.7 ms (Fig.1-4b).

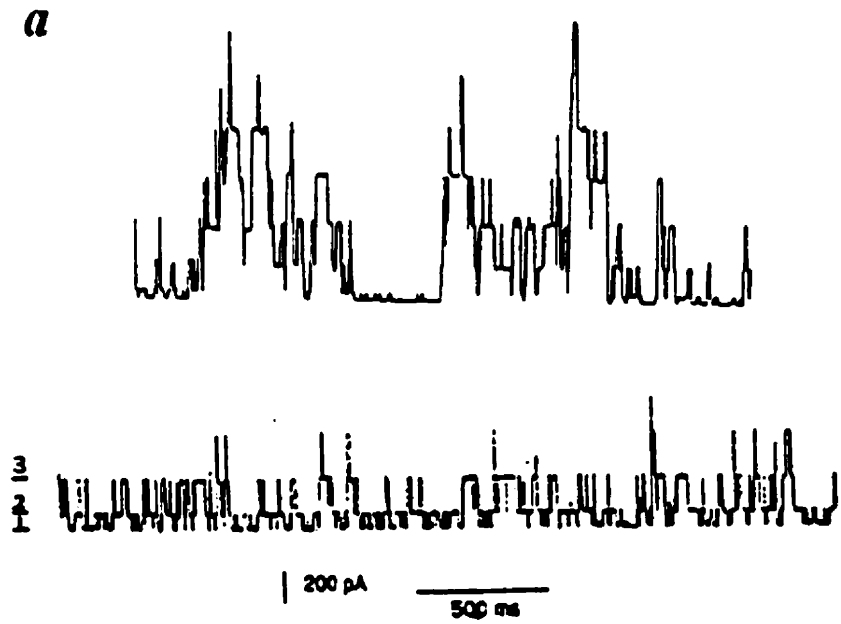

Fig.1-4. The single-channel records of alamethicin monomers. (a). The multiple conductance level channel activity of single alamethicin monomer channels in 0.5M KCl solution with 125 mV applied potential (Taken from Sansom, M. S. P. 1991 [18]). (b). Monomer conductance activity under the same condition as in a except: 1M KCl solution, 160 mV applied potential. The current levels observed are indicated by horizontal bars with the level number (Taken with permission from Shaochun You *et al*, 1996 [19]).

Shaochun You *et al.* [19] have suggested that oligomer association and conductance states can be stabilized by formation of a covalent alamethicin dimer by linking two peptides at their C-termini with a flexible linker. Tethering appears to reduce the chance of a monomer leaving the channel and limits the size of bundles so that only relatively small sized structures predominate. The *I-V* relationships of their two alamethicin dimers (alm-PAPDA and alm-BAPHDA where the linkers are pimelic acid piperazine diamide and bis(N-3-aminopropyl)-1,7-heptanediamide, respectively) channels are similar to those of channels formed by alamethicin monomer, indicating the linkers do not affect the pore structure of the channel. Alamethicin dimer channels also have predominantly three different conductance states (Fig.1-5), however, there is a large difference in the lifetimes of different conductance states between dimer and monomer channels. The upper and lower states (level 1 and level 3) of the dimer channels appear to be selectively

stabilized, whereas the intermediate states (level 2) are brief with a lifetime similar to the corresponding state of monomer channels. The preferred maximum conductance level has a mean lifetime of 287 ms for alm-BAPHDA and 80 ms for alm-PAPDA, corresponding to 170-fold and 48-fold longer than the related channels formed from alamethicin monomers. In addition, Shaochun You *et al.* [19] suggested that the alamethicin dimer channel is formed by bundles of six alamethicin helices, i.e., by bundles of three covalent dimers.

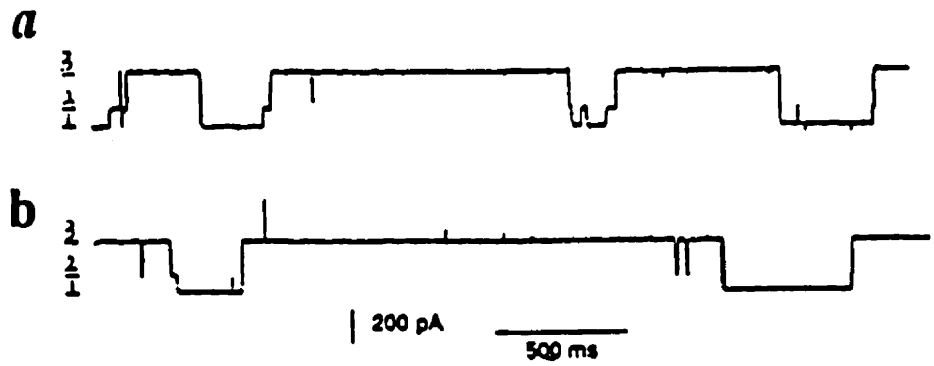

Fig.1-5. Single-channel recordings of channels formed by (a) alm-PAPDA dimers and (b) alm-BAPHDA. (Taken with permission from Shaochun, You, *et al.* 1996 [19])

1.2 Protein Identification Using Electrospray Ionization Mass Spectrometry (ESI-MS)

ESI-MS [20-21] has proven to be a powerful method for the analysis of peptides and other biological compounds due to its speed, sensitivity, and ease of sample introduction. ESI involves formation of gas-phase ions from ions in solution subjected to electrospray at one atmosphere and the transfer of the gas-phase ions to the vacuum of a mass analyzer.

The types of mass spectrometers available for ESI include time-of-flight, quadrupole, quad-rupole ion trap, Fourier transform ion cyclotron resonance and magnetic sector mass spectrometers. The characteristic feature of ESI, which

distinguishes it from other ionization techniques, is that it generally imparts multiple charges to larger analyte molecules under mild conditions, so that even very large molecules (up to 150 kDa) can be detected. The ESI-MS of proteins has generally been performed in the positive ionization mode. These positive ions generally arise by attachment of protons, alkali cations, or ammonium ions to the protein. Multiprotonated molecules give rise to a series of consecutive peaks along the *m/z* scale denoted as $(M + nH)^{n+}$, where M is mass of the neutral molecule and n is the number of positive charges. From the ESI mass spectrum, the charges on the fragments and accurate molecular masses can be determined using the equation (if the added ions are protons): $m/z = (M + n)/n$ [22].

1.3. Structure Determination of Peptides by NMR Spectroscopy

A knowledge of the conformation of peptides is the basis for understanding their biological activities. NMR spectroscopy has proven to be a very powerful technique for the structural studies of peptides and proteins in solution. The application of two-dimensional NMR methods to peptides and proteins was pioneered by Richard Ernst and Kurt Wüthrich [23] in the early 1980s and later extended to three-dimensional methods by others [24-25]. A 2D experiment is usually composed of four basic time periods: Preparation (T_{rd})-evolution (t_1)-mixing (τ_m)-detection (t_2). It is obtained by allowing the evolution time t_1 to be incremented in equal steps of Δt_1 determined by the desired spectral width, SW_1. Separate data acquisitions composed of NS transients are performed for each value of t_1 to give TD_1 FIDs, each FID containing TD_2 total data points. The detected resonances will be modulated as a function of t_1 for all pairs of spins which are J-coupled or dipolar. Once the complete data set has been acquired, it is Fourier transformed with respected to t_1 and t_2 to give a two-dimensional spectrum that is a function of two frequencies, F_1 and F_2. 3D spectroscopy is an extension of the 2D experiment by adding further evolution and mixing periods.

1.3.1. Assignment of Proton Signals

Kurt Wüthrich has outlined the standard approach for the sequential assignments of a small protein [26]. Generally, sequential resonance assignment includes the assignment of each ^1H signal to a specific type of spin system and the assignment of these spin systems to their sequential position in the peptide chain. A spin system is a group of spins that are connected by scalar (through-bond) spin-spin *J* couplings. In most cases, sequential resonance assignment can be achieved with a combination of COSY, TOCSY, and ROESY or NOESY spectra. Fig. 1-6 shows the spin system and some sequential distances useful for assignment. The distance between the hydrogen atoms A and B located in the amino acid residues in the sequence positions *i* and *j*, is denoted as d_{AB} (*i*, *j*). The indices *i* and *j* are usually omitted for the sequential distances.

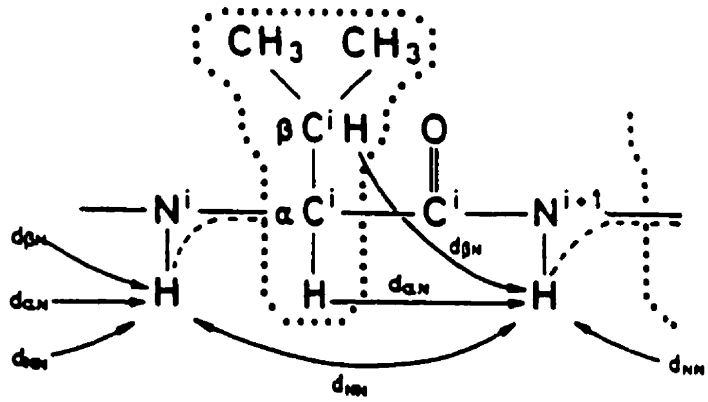

Fig.1-6. The spin system in the individual residue (inside dotted lines), the αH-NH COSY connectivities (broken lines) and the sequential links between adjacent residues (arrows). $d_{NN} \equiv d(NH_i, NH_{i+1})$, $d_{\alpha N} \equiv d(\alpha H_i, NH_{i+1})$, $d_{\beta N} \equiv \min\{d(\beta H_i, NH_{i+1})$. Min indicates that the shortest distance to any of the β protons is taken. (Taken with permission from Wüthrich, K. 1986 [26]).

Each spin system corresponds to the resonances of an individual amino acid residue since there is no proton spin-spin coupling across the peptide bond. Taken together, the 20 amino acid residues give rise to 10 different COSY connectivity patterns for the aliphatic protons and four motifs for the aromatic rings. The presence of a COSY cross peak indicates that the coupled nuclei are two or three

bonds apart. Shorter spin systems like Ala (A_3X), Ser (AMX) and Cys (AMX) can be identified using correlated spectroscopy (COSY). For longer spin systems such as Arg [$A_2(T_2)MPX$], Lys ($A_2(F_2T_2)MPX$) and Leu (A_3B_3MPTX), TOCSY is usually needed to give the complete side-chain assignment. The aromatic side chains in Phe, Tyr, Trp, and His are identified from the observation of the short βH-ring proton distances in NOESY spectra.

Sequential assignment is achieved by correlating one amino acid spin system with the spin systems of its neighboring residues. This assignment usually relies on short-range, through-space connectivities observed in NOESY or ROESY spectra. The three most useful NOE effects involved in sequential assignment arise from the distances d_{NN}, $d_{\alpha N}$ and $d_{\beta N}$. The sequential assignments for Pro should also include $d_{N\alpha}$. If a short $d_{\alpha N}$ (δCH_2 of Pro is used instead of NH) is observed between two amino acid spin systems then these residues are likely to be adjacent in the sequence. However, the identification of neighboring residues by sequential NOE connectivities is ambiguous because the short distances $d_{\alpha N}$ (i, j), d_{NN} (i, j), or $d_{\beta N}$ (i, j) may also prevail between intraresidue, medium or long-range non-neighboring residues. Wüthrich *et al* [26] showed that 88% of (NH, NH), 88% of (αH, NH) and 76% of (βH, NH) NOEs with an interproton distance of ≤ 3.0 Å involve adjacent residues. Assignment is possible because of multiple connectivities between sequential residues. So assignment is a trial-and-error process where connectivities are proposed and either confirmed or disproved by subsequent assignments.

1.3.2. Structure Determination from NMR Data

After sequence-specific assignments, the solution structure of a protein can be obtained in two stages. The first stage involves the determination of the secondary structure which can be identified from NMR data such as chemical shifts, nuclear Overhauser enhancements (NOE), amide-proton exchange rates and spin-spin

coupling constants. The second stage of the structure determination process involves the use of computational methods such as distance geometry and molecular dynamic calculations which are not described in this report.

1.3.2.1. From Chemical Shift to Secondary Structure

Chemical shifts are perhaps the most accessible measured quantities in all of NMR data [27-28]. They can be helpful in identifying secondary structure and backbone flexibility by comparison with random coil chemical shift values since they are very sensitive to the secondary structure. The random coil state is an extreme case of an unstructured polypeptide, which is presumed to have no specific non-local interactions between residues. The changes in chemical shift ($\Delta\delta$) relative to a random coil chemical shift (δ^{ran}) are calculated using the equation: $\Delta\delta = \delta^{obs} - \delta^{ran}$. In general, rigid helices or β-strands would be expected to have chemical shifts far from random coil values, while flexible helices or β-strands would be expected to have "averaged" chemical shifts closer to random coil values [29]. The average shift changes for ^{1}H, ^{13}C carbonyl and ^{15}N in helix and β-strand are summarized in Table 1-1. Wishart, D. S. *et. al.* [29] also indicate that a minimum of three or four consecutive amino acid chemical shifts are needed to define a helix or a β-strand structure.

Table 1-1 Average Secondary Shift for Various Nuclei

Relative to Random Coil Values (in ppm)

Nucleus	Helix	β Strand
α-^{1}H	-0.38	0.38
N-^{1}H	-0.19	0.29
2-^{13}C	2.6	-1.4
1-^{13}C	1.7	-1.4
^{15}N	-1.7	1.2

Rewritten from Wishart, D. S. 1994 [27]

1.3.2.2. From NOEs to Distances and Secondary Structure

The NMR absorption is a consequence of a transition between nuclear energy levels stimulated by an applied radio-frequency field. The system of two spin (1/2) nuclei, *i* and *s* with the same γ but different chemical shifts, has four energy levels in the absence of J-coupling. Fig. 1-7 presents the several possible pathways by which the system could relax [30].

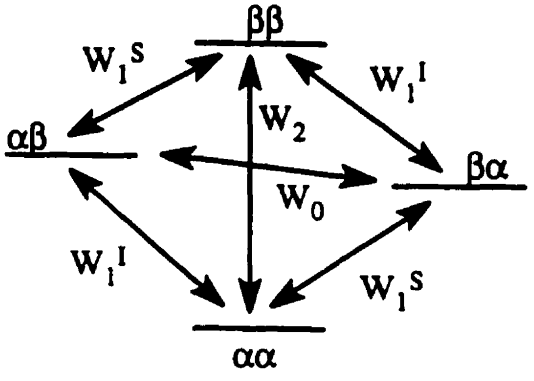

Fig. 1-7. Relaxation pathways of an AX system, where W_0, W_1 and W_2 represent the zero-, single- and double-quantum transitions, respectively.

The NOE is a change in intensity of one spin while the second spin is saturated and is given by:

$$\eta_i(s) = \frac{W_2 - W_0}{2W_1^i + W_2 + W_0} \qquad (1\text{-}1)$$

The NOE arises due to cross relaxation (W_0 and W_2), which leads to a transfer of longitudinal magnetization via dipolar coupling (through space) between nuclei separated by less than 5Å [26]. The efficiency of dipolar relaxation depends on field strength and molecular motion expressed by the molecular rotational correlation time τ_c. The cross-relaxation rate σ is obtained from Eq. 1-2 [31].

$$\sigma = W_2 - W_0 = \frac{\gamma^4 h^2 \tau_c}{4\pi^2 10 r^6}\left(\frac{6}{1 + 4\omega^2\tau_c^2} - 1\right) \qquad (1\text{-}2)$$

where *h* is Planck's constant and γ is the gyromagnetic ratio. At a given spectrometer

frequency ω, the size of the cross-relaxation rate σ between two protons is dependent on the inverse sixth power of the internuclear distance *r*. Thus, the NOE can be translated into an interproton distance.

For small molecules, for which rotational correlation is rapid, i.e., $\omega_0 << 1/\tau_c$, double-quantum transitions W_2 are favored and the NOESY spectra show negative cross-peaks (positive NOEs up to + 0.5 when $\omega_0\tau_c < 0.1$) [32]. For large molecules with longer τ_c ($\omega_0 >> 1/\tau_c$), the NOESY spectra will show positive cross-peaks (negative NOEs up to -1 when $\omega_0\tau_c > 10$). A strong NOE usually appears as an intense cross-peak even at short mixing times. Weak NOEs appear only at longer mixing times. In the case of the medium-sized molecules with $\omega_0 \approx 1/\tau_c$, the NOE effect is small or zero. In this case, the ROESY technique should be used in which NOE buildup is measured in the rotating frame. NOEs in the ROESY experiment are always positive (Fig. 1-8). An advantage of ROESY is that if it is performed in a phase-sensitive mode, the diagonal peaks and any cross peaks due to chemical exchange will be positive, while the NOE cross peaks will be negative.

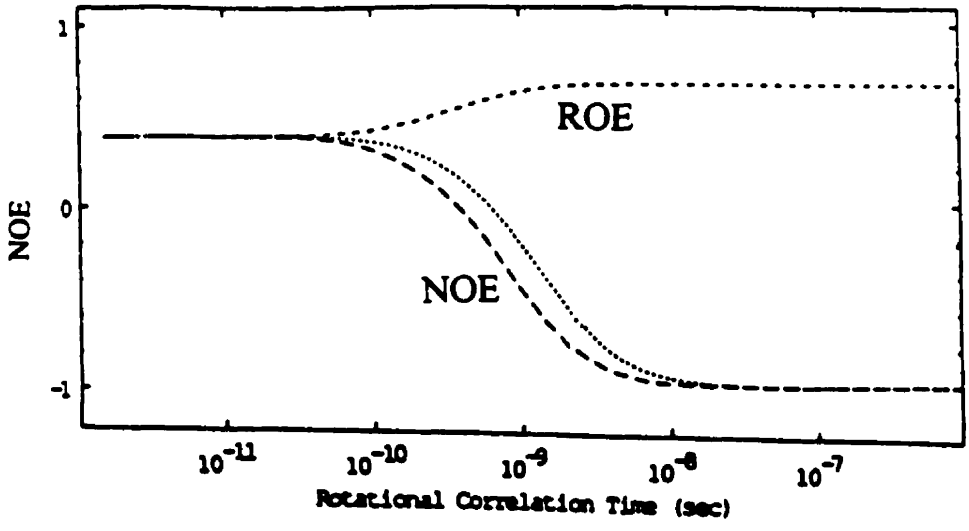

Fig. 1-8. The relationship between NOE and ROE with correlation τ_c(ns). (Adapted from Adelinda A. Yee and Joe D.J. O'Neil, 1991 [31])

After assignment of NOE cross peaks, which usually is done on the basis of chemical shifts, the intensity of the cross-peaks are measured by integration [33]. In 2D spectra, the integral corresponds to the volume of the cross peak. The factors that influence the accuracy of measurement of intensities are lineshape, window function, peak overlap and method of measurement. A simpler way to estimate cross-peak volume is to count the number of contour levels on a single NOESY spectrum with a short mixing time [26]. This method evaluates only the height and is valid only if all cross-peaks have the same lineshape. When a small peptide has fast overall motion, the intensities (α) of cross peaks in NOESY and ROESY spectra are proportional to the cross-relaxation rate σ and thus to the distance r between the nuclei:

$$\alpha_{ij} \propto \sigma_{ij} \propto r_{ij}^{-6} \qquad (1\text{-}3)$$

Since the NOE intensity is approximately proportional to r^{-6}, thus, an increase in the distance by a factor of 1.5 leads to a decrease in the intensity by a factor of about 10. The unknown interproton distances can be obtained by calibration of the cross-peak intensities against a known fixed distance which is usually the distance between diastereotopic germinal protons of a methylene proton pair (r_{ref} = 1.75 Å) or between aromatic ring protons (r_{ref} = 2.42 Å) [26]:

$$r_{ij} = r_{ref} (\alpha_{ref}/\alpha_{ij})^{1/6} \qquad (1\text{-}4)$$

This equation assumes that the protons giving rise to the NOE are not interacting with any other protons. Distances smaller than the reference are overestimated and longer distances can be underestimated depending on different correlation times. The error in distance determination increases as the correlation time and the mixing time increase (between ± 3% and ± 20%) [34]. One of the

ways to deal with the inaccuracy of the distance determination is to classify intensities into three groups: strong, medium, and weak cross-peaks corresponding to the distances 1.8-2.8Å, 1.8-3.5Å, and 1.8-5.0Å, respectively [35].

The seven sequential and medium range distances $d_{\alpha N}$, $d_{\alpha N}$ (i, i+2), $d_{\alpha N}$ (i, i+3), $d_{\alpha N}$ (i, i+4), d_{NN}, d_{NN} (i, i+2) and $d_{\alpha\beta}$(i, i+3) are of potential interest for protein structure determination (Fig.1-9).

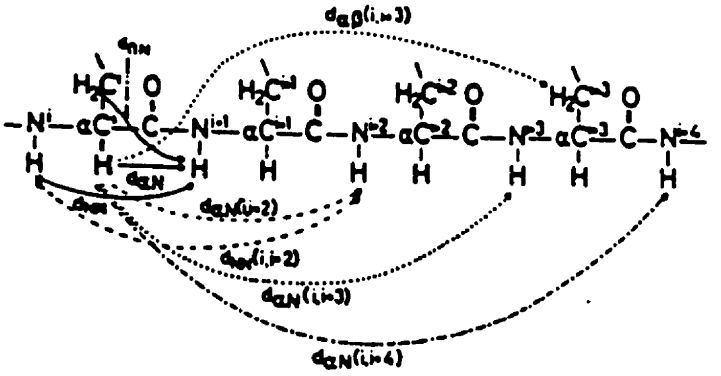

Fig.1-9. Selected sequential and medium-range ^{1}H-^{1}H distances in polypeptide chains (Taken with permission from Wüthrich *et. al.*, 1986 [26]).

Secondary structures have characteristic NOE patterns and scalar coupling constants (Table 1-2). Generally, α-helices have strong sequential (NH_i, NH_{i+1}) NOEs. The (αH_i, NH_{i+1}), (αH_i, NH_{i+3}) and (αH_i, βH_{i+3}) NOEs are of lower intensity than (NH_i, NH_{i+1}) NOEs, but are observable. Strong sequential (αH_i, NH_{i+1}) and almost unobservable sequential (NH_i, NH_{i+1}) cross peaks indicate the presence of a β-sheet. Interstrand (αH_i, αH_j) NOEs can distinguish if a β-sheet is parallel or anti-parallel. The tight turns have short distances $d_{\alpha N}$ and d_{NN} and show similar distance constraints to those in helical structures. The distinction between α-helices and 3_{10} helix relies on observing (αH_i, NH_{i+4}) NOEs in the former and (αH_i, NH_{i+2}) NOEs in the latter.

Table 1-2 Internuclear Distances, Coupling Constants $^3J_{\alpha N}$, and Amide Exchange Rates of Secondary Structures (Rewritten from Brasukov, I. L. & Lu, Y. L., 1993 [43])

Parameter[a]	α-Helix	3_{10}-Helix	β-Anti-parallel[b]	β-Parallel
$d_{\alpha N}(i, i)$	2.6	2.6	2.8	2.8
$d_{\alpha N}(i, i + 1)$	3.5	3.4	**2.2**	**2.2**
$d_{\alpha N}(i, i + 2)$	4.4	**3.8**		
$d_{\alpha N}(i, i + 3)$	**3.4**	3.3		
$d_{\alpha N}(i, i + 4)$	4.2	(> 4.5)		
$d_{NN}(i, i + 1)$	**2.8**	**2.6**	4.3	4.2
$d_{NN}(i, i + 2)$	4.2	4.1		
$d_{\beta N}(i, i + 1)$	2.5-4.1	2.9-4.4	3.2-4.5	3.7-4.7
$d_{\alpha\beta}(i, i + 3)$	2.5-4.4	3.1-5.1		
$d_{\alpha\alpha}(i, j)$			**2.3**	4.8
$d_{\alpha N}(i, j)$			3.2	3.0
$d_{NN}(i, j)$			**3.3**	4.0
$^3J_{H^N-H^\alpha}$	(< 4)	(< 4)	(> 9)	(> 9)
NH exchange rate	slow[c]	slow[c]	slow[d]	slow[d]

[a]The most readily available parameters are highlighted in **bold.**
[b]$d_{\alpha\alpha}(i, j)$, $d_{\alpha N}(i, j)$, and $d_{NN}(i, j)$ refer to interstrand distances.
[c]The first four residues in the α-Helix and the first three residues in the 3_{10}-Helix will have fast amide proton exchange rates.
[d]Every second residue in the flanking strand will have slow amide proton exchange rates.

1.3.2.3. Chemical Exchange

Chemical exchange refers to the process in which a nucleus exchanges between two or more environments and causes changes to its observable NMR parameters. These may be intramolecular or intermolecular processes, including not only proton exchange of labile hydrogens and slow conformational equilibria, but also internal motions of a flexible molecule [36-37].

All effects of an exchange processes on the NMR spectrum depend on its rate k, compared with the nuclear relaxation rate T_1^{-1} (R_1) and correlation rate τ_c^{-1}[23]. When $k < T_1^{-1}$ (slow exchange on the relaxation time scale), exchange has no influence on the NOE and the enhancements are just those expected in the absence of exchange. When $k > T^{-1}$ (fast exchange on the relaxation time scale), the various relaxation rates are averaged by the exchange but the effect on NOE depends on

the chemical shift time scale and NOEs can be measured. Generally, separate resonances are seen for the nucleus in two or more states in slow exchange on the chemical shift time scale. For fast exchange on the chemical shift time scale, a single averaged resonance is observed and NOE measurements are impossible.

When the exchange rate is slower than molecular tumbling ($k << \tau_c^{-1}$), exchange processes that do not change the distance r_{IS} have no effect on NOE. If $k > \tau_c^{-1}$, exchange processes that do not affect r_{IS} can affect enhancement and thus interproton distance r_{IS} measurement.

The methods used for the analysis of exchange effects are lineshape analysis and magnetization transfer (slow exchange on chemical shift time scale only), which try to determine the nature of the contributing conformers. In the two-dimensional experiment (NOESY or ROESY), when the exchange rate is fast compared to the mixing time (τ_m), but slow on the chemical shift time scale ($R < k << \delta_A - \delta_B$), the spectrum will display an exchange cross peak. In a ROESY spectrum, the cross peaks can be from cross-relaxation (NOE), exchange effects or transferred NOEs which result from a two-step magnetization transfer; for example, cross-relaxation between two spins in state A followed by chemical exchange to state B. For the simplest case of first-order two-site exchange with equal populations and equal relaxation rates, the exchange rate k can be determined from the ratio of the cross and diagonal peak intensities I_{AA}/I_{AB} at a short mixing time t_m [38]:

$$I_{AA}/I_{AB} = (1-kt_m)/kt_m \qquad (1\text{-}5)$$

Amide-proton exchange rates can provide additional information about protein secondary structure and dynamics. Amide protons that are unexchanged after 24 hours in D_2O are considered slowly exchanging [25] and indicate the existence of hydrogen bonds in regular secondary structures. Fast amide proton exchange usually implies the absence of secondary structure elements.

1.3.2.4. From Coupling Constants to Dihedral Angles

Scalar coupling constants can provide local structural information which is complementary to that from the NOE data. Of particular interest is the NH-$C^{\alpha}H$ couplings constant, $^3J_{NH\alpha}$, which is directly related to the polypeptide backbone dihedral angle ϕ (Fig.1-10), and the two αH-βH coupling constants across the C^{α}-C^{β} bond, $^3J_{\alpha\beta 2}$ and $^3J_{\alpha\beta 3}$, which give the side-chain torsion angle χ_1 by the Karplus equations [39]:

$$^3J_{NH\alpha} = 6.4\cos^2(\phi - 60°) - 1.4\cos(\phi - 60°) + 1.9 \qquad (1\text{-}6)$$

$$^3J_{\alpha\beta 2} = 9.5\cos^2\chi_1 - 1.6\cos\chi_1 + 1.8 \qquad (1\text{-}7)$$

$$^3J_{\alpha\beta 3} = 9.5\cos^2(\chi_1 - 120°) - 1.6\cos(\chi_1 - 120°) + 1.8 \qquad (1\text{-}8)$$

In these equations, the coupling constants are in Hertz. The parameters used for $^3J_{NH\alpha}$ are those according to Pardi *et al.*[40]. The parameters used for two $^3J_{\alpha\beta}$ are those according to De Marco *et al.*[41]. The two methylene protons of CH_2- are denoted as β_2 and β_3.

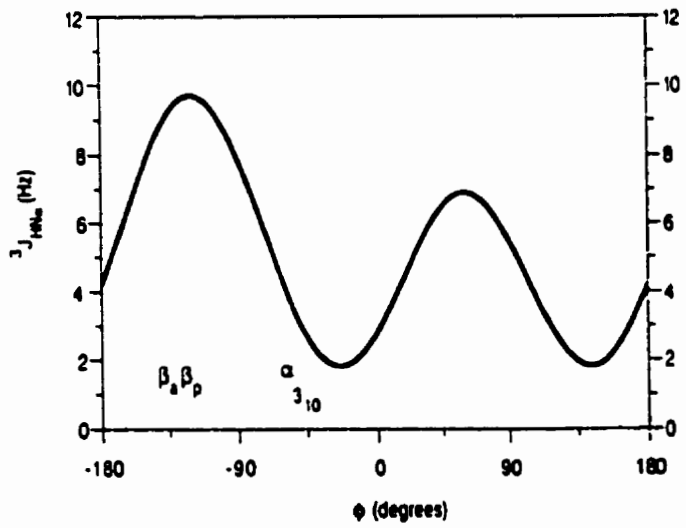

Fig.1-10 The relationship between the $^3J_{NH\alpha}$ and the main-chain dihedral angle ϕ using equation 1-6. ϕ values for idealized α-helices, 3_{10}-helices, parallel, and antiparallel β-sheets are denoted as α, 3_{10}, β_p and β_a, respectively. (Taken with permission from Wüthrich, K.1986 [26]).

Smith, L. J. *et. al.* [42] demonstrated that the calculated mean $^3J_{NH\alpha}$ coupling constants for α helices, 3_{10} helices and β-sheets from a data base of 85 high resolution protein crystal structures are 4.8, 5.6 and 8.5 Hz, respectively. These differ significantly from the ideal values of 3.9 Hz (ϕ = -57°) for α-helices, 3.0 Hz (ϕ = -49°) for 3_{10}-helices and 9.7/8.9 Hz (ϕ = -119°) for parallel and (ϕ = -139°) for antiparallel β-sheets. Furthermore, a wide range of ϕ, φ angles was seen for α helices, 3_{10} helices and β-sheets in the data base and this results in a very broad $^3J_{NH\alpha}$ coupling constant distribution. However, a qualitative analysis of the DQF-COSY spectrum is achieved by grouping the coupling constants into the categories: $^3J_{NH\alpha} > 8$ Hz for β-sheets, $^3J_{NH\alpha}$ = 6-8 Hz disordered segments and $^3J_{NH\alpha} < 6$ Hz for helices [43].

In small peptides, $^3J_{NH\alpha}$ can be measured from one-dimensional NMR spectra because of the separation of the components of the doublet at the amide proton resonance frequency. For proteins, 2D methods must be used for such measurement due to resonance overlap in 1D. $^3J_{NH\alpha}$ can be measured using phase-sensitive COSY or DQF-COSY spectra where the separation of the antiphase components of the NH-C^{α}H cross peak in ω_2 is a measure of $^3J_{NH\alpha}$. This method is subject to errors if the linewidth is larger than the coupling constant. The minimum separation between the antiphase components is equal to about 0.576 times the linewidth at half-height [44]. If the true separation is smaller than this, the observed coupling constants in antiphase cross peaks are unreliable.

Measurement of $^3J_{\alpha\beta}$ directly from a 1D spectrum is usually impossible. Qualitative estimation of the two coupling constants, $^3J_{\alpha\beta 2}$ and $^3J_{\alpha\beta 3}$ can be obtained from DQF-COSY spectra where the peak-to-peak separation of the αβ multiplet depends on $^3J_{\alpha\beta}$. Three rotamers give very different values for the $^3J_{\alpha\beta 2}$ and $^3J_{\alpha\beta 3}$. It is sometimes possible to make a stereospecific assignment of β-protons

based on $^3J_{\alpha\beta}$ measurements and intraresidue NOEs (H^{α}-$H^{\beta 2}$), (H^{α}-$H^{\beta 3}$), (H^{N}-$H^{\beta 2}$) and (H^{N}-$H^{\beta 3}$) (Table 1-3) [43]. A more sensitive measure of $^3J_{\alpha\beta}$ is obtained from E-COSY-type spectra [45] by measuring the displacement in cross peak components caused by the passive scalar coupling in the well-resolved αH-βH cross peak as shown in Fig.1-11. An alternative coupling constant, $^3J_{N\beta}$, which can be obtained from a ^{15}N-coupled ^{1}H NOESY or a COSY-type experiment, also can be used in the stereospecific assignment of β-proton resonances [46].

Table 1-3 NMR Parameters Used to Define the Three Possible Conformations Around the Cα-Cβ Bond. (Rewritten from Barsukov, I. L. 1993 [43])

χ_1	60°	180°	−60°
	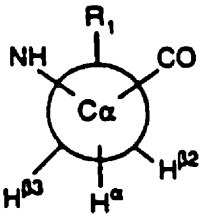	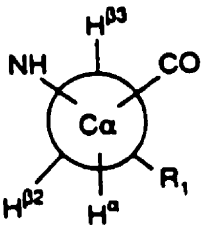	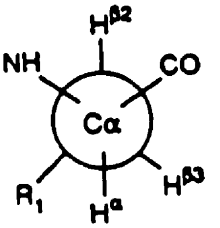
$^3J_{H^{\alpha}.H^{\beta 2}}$ (Hz)	2.6–5.1	2.6–5.1	11.8–14.0
$^3J_{H^{\alpha}.H^{\beta 3}}$ (Hz)	2.6–5.1	11.8–14.0	2.6–5.1
$^3J_{H^{N}.H^{\beta 2}}$ (Hz)	−6	−1	−1
$^3J_{H^{N}.H^{\beta 3}}$ (Hz)	−1	−1	−6
NOE(H^{α}-$H^{\beta 2}$)[a]	s	s	m–w[b]
NOE(H^{α}-$H^{\beta 3}$)	s	w–m[b]	s
NOE(H^{N}-$H^{\beta 2}$)	w–m[b]	s–m[b]	s
r (H^{N}-$H^{\beta 2}$)[c]	3.5–4.0	2.5–3.4	2.2–3.1
NOE(H^{N}-$H^{\beta 3}$)	s–m[b]	s	w–m
r (H^{N}-$H^{\beta 3}$)	2.5–3.4	2.2–3.1	3.5–4.0

[a] S = strong, m = medium, w = weak.
[b] For large proteins, when efficient spin diffusion is prevalent, the NOEs are biased towards stronger intensities. In this case a ROESY experiment is advisable.
[c] r(H^{N}-H^{β}) is the approximate interproton distance in Å.

Fig. 1-11. An example of measurement of two coupling constants $^3J_{\alpha\beta}$ from an E. COSY experiment with one large ($^3J_{\alpha\beta A}$ = 10.8 Hz) and one small ($^3J_{\alpha\beta B}$ = 4.5 Hz) $^3J_{\alpha\beta}$ value. It is assumed that β_A proton has a higher chemical shifts and β_B proton has a lower chemical shift. (Taken with permission from Lorna J. Smith, 1991[47])

1.3.3. Protein Structures by NMR Restraints

There are many procedures for protein tertiary structure determination from NMR data. All these approaches aim to sample conformational space whilst at the same time satisfying a set of experimental constraints. One approach is homologous model building which utilizes existing knowledge of tertiary structure. This can be performed either by using interactive molecular graphics (for example, CONFOR program [48]) or using a physical model. An alternative method is adopted by two types of distance geometry: metric matrix distance geometry (DGEOM [49] and XPLOR/dg [50]) and distance geometry in torsional space (DISMAN [51]). Restrained molecular dynamics (AMBER [52] and DISCOVER [53]) can be used to refine model-built structures and dynamical simulated annealing (XPLOR [54]) allows potential energy barriers to be crossed.

1.4. Aim of the Present Work

The purpose of this research was to synthesize an alamethicin dimer and to characterize the structure and dynamics of the dimer using ^1H and ^{15}N NMR spectroscopy. The chemical shifts, NOEs and scalar coupling constants of the

dimer will be measured. From these NMR data, it may be possible to determine the secondary structure of the dimer and interactions at the dimer interface, including backbone-backbone and side-chain contacts between the monomers. This information would be useful in efforts to build a model of the alamethicin pore and may lead to insights into the antibiotic activity of alamethicin.

References

1. Mathew, M. K., & Balaram, P. (1983) *Mol. Cell Biochem. 50*, 47-64.
2. Breed, J., Kerr, I. D. & Sansom, M. S. P. (1995) *Biopolymers 35*, 639-655.
3. Brewer, D., Mason, F. G., & Taylor, A. (1987) *Can. J. Microbiol., 33*, 619-625.
4. Pandey, R. C., Cook. Jr., J. C. and Rinehart Jr. K. L. (1977) *J. Am. Chem. Soc. 99*, 8469
5. Fox, R. O. & Richards, F. M. (1982) *Nature 300*, 325-330.
6. Banerjee, U.Tssui, F. P., Balasubramanian, T. N. & Chan, S. I. (1983) *J. Mol. Biol. 165*, 757.
7. Esposito, G., Carver, J. A. & Campbell, I. D. (1987) *Biochemistry 26*, 1043-1050.
8. Yee, A. A. & O'Neil J. D. J. (1992) *Biochemistry 31*, 3135-3143.
9. Boheim, G., Hanke, W. & Jung, G. (1983) *Biophys. Struct. Mech. 9*, 181-191.
10. Ritov, V. B. & Shimon, R. G. (1992) *Gen. Physiol. Biophy. 11*, 49-58.
11. Woolley, G. A. & Wallace B. A. (1992) *J. Memr. Biol. 129*, 109-136.
12. Sansom, M. S. P., (1993) *Eur. Biophys. J. 22*, 105-124.
13. Sansom, M. S. P., (1991) *Eur. Biophys. J. 20*, 229-240.
14. Mak, D. D. & Webb, W. W (1995) *Biophys. J.* 69, 2323-2336.
15. Hall, J. E. & Vodyanoy, I. (1984) *Biophys J. 45*, 233-247.
16. Boheim, G. J. (1974) *Membrance Biol. 19*, 277-303.
17. Gordon, L. G. M., & Haydon D. A. (1972) *Biochim. biophys. Acta. 255*, 1014-1018.
18. Sansom, M. S. P., (1991) *Prog. Biophys. Mol. Biol. 55*, 139-236.
19. Shaochun Y., Shuyun, P., Linda, L, Breed, J., Sansom, M. S. P. & Woolley, G. A (1996) *Biochemistry 35*, 6225-6232.
20. Kebarle, P. & Tang, T. (1993) *Anal. Chem. 65*, 975.
21. Richard B. Cole (1997) <<*Electrospray Ionization Mass Spectrometry*>>, New York
22. Biemann, K. (1992) *Annu. Rev. Biochem. 61*, 977-1010.

23. Wüthrich, K., Wider, G., Wagner, G. & Bram, W. (1982) *J. Mol. Biol. 155*, 311.

24. Kay, L. E., Ikua, M., Tschudin, R., & Bax, A. (1990) *J. Magn. Reson. 89*, 496.

25. Pelczer, I. & Szalma, S.(1991) *Chem. Rev. 91*, 1507.

26. Wüthrich, K. (1986) <<*NMR of Proteins and Nucleic Acids*>>, John-Wiley and Sons, Inc., New York

27. Wishart, D. S. & Sykes, B. D. (1994) *Methods in Enzymology 239*, 363-392.

28. Wishart, D. S. & Sykes, B. D. (1994) *J. Biomol. NMR 4*, 171-180.

29. Wishart, D. S., Sykes, B. D. & Richards, F. M. (1991) *J. Mol. Biol. 222*, 311-333.

30. Andrew E Derome (1987) <<*Modern NMR Techniques for Chemistry Research*>>, Pergamon Press, Oxford

31. Yee, A. A. & O'Neil J. D. J. (1992) *Biochemistry 31*, 3135-3143.

32. Neuhaus, D. & Willison, M. (1989) <<*The Nuclear Overhauser Effect*>>, VCH Publisher, Inc., New York

33. Stoven, V., Mikou, A., Piretean, D. & Lallemand, Y. Y. (1989) *J. Magn. Reson. 82*, 163.

34.Gronenborn, A. M. & Clore. G. M. (1985) *Prog. NMR Spectrosc. 17*, 95.

35. Kuntz, I. D., Thomason, J. F. & Oshiro, S. M. (1989) *Methods in Ezymology 177*, 159-204.

36. Berkowitz, B. & Balaban, R. S. (1989). *Methods in Enzymology 176*, 330-341.

37. Bain, A. D. (1998) *Biochem. Cell Biol. 76*, 171-176.

38. Dobson, C. M., Lian, L. Y., Redfield, C.& Topping, K. D. (1986). *J. Magn. Reson. 69*, 201.

39. Karplus, M. (1959). *J. Phy. Chem. 30*, 11.

40. Pardi, A., Billeter, M. & Wüthrich, K. (1984) *J. Mol. Biol. 180*, 741.

41. De Marco, A., Llinas, M. & Wüthrich, K. (1978) *Biochemistry 17*, 617.

42. Smith, L. J. Bolin, K. A. et, al, (1996) *J. Mol. Biol. 255*, 494-506.

43. Barsukov, I. L. & Lu, Y. L. (1993) <<*NMR of Macromolecules*>>. Edited by Roberts, G. C. K., Oxford University Press Inc., New York, pp 325.

44. Neuhaus, D., Wagner, G., Vsak, M., Kagi, H. R. & Wüthrich, K. (1995) *Eur. J. Biochem. 151*, 257.

45. Griesinger, C. SΦrensen, O. W. & Ernst, R. R (1987). *J. Magn. Reson. 75*, 474-492.

46. Montelione, G. T., Winkler, M. E. & Wagner, G. (1989) *J. Magn. Reson. 82*, 198.

47. Lorna J. Smith, Michael J. Sutcliffe&Christopher M. Dobson (1991) *Biochemistry 30*, 986.

48. Billeter, M., Engeli, M. & Wüthrich, K. (1985). *J. Mol. Graphics 3*, 79.

49. Havel, T. F. (1991). *Prog. Biophys. Molec. Biol. 56*, 43.

50. Kuszewski, J., Nilges, M., & Brunger, A. T. (1992) *J. Biomolec. NMR 2*, 33.

51. Braun, W. (1987) *Q. Rev. Biophys. 19*, 115.

52. Weiner, S. J., Kollman, P. A., Case, D. A. & Weiner, P. (1984) *J. Am. Chem. Soc. 106*, 765.

53. Discover manual version 2.8 (1992) Biosym Technologies Inc., San Diego, CA.

54. Brünger, A. T. (1992) Xplor Manual version 3.0, Yale University, New Haven, CT.

Chapter 2

Experimental

2.1. Alamethicin Monomer Purification

Unlabeled and ^{15}N-labeled alamethicin were extracted from the culture medium of *T.viride* grown in a complex medium and a semi-basal medium respectively using the modified procedures described by Adelinda A.Yee [1]. The freeze-dried alamethicin extracts were purified using reversed-phase high-performance liquid chromatography (HPLC) with detection using a SP8450 UV/visible spectrophotometer (Perkin-Elmer). A Supelcosil™ SPLC-18 column (Supelco Inc., 10 mm × 25 cm) was used to purify unlabeled alamethicin monomers. For purification of ^{15}N labeled alamethicin monomer, an ultrasphere ODS C-18 column (Beckman Inc., 10 mm × 25 cm) was used. The HPLC columns were periodically tested with 20μl test samples consisting of 5μl acetophenone, 5μl nitrobenzene and 500μl toluene dissolved in 1L of mobile phase [1], eluted with 70% methanol and 30 % deionized water at 3 ml/min (254 nm). A guard cartridge column filled with Pelliguard packing was used.

For peptide purification, the mobile phases consisted of solvent A (0.05 N acetic acid adjusted to pH 3.5 with triethylamine), solvent B (tetrahydrofuran : acetonitrile : solvent A = 8 : 1 : 2) and solvent C (HPLC-grade methanol). The mobile phases were filtered through a Nylon-66 membrane filter (0.45 μm pores) and were degassed for 20 min in an ultrasonic bath in order to prevent air bubbles in the system. Samples were dissolved in HPLC-grade methanol and centrifuged. Before each sample injection, the column was equilibrated for at least 30 min with mobile phase at a flow rate of 1 ml/min. The injection volume of peptide solution varied between 50 and 500 μl. The UV detector was operated at 210 nm. The

solvent elution gradients for alamethicin monomer purification are indicated in Table 2-1. All solvents were of HPLC grade from Aldrich Chemical Co. For dimer purification and alamethicin monomer repurification in order to eliminate triethylammonium acetate impurities, 100% HPLC-grade methanol was used as mobile phase.

Table 2-1 Solvent Program in the HPLC Purification of Alamethicin

time (min)	flow (ml/min)	A (percentage)	B (percentage)	C (percentage)
10	2.0	60	40	0
20	1.0	46	54	0
45	1.0	46	54	0
50	1.5	0	100	0
51	2.0	0	0	100
60	2.0	0	0	100

2.2. Preparation of Alamethicin Dimers:

Dodecanedioyl dichloride and pyridine were purchased from Adrich Chemical Co. Pyridine and tetrahydrofuran (THF) were distilled using standard methods [2]. The synthetic route to the alamethicin dimer is shown in Fig. 2-1:

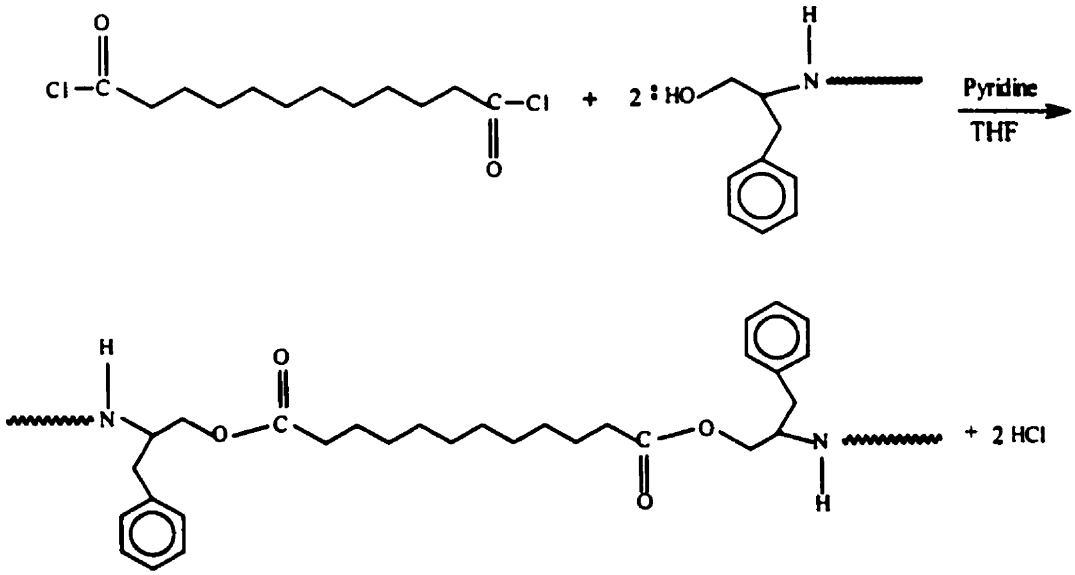

Fig.2-1. The route for the synthesis of the alamethicin dimers. ~~~~~ represents the Gln_{19}-Ac segment of alamethicin.

This nucleophilic substitution reaction is the esterification of 2 equivalents of a primary alcohol (phenylalaninol) with 1 equivalent of a diacid chloride (dodecanedioyl dichloride) via the addition-elimination mechanism as follows [3]. The addition of the phenylalaninol hydroxyl to the carbonyl group of the acid dichloride yields a tetrahedral intermediate. The negative charge on oxygen in the intermediate then expels readily the leaving group (-Cl^-), generating a compound as product (dimer). Pyridine base is present as a catalyst, to neutralize the HCl formed and to prevent side reactions.

Two dimer preparations were made. In the first, ^{15}N labeled Aib_6-alamethicin was dimerized (Fig.2-2a). In the second, a mixture of Aib_6-alamethicin and Ala_6-alamethicin were dimerized, yielding a mixture of three dimers as indicated in Fig.2-2b.

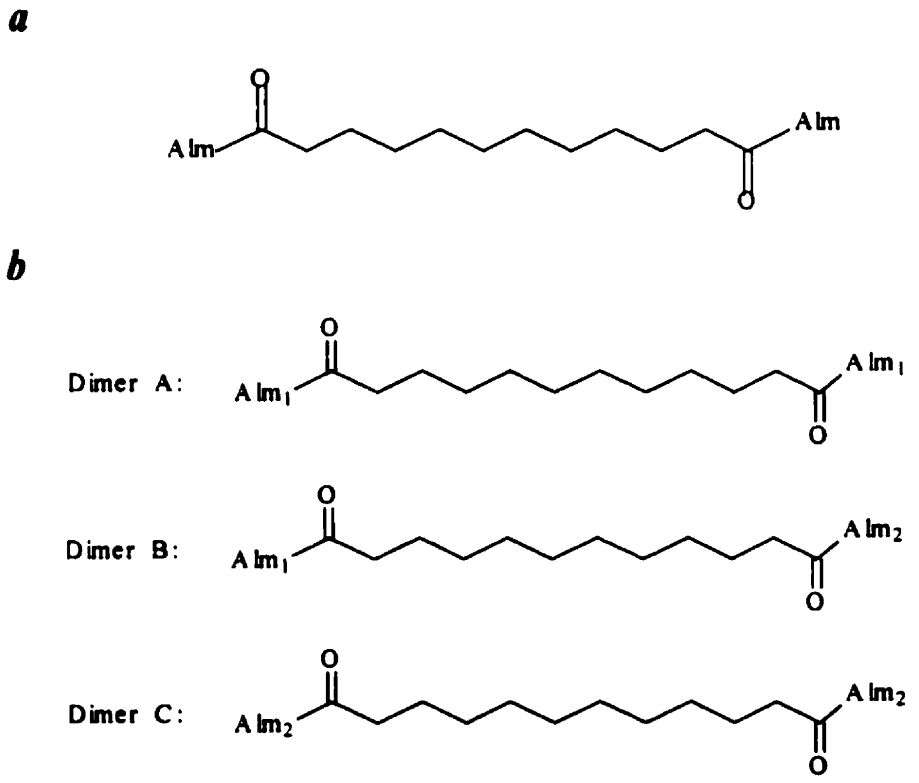

Fig.2-2. The Chemical structures of ^{15}N labeled (a) and unlabeled (b) alamethicin dimers. The Alm_1 has Aib6 and Alm_2 has Ala6. The sequences for Alm_1 and Alm_2 are shown in Fig 1-1.

a. Synthesis of ^{15}N Labeled Alamethicin Dimer

HPLC-purified unlabeled alamethicin monomer was recrystallized in boiling acetonitrile solvent and used for the dimer reaction. 20 mg (1×10^{-5} mol, 3 equiv.) of ^{15}N labeled alamethicin white powder in a 1ml dry flask was dried for one day at room temperature under vacuum and then dissolved in 0.3 ml of dry THF. To this was added 0.1 ml of distilled pyridine. The resulting solution was cooled in an ice-water bath for 10 min before reaction. In another 5 ml dry flask, 166 µl of dodecanedioyl dichloride was dissolved in 5 ml of dry THF and stored under nitrogen. 25 µl of the acid chloride (3.3×10^{-6} mol, 1 equiv.) solution was added to the alamethicin solution dropwise under nitrogen. The reaction mixture was stirred on ice for 2 hours and then at room temperature for 2 days.

Thin-layer chromatography of the reaction mixture (mobile phase: chloroform/methanol/H_2O = 70:15:2) showed one more nonpolar compound than present in a solution of pure alamethicin monomer. The solvent was evaporated from the reaction mixture under vacuum to eliminate most of the pyridine and the remnant was redissolved in methanol. The solution was loaded onto a reversed-phase HPLC column in aliquots of 50-100 µl and eluted by 100% HPLC-grade methanol at 1.5 ml/min. 1.2 mg of labeled dimer was obtained with 7.5 % yield.

b. Synthesis of Unlabeled Alamethicin Dimer

Unlabeled alamethicin monomer mixture (from Sigma) was used for the dimer reaction. Analogous to the procedure described for formation of ^{15}N labeled alamethicin dimer, 20 mg (1×10^{-5} mol) of unlabeled alamethicin mixture, 0.1ml pyridine and 1.26 µl (5×10^{-6}mol) of undiluted dodecanedioyl dichloride in 5 ml of THF were reacted for 2 days and worked up to obtain approximately 1mg dimer as a white solid with 8.6 % yield.

2.3. Identification of Alamethicin Dimers by ESI-MS

Freeze-dried alamethicin dimers were dissolved in 0.1 ml of methanol and analyzed by ESI-MS. All experiments were conducted on a Quattro LC triple quadrupole mass spectrometer (Micromass, UK) equipped with a Z-spray™ ionization source in the positive ion mode. Solutions of peptide (10^{-5}M) in CH_3CN : methanol : H_2O (3 : 3 : 4) were injected using a 20-μl injection loop. The carrier solvent was CH_3CN : H_2O (50 : 50) at 10 μl/min. The cone voltage varied from 20 V to 60 V. Table 2-2 shows the masses of the common amino acids used for the calculation of protein mass. In addition, the masses of Aib and Pho in alamethicin are 85 and 150 Da, respectively. The mass of the linker is 196 Da.

Table 2-2 Residue Mass [-NH-CHR-CO-] of Common Amino Acids

Amino acid	Three letter code	Mass	Amino acid	Three letter code	Mass
Glycine	Gly	57	Aspartic acid	Asp	115
Alanine	Ala	71	Glutamine	Gln	128
Serine	Ser	87	Lysine	Lys	128
Proline	Pro	97	Glutamic acid	Glu	129
Valine	Val	99	Methionine	Met	131
Threonine	Thr	101	Histidine	His	137
Cysteine	Cys	103	Phenylalnine	Phe	147
Isoleucine	Ile	113	Arginine	Arg	156
Leucine	Leu	113	Tyrosine	Tyr	163
Aspargine	Asn	114	Tryptophan	Trp	186

Rewritten from Biemann, K. 1992 [4]

2.4 NMR Spectroscopy

Alamethicin dimer was dissolved in 0.5 ml of CD_3OH to a concentration of approximately 1 mM and placed in a 5-mm NMR tube (Wilmad 535). All NMR spectra were obtained using a Bruker AMX 500 spectrometer with a 5-mm ^1H probe head.

All experiments were carried out non-spinning. Setting up the instrument involved four fundamental steps: locking the sample, tuning the probe, shimming

the field and calibrating the pulses. Quadrature detection mode for 1D experiments was achieved using *qseq* (sequential alternate sampling). 2D experiments used time proportional phase increment (TPPI) [5] for quadrature detection in the F_1 dimension and *qsim* (simultaneous sampling) in the F_2 dimension. Presatuation was used for water suppression, which was achieved by a selective low-power irradiation of the water signal. For spectra acquired on ^{15}N-labeled alamethicin, composite-pulse decoupling (CPD) [6] was used during acquisition to eliminate the splitting and broadening caused by the scalar coupling between the ^{15}N nuclei and protons. The evolution of heteronuclear coupling in experiments such as HSQC was refocused by a 180° pulse applied to ^1H in the middle of t_1. A number of scans per FID, which was always some multiple of the basic cycle length, was used to increase signal-to-noise. Dummy scans were used to establish a steady-state magnetization before data was acquired. The acquisition parameters for each experiment are given in the related figure legends. The interrelationships between some acquisition parameters for three different sampling modes are summarized below :

Table 2-3 Parameters Involved in the Data Acquisition [7]

Parameters	QDseq	QDsim	TPPI
ADC digitization mode	A, B, A, B, ...	(A, B), (A, B), ...	A, A, A, ...
rf Offset position	Center of SW	Center of SW	Edge of SW
Total data points (real + imag.)	TDi	TDi	TDi
Number of time-domain increments	TDi/2	TDi/2	TDi
Time-domain increment	$\Delta ti = 1/SW_i$	$\Delta ti = 1/SW_i$	$\Delta ti = 0.5/SW_i$
Dwell time	$dw_i = \Delta t_i/2$	$dw_i = \Delta t_i$	$dw_i = \Delta t_i$
Nyquist frequency	$f_{Ni} = 0.25/dw_i = SW_i/2$	$f_{Ni} = 0.5/dw_i = SW_i/2$	$f_{Ni} = 0.5/dw_i = SW_i$
Maximum evolution	$t_i^{max} = t_i^0 + (N_i-1)\,\Delta t_i$	$t_i^{max} = t_i^0 + (N_i/2-1)\,\Delta t_i$	$t_i^{max} = t_i^0 + (N_i-1)\,\Delta t_i$
Acquisition time	$aq_i = TD_i\Delta t_i/2$	$aq_i = TD_i\Delta t_i/2$	$aq_i = TD_i\Delta t_i$
Digital resolution	$R_i = 2SW_i/TD_i$	$R_i = 2SW_i/TD_i$	$R_i = 2SW_i/TD_i$
Digital resolution after zero-filling	$R_i = SW_i/SI_i$	$R_i = SW_i/SI_i$	$R_i = SW_i/SI_i$
Type of FT	Real	Complex	Real

The NMR data were processed on a SUN workstation using XSPEC® software based on UXNMR®. The basic steps of processing involve zero-filling, window multiplication, Fourier transformation, spectrum phasing and base line correction. Window functions were applied for maximization of resolution by minimizing linewidths and/or for reducing noise. Zero-filling was used for resolution enhancement by increasing the number of points in each domain. Phase correction was done using zero-order and first-order phase constants. 1D spectra were base-line corrected with a 5th-order polynomial function. 2D spectra were base-plane corrected with automatic baseline correction in both dimensions. All ^{1}H chemical shifts are referenced to 2,2-dimethyl-2-silapentane-5-sulfonate (DSS). ^{15}N chemical shifts in ppm are relative to 2.9 M $^{15}NH_4Cl$ in 1 M HCl, which resonates at 24.93 ppm with respect to liquid NH_3 [8].

The pulse sequences for 2D experiments in this report are shown in Fig.2-3:

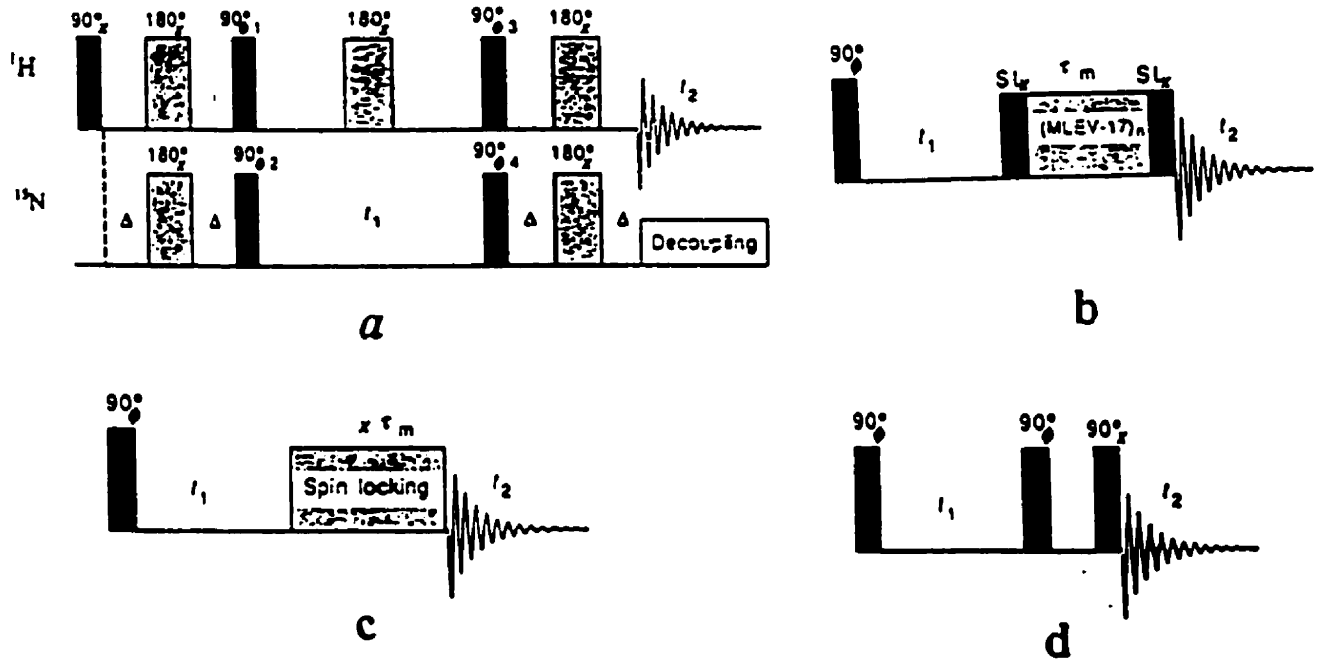

Fig. 2-3. The 2D pulse sequences for the alamethicin dimers (adapted from [9]). (a) The HSQC pulse sequence for ^{15}N dimer. (b) The TOCSY pulse sequence for the unlabeled dimer and ^{15}N dimer (^{15}N cpd decoupling during acquisition was added). (c) The ROESY pulse sequences for the unlabeled dimer and for ^{15}N dimer (180° ^{1}H decoupling during t_1 and ^{15}N cpd decoupling during acquisition were added). (d) The DQF-COSY pulse sequence for the unlabeled dimer and for ^{15}N dimer (180° ^{1}H decoupling during t_1 and ^{15}N cpd decoupling during acquisition were added). ($\Delta=1/4\ J^{15}_{N\text{-}\alpha_H}$).

References

1. Adelinda A.Yee thesis <<*Isotopic labeling of alamethicin with ^{15}N and its conformation in methanol by ^{1}H and ^{15}N NMR*>> (1991).
2. Oerrin, D. D. & Armarego, W. L. F. (1989) <<*Purification of Laboratory Chemicals*>>, Pergamon Press, New York.
3. Mcmurry, J. (1984) <<*Organic Chemistry*>>, Brooks/Cole, California.
4. Biemann, K. (1992) *Annu. Rev. Biochem. 61*, 977-1010.
5. Marion, D. & Wüthrich, K (1983) *Biochem. Biophys. Res. Comm. 113*, 967.
6. Wimperis, S. (1990) *J. Magn. Reson. 86*, 46.
7. Croasmun, W. R. & Carlson R. M. K. (1994) <<*Two-Dimensional NMR Spectroscopy*>>, pp 205, VCH Publishers, Inc., USA.
8. Levy, G. C., & Lichter, R. L. (1979) *Nitrogen-15 Nuclear Magnetic Resonance Spectroscopy,* John Wiley and Sons, Toronto.
9. Frank, J. M. van de Ven (1995) <<*Multidimensional NMR in Liquids*>>, VCH Publisher, Inc., New York.

Chapter 3

Results

3.1. Purification of Alamethicin Dimers by HPLC

Fig. 3-1 shows the HPLC elution profiles for the alamethicin dimer reaction mixtures. In the ^{15}N labeled dimer mixture (*a*), pyridine (A) was eluted first at 6.9 minutes since it is the most polar component in the mixture. The unreacted alamethicin monomer (B) was eluted at 11.0 min, which is the same retention time as alamethicin by itself. Peak C at retention time 14.1 min might be the monomer plus linker since it is less polar than monomer, but more polar than the dimer (no characterization of this peak was done). The dimer (D) was the last component to be washed out at 16.4 minutes. The components in the unlabeled dimer mixture were eluted in the same order as those of the ^{15}N labeled mixture (Fig. 3-1b). The two unreacted alamethicin monomers (Ala_6; Aib_6) eluted at 8.5 and 8.9 minutes, respectively. Presumably, the two monomers plus linkers eluted at 10.6 and 12.3 minutes, respectively. The unlabeled dimer (E) was eluted last and showed a broadened peak at 14.0 minutes due to the presence of three types of dimers in the mixture.

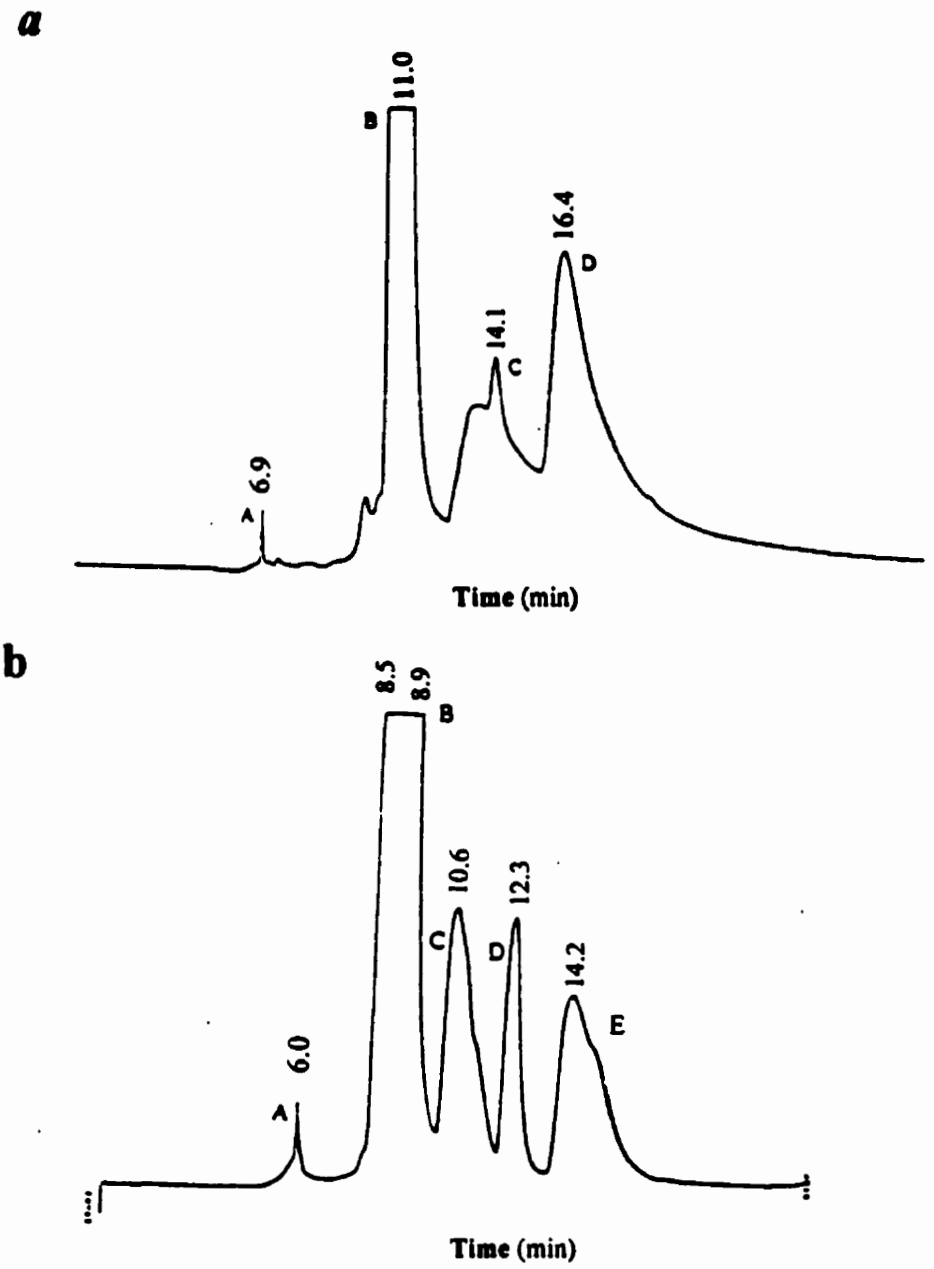

Fig. 3-1. HPLC chromatograms of (a) ^{15}N labeled alamethicin dimer reaction mixture and (b) unlabeled alamethicin dimer reaction mixture.

3.2. Electrospray Ionization Mass Spectrometry

3.2.1. Mass Spectra of ^{15}N Labeled Alamethicin Monomer

Alamethicin has three glutamine residues, which are the most likely sites of deposition of protons and other ions during electrospray ionization of the protein. The mass spectrum of ^{15}N-alamethicin monomer used for the dimer reaction is

shown in Fig. 3-2. The peaks of singly-charged parent ions (P) appear as isotopic multiplets caused primarily by the natural abundance of ^{13}C. Singly-charged parent ions (P1 = 2000.1; P2 = 2022.0) arise from the addition of H^+ and Na^+ to the peptide. Doubly-charged ion peaks (P3 = 1000.6; P4 = 1011.5; P5 = 1022.5) are due to the addition of two H^+, or one H^+ and one Na^+, and two Na^+, respectively. The other peaks in the spectrum occur as a result of fragmentation of the peptide during the electrospray ionization process. For example, F1 is the singly protoned C-terminal fragment which arises from fragmentation of the Pro_{14}-Val_{15} peptide, as indicated in Fig. 3-3. The remaining peak assignments are listed in Table 3-1 where they are compared to the masses calculated from the alamethicin sequence using amino acid masses given in Table 2-2.

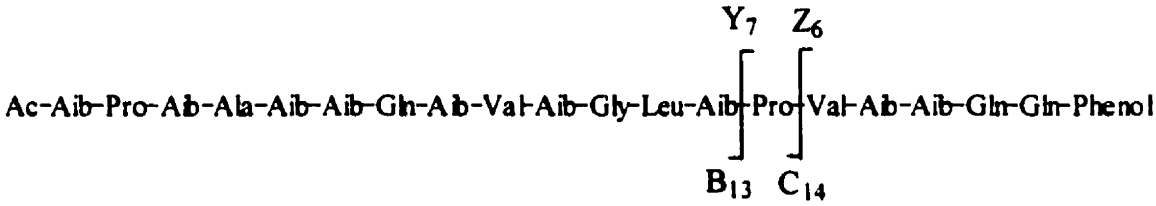

Fig.3-3. Fragment ion patterns of ^{15}N alamethicin. Y, B fragments mean the cleavage happens between C=O and NH bond and C, Z fragments mean the cleavage happens at NH and $^{\alpha}C$ bond. Two Daltons have to be added to Y and C fragments because they retain the original hydrogen and pick up one more proton from the other side of the peptide.

Table 3-1 Mass Assignments of ^{15}N Alamethicin Monomer

Peaks	Assignment	Observed *m/z*	Measured mass	Theoretical mass
P1	$(M+H)^+$	2000.1	M = 1999.1	M = 1999
P2	$(M+Na)^+$	2022.0	M = 1999.0	M = 1999
P3	$(M+2H)^{2+}$	1000.6	M = 1999.2	M = 1999
P4	$(M+H+Na)^{2+}$	1011.5	M = 1999.0	M = 1999
P5	$(M+2Na)^{2+}$	1022.5	M = 1999.0	M = 1999
F1	$(Z_6+H)^+$	667.4	Z_6 = 666.4	Z_6 = 667
F2	$(Y_7H+H)^+$	782.5	Y_7H = 781.5	Y_7H= 782
F3	$(B_{13}+H)^+$	1217.6	B_{13} = 1216.4	B_{13} = 1217
F4	$(C_{14}H+H)^+$	1333.7	$C_{14}H$ = 1332.7	$C_{14}H$ = 1332

Fig. 3-2. Mass spectrum of ^{15}N-alamethicin monomer in methanol. Cone voltage (c.v.) = 30 V. Desolvation temperature = 130 °C. The spectrum was acquired at a scan rate of 300 u/s. The peaks of alamethicin parent ions are labeled as P and the peaks for fragment ions are labeled as F. For m/z greater than 1700, the peak scales were increased to show the parent ions.

Fig. 3-2 Mass spectrum of 15N alamethicin monomer

3.2.2. Mass Spectra of the Unlabeled Alamethicin Monomer

Fig. 3-4 shows the mass spectrum of unlabeled alamethicin monomer purchased from Sigma Inc., which is a mixture of two types of alamethicin (Ala_6, M_a; Aib_6, M_b). The molecular ions of alamethicin (Ala_6) show up as singly-charged (P1 = 1963.3; P3 = 1985.4) and doubly-charged (P5 = 1004.4) species, similar to the parent ions of alamethicin (Aib_6) which also appear as singly-charged (P2 =1977.4; P4 = 1999.3) and doubly-charged (P6 = 1011.9) species by adding one proton, one sodium ion, and two sodium ions, respectively. In the expanded region of Fig. 3-4, each of the components in the isotopic multiplets of the $(M + H)^+$ and $(M + Na)^+$ ions differ by one Dalton and the most abundant species reflects the ^{13}C contributions of about 150 carbon atoms, with 1.13% per atom. Bond cleavages at Aib_{10}-Gly_{11} and Aib_{13}-Pro_{14} were also observed, as shown in Fig 3-5. The largest peak, F1, which contributed to the C-terminal fragment $(Y_7H+ H)^+$, is due to bond cleavage between Aib_{13} and Pro_{14}. Table 3-2 provides a summary of the peak assignments.

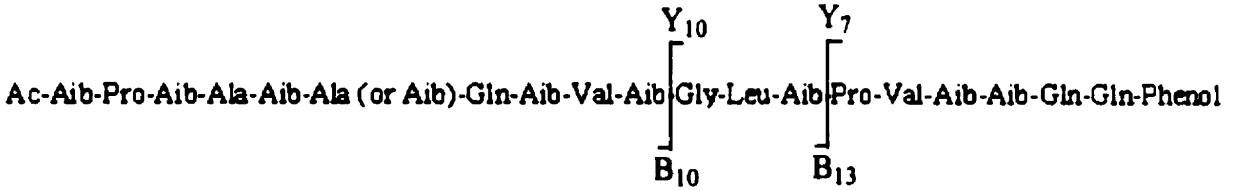

Fig.3-5. Fragment ion patterns of unlabeled alamethicin mixture.

Fig. 3-4. Mass spectrum of the unlabeled alamethicin mixture. The parameters are the same as those listed for Fig. 3-2.

Fig. 3-4 Mass spectrum of 14N alamethicin monomer

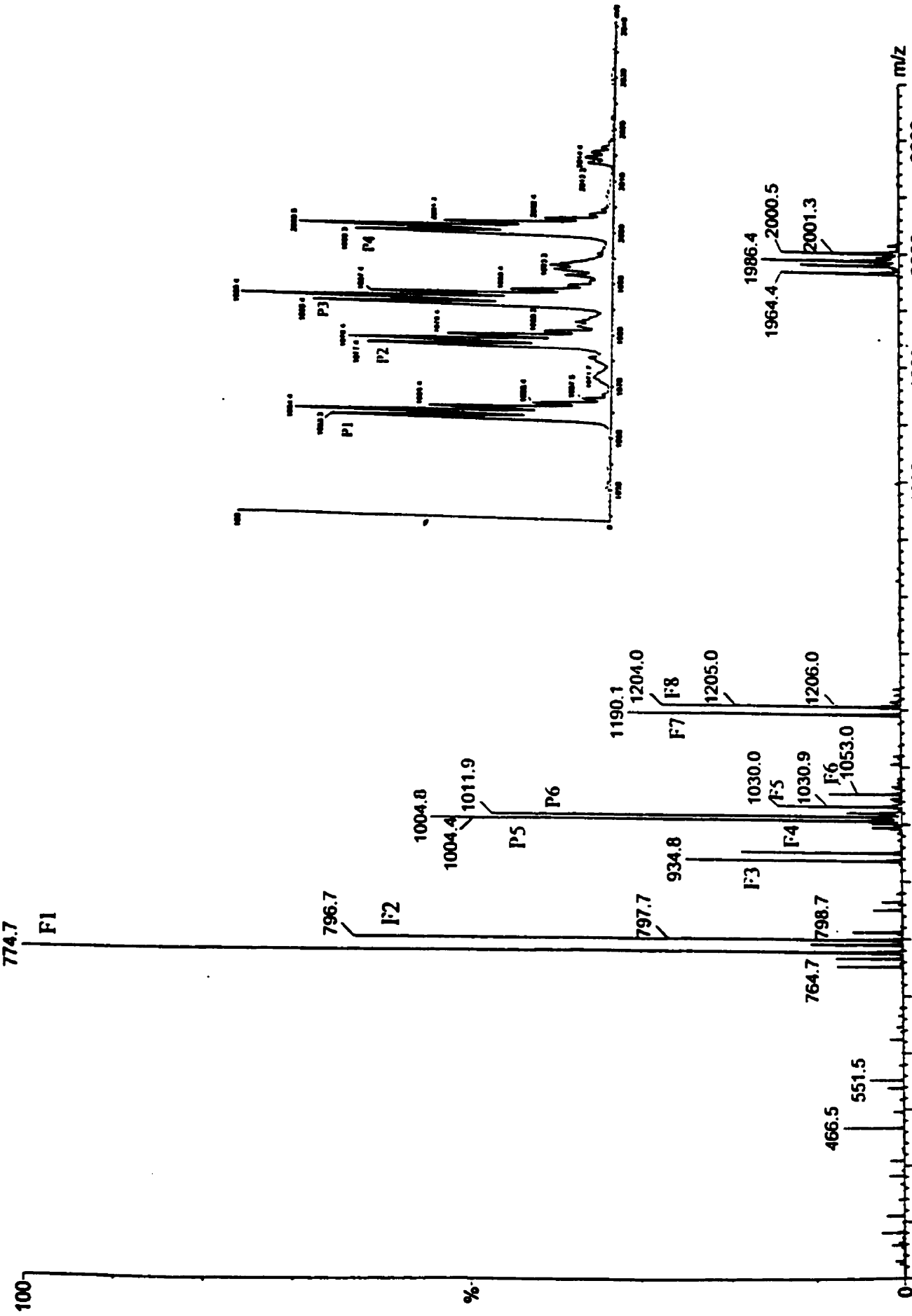

Table 3-2. Mass Assignments of Unlabeled Alamethicin Mixture

Peaks	Assignment	Observed *m/z*	Measured mass	Theoretical mass Monoisotopic
P1	$(M_a+H)^+$	1963.3	M_a = 1962.3	M_a = 1962
P2	$(M_b+H)^+$	1977.4	M_b = 1976.4	M_b = 1976
P3	$(M_a+Na)^+$	1985.4	M_a = 1962.4	M_a = 1962
P4	$(M_b+Na)^+$	1999.3	M_b = 1976.3	M_b = 1976
P5	$(M_a+2Na)^{2+}$	1004.4	M_a = 1962.8	M_a = 1962
P6	$(M_b+2Na)^{2+}$	1011.9	M_b = 1977.8	M_b = 1976
F1	$(Y_7H+H)^+$	774.7	Y_7H= 773.7	Y_7H= 774
F2	$(Y_7H+Na)^+$	796.7	Y_7H =773.7	Y_7H= 774
F3	$(B_{10}+H)^+$ of M_a	934.8	B_{10a} = 933.8	B_{10a} = 934
F4	$(B_{10}+H)^+$ of M_b	948.9	B_{10b} = 947.9	B_{10b} = 948
F5	$(Y_{10}H+H)^+$	1030.0	$Y_{10}H$ = 1029.0	$Y_{10}H$= 1029
F6	$(Y_{10}H+Na)^+$	1051.8	$Y_{10}H$ = 1028.8	$Y_{10}H$= 1029
F7	$(B_{13}+H)^+$ of M_a	1190.1	B_{13a} = 1189.1	B_{13a} = 1189
F8	$(B_{13}+H)^+$ of M_b	1204.0	B_{13b} = 1203.0	B_{13b} = 1203

3.2.3. Mass Spectrum of the ^{15}N Labeled Alamethicin Dimer

The mass spectrum of the ^{15}N-dimer is shown in Fig. 3-6, exhibiting a distribution of multiprotonated fragments and molecular ions. The expected mass of the dimer is 4190.0 Da. The observed molecular masses ranged from 4190.1 to 4191.5 Da as calculated from mass to charge values with 2, 3, 4 and 5 positive charges. Fragment ions smaller than the dimer by 212 Da are observed with the same charges as the corresponding molecular ions, and may be caused by cleavage at the Aib_1-Pro_2 backbone and side chain (Fig.3-7). The spectrum also shows the presence of some unreacted alamethicin monomers which appear as singly-charged parent ions (P_{1m} = 1999.7) and doubly-charged parent ions (P_{2m} = 1000.2). Table 3-3 provides a summary of the peak assignments.

Fig. 3-6. Mass spectrum of the ^{15}N-alamethicin dimer. The parameters are the same as those shown in Fig. 3-2. Peaks from the alamethicin monomer ions are labeled as P_{1m} and P_{2m}.

Fig. 3-6 Mass spectrum of 15N alamethicin dimer

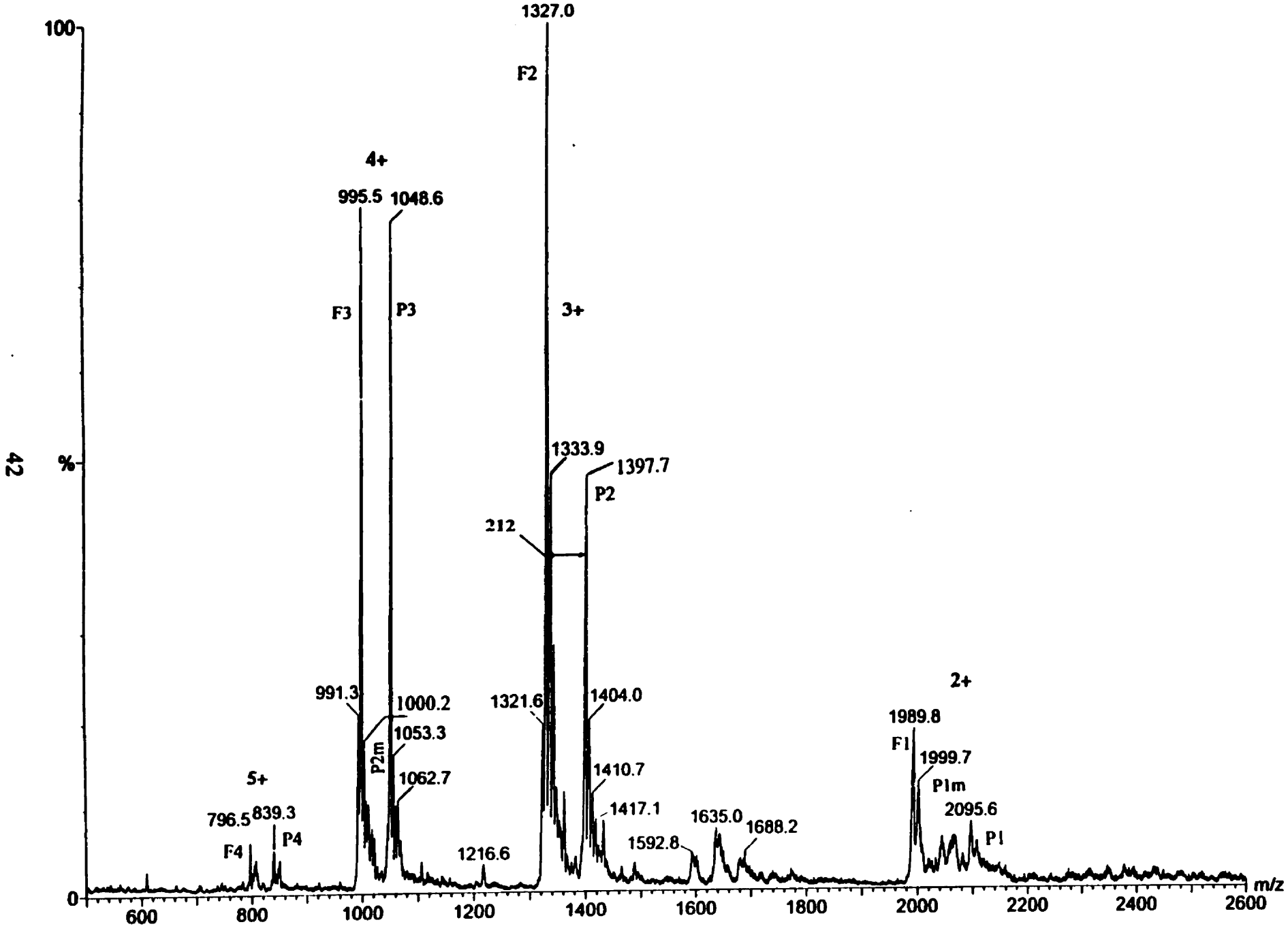

Fig. 3-7. Possible fragmentation of ^{15}N-alamethicin dimer. ~~~~~ represents the linker and other monomer.

Table 3-3. Mass Assignments of ^{15}N-Alamethicin Dimer

Peaks	Assignment	Observed *m/z*	Measured mass	Theoretical mass
P1	$(D + 2H)^{2+}$	2096.1	D = 4190.2	D = 4190
P2	$(D + 3H)^{3+}$	1397.7	D = 4190.1	D = 4190
P3	$(D + 4H)^{4+}$	1048.6	D = 4190.4	D = 4190
P4	$(D + 5H)^{5+}$	839.3	D = 4191.5	D = 4190
P_{1m}	$(M + H)^{+}$	1999.7	M = 1998.7	M = 1999
P_{2m}	$(M + 2H)^{2+}$	1000.2	M = 1998.4	M = 1999
F1	$(F + 2H)^{2+}$	1989.8	F = 3977.6	
F2	$(F + 3H)^{3+}$	1327.0	F = 3978.0	
F3	$(F + 4H)^{4+}$	995.5	F = 3978.0	
F4	$(F + 5H)^{5+}$	796.5	F = 3977.5	

3.2.4. Mass Spectrum of the Unlabeled Alamethicin Dimer

Because our unlabeled alamethicin preparation consisted of a roughly equal mixture of two peptides differing in one amino acid, dimer synthesis should have produced equal amounts of two different homodimers (D_a and D_c) and one heterodimer (D_b) twice as abundant as each of the homodimers. Fig. 3-8 shows the mass spectrum of the unlabeled alamethicin dimers, where the expected 1:2:1 ratio of the three types of dimer was observed (P3, P4, P5). Doubly-charged parent ions of dimer have mass to charge ratios of 2082.8, 2090.4 and 2097.4, corresponding to $(D_a + 2Na)^{2+}$, $(D_b + 2Na)^{2+}$, and $(D_c + 2Na)^{2+}$, respectively. The singly-charged fragments such as F1 (1964.4), F3 (1985.4) and F6 (2211.5) are consistent with peptides arising from the cleavages between $PhoI_{20}$ and the linker, as shown in Fig. 3-9. Assignments of peaks for unlabeled dimer are listed in Table 3-4:

Fig. 3-8. Mass spectrum of the unlabeled alamethicin dimer mixture. The parameters are same as those listed for Fig. 3-2.

Fig. 3-8 Mass spectrum of 14N alamethicin dimer

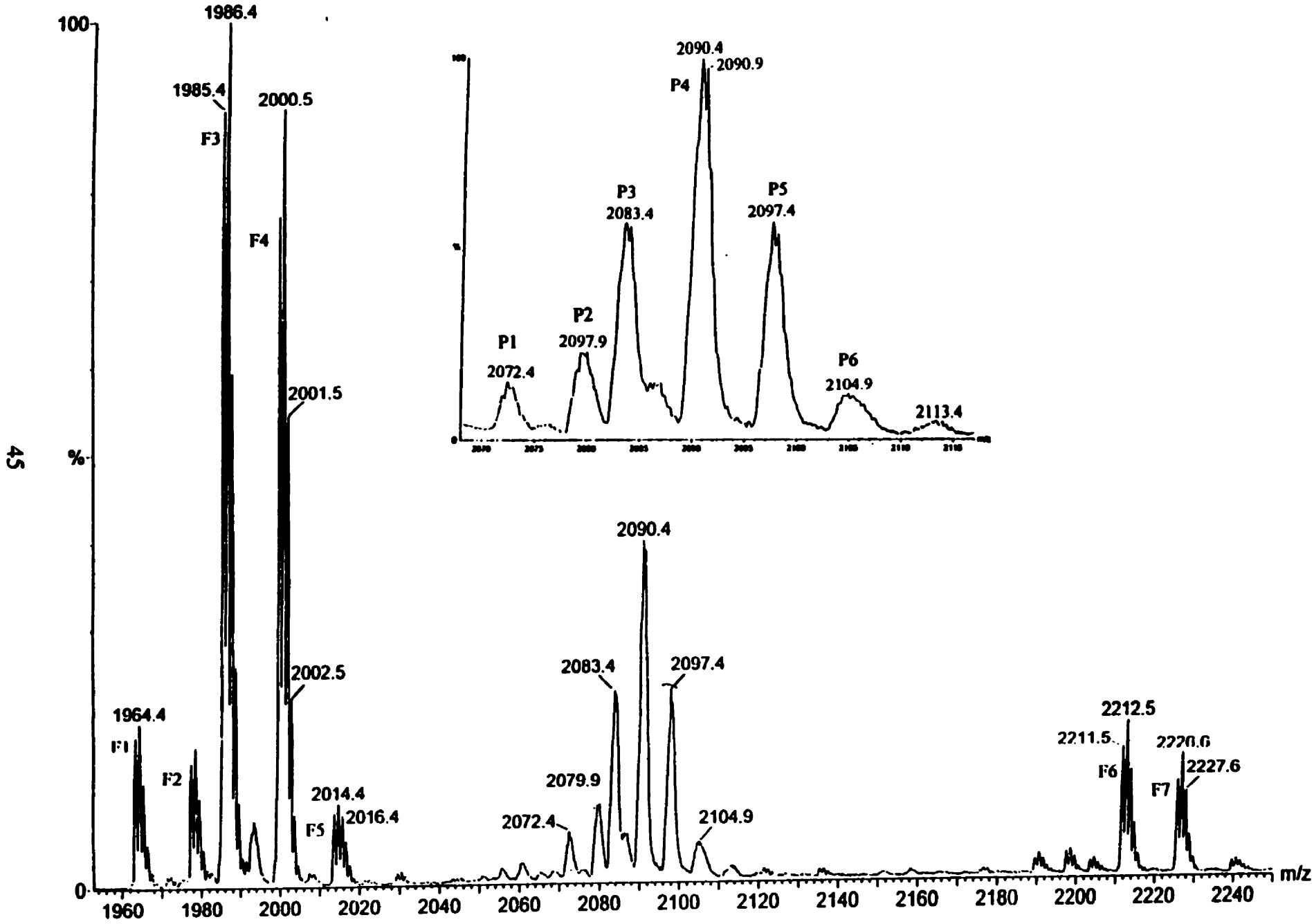

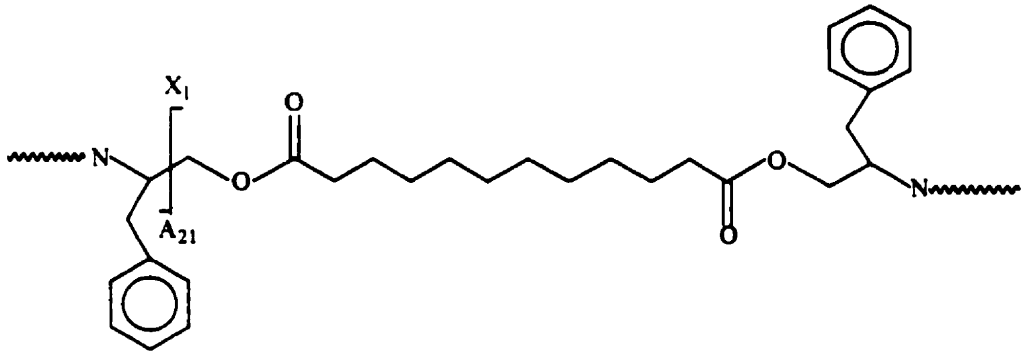

Fig.3-9. Fragment ion patterns of unlabeled alamethicin dimer. A_{21} fragments obtain the original protonating hydrogens, forming intact molecules, and then get another one hydrogen. ~~~~ represents Alm_1 or Alm_2.

Table 3-4 Mass Assignments of the Unlabeled Alamethicin Dimer

Peaks	Assignment	Observed *m/z*	Calculated mass	Theoretical mass
P1	$(D_a + H + Na)^{2+}$	2071.4	$D_a = 4118.8$	$D_a = 4119$
P2	$(D_a + H + K)^{2+}$	2079.7	$D_a = 4119.4$	$D_a = 4119$
P3	$(D_a + 2Na)^{2+}$	2082.8	$D_a = 4129.6$	$D_a = 4119$
P4	$(D_b + 2Na)^{2+}$	2089.8	$D_b = 4133.6$	$D_b = 4133$
P5	$(D_c + 2Na)^{2+}$	2097.3	$D_c = 4148$	$D_c = 4147$
P6	$(D_c + K + Na)^{2+}$	2104.7	$D_c = 4147.4$	$D_c = 4147$
F1	$(A_{21a}H + H)^{+}$	1963.4	$A_{21a}H = 1962.4$	$A_{21a}H = 1962$
F2	$(A_{21b}H + H)^{+}$	1977.2	$A_{21b}H = 1976.2$	A_{21b} H= 1976
F3	$(A_{21a} + Na)^{+}$	1985.4	$A_{21a} = 1962.4$	$A_{21a}H = 1962$
F4	$(A_{21b} + Na)^{+}$	1999.3	$A_{21b} = 1976.3$	A_{21b} H= 1976
F5	$(A_{21b}H + K)^{+}$	2014.4	$A_{21b}H = 1975.4$	A_{21b} H= 1976
F6	$(X_{1a} + Na)^{+}$	2211.5	$X_{1a} = 2187.5$	$X_{1a} = 2188$
F7	$(X_{1b} + Na)^{+}$	2225.6	$X_{1b} = 2202.6$	$X_{1b} = 2202$

3.3. NMR Spectroscopy of ^{15}N Alamethicin Dimer

The ^{1}H and ^{15}N resonances of alamethicin dimer were assigned using 1D-^{1}H, DQF-COSY, TOCSY, ^{1}H-^{15}N HSQC, and ROESY spectra following the procedures described by Wüthrich [2] and making use of the previous assignments of alamethicin monomer [3]. Briefly, the Wüthrich method involves identification of ^{1}H spin systems of amino acids with the use of correlation experiments and sequence-specific assignment of spin systems using Nuclear Overhauser Effect Spectroscopy (NOESY). For convenience, a complete listing of the assigned ^{1}H and ^{15}N resonances is given in Table 3-5.

3.3.1. 1D NMR Spectrum of ^{15}N Alamethicin Dimer

A 1D ^{15}N decoupled ^{1}H NMR spectrum of ^{15}N labeled alamethicin dimer is shown in Fig. 3-10a. An expanded view of the amide plus aromatic regions of the spectrum is shown in Fig. 3-10b. The same regions of the alamethicin monomer spectrum are shown in Fig. 3-10c. ^{1}H NMR lines of the amide protons of the backbone and side-chains as well as phenyalaninol ring protons appear between 6.5 and 8.7 ppm. The signal-to-noise ratio in the dimer spectrum is lower than that in the monomer spectrum due to a lower concentration in the former. The linewidths in the dimer spectrum are broader (for example, $\Delta\nu_{1/2}$ = 5.44 Hz for Aib_{10}) than in the monomer spectrum ($\Delta\nu_{1/2}$ = 2.78 Hz for Aib_{10}) likely because of the increased mass and slower rotational correlation of the dimer. In the dimer spectrum, the Gly_{11} amide proton is the only resonance that shows up as a triplet (8.4 ppm) because it is coupled to two α-protons. All the Aib amide protons appear as singlets because of the lack of an α proton. The peaks for the amide protons of Aib_5 and Aib_6 are overlapped in both monomer and dimer spectra. As expected, other amide protons such as those of Ala_4, Val_9 and Leu_{12} show up as doublets in

spectra of monomer and dimer and these can be used to measure $^3J_{N\alpha}$. A major difference between the ^1H spectra of monomer and dimer is that all amide resonances for residues between Val_{15} and Pho_{20} are reduced in intensity in the dimer compared to the monomer spectrum. Also, additional resonances appear in the dimer spectrum which are not observed in the monomer spectrum. Peaks in the set denoted as *a* have the chemical shift of amide protons close to those in the monomer spectrum, whereas another set of peaks appears nearby (denoted as *b*). The intensities of the *b* peaks are stronger than the *a* peaks. Careful inspection of the Leu_{12} amide resonance suggests that it may consist of two peaks very close in chemical shift. In the monomer spectrum, the aromatic protons belonging to the Pho_{20} ring resonate between 7.0 and 7.3 ppm as three sets of triplets. In the spectrum of the dimer, the pattern is more complicated.

Fig 3-10. High-resolution one-dimensional ^1H NMR spectrum of ^{15}N dimer and monomer with water suppression using presatuation (2s, 50dB) and ^{15}N decoupling during acquisition using GARP [4]. The dimer spectrum was recorded with 32 k points, 2 k number of scans (NS), 64 dummy scans (DS), 14.9 μs 90° ^1H pulse width, 5400Hz sweep width (SW), and acquisition time 6.03 sec. Total acquisition time was about 5h. The data were processed using a Lorentz-Gaussian multiplication (GM) window function with LB = -4 and GB = 0.02. (a) The full spectrum of dimer. (b) Expanded low-field region of the dimer. The two sets of cross-peaks are indicated as *a* and *b* (*a* peaks have chemical shifts close to alamethicin monomer). (c) Expanded low-field region of the monomer spectrum with the same acquisition parameters as those of dimer except NS = 1 k. Assigned resonances of backbone NHs are labeled with one letter code with numbers indicating residue position in the peptide sequence. Side-chain resonances are indicated in the spectra.

Fig. 3-10a The 1D spectrum of ^{15}N alamethicin dimer

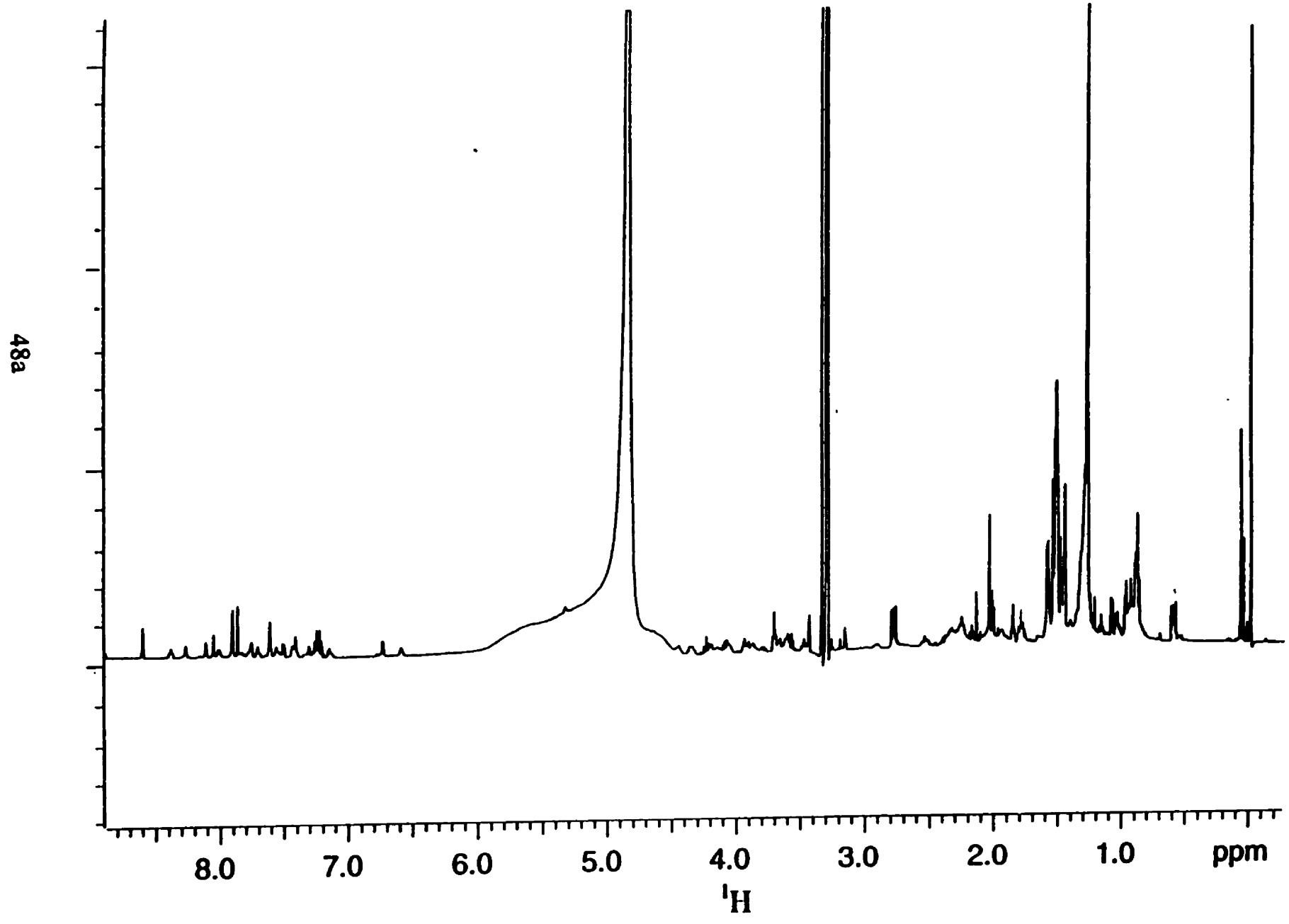

Fig.3-10b The amide region of 1D spectrum of ^{15}N alamethicin dimer

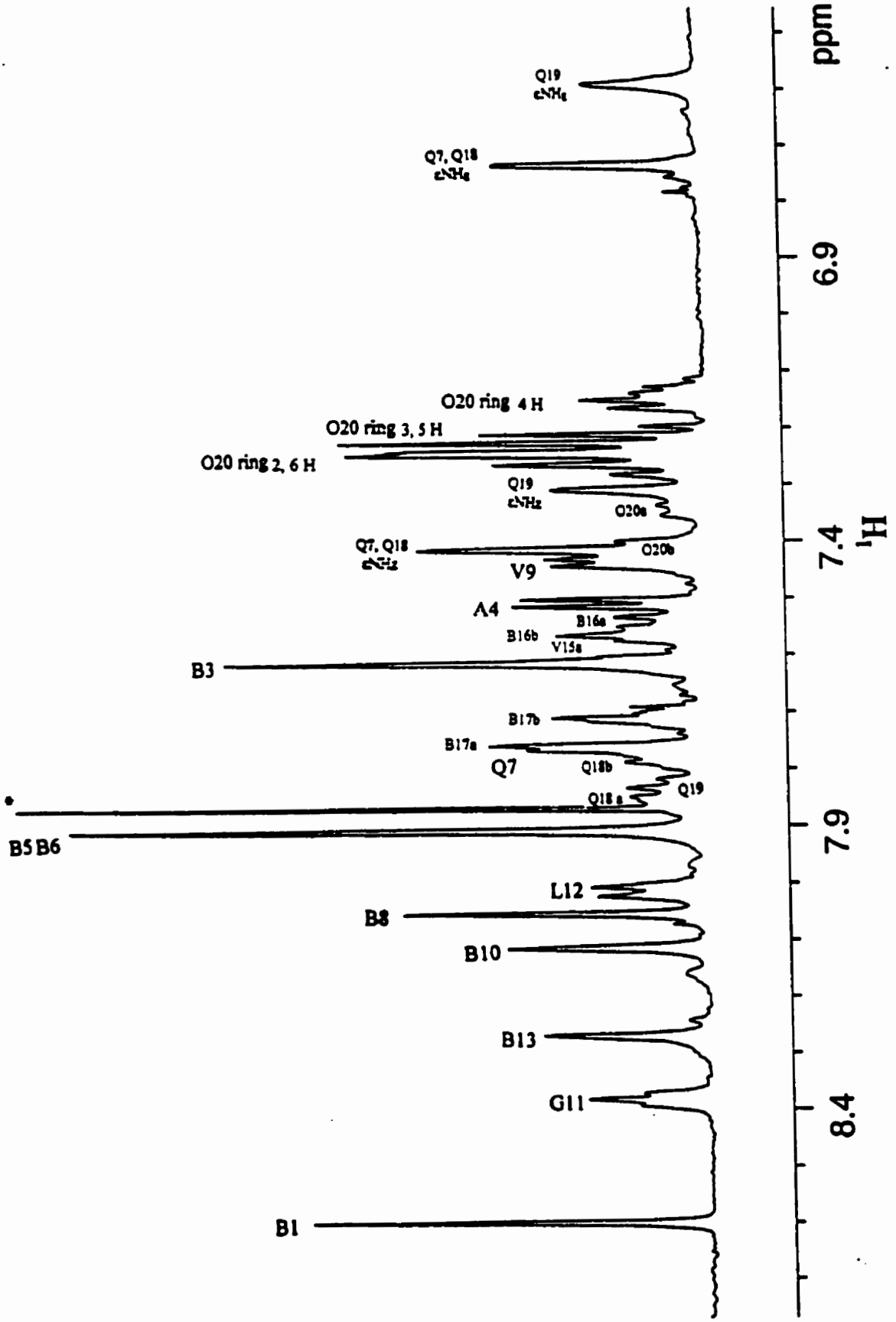

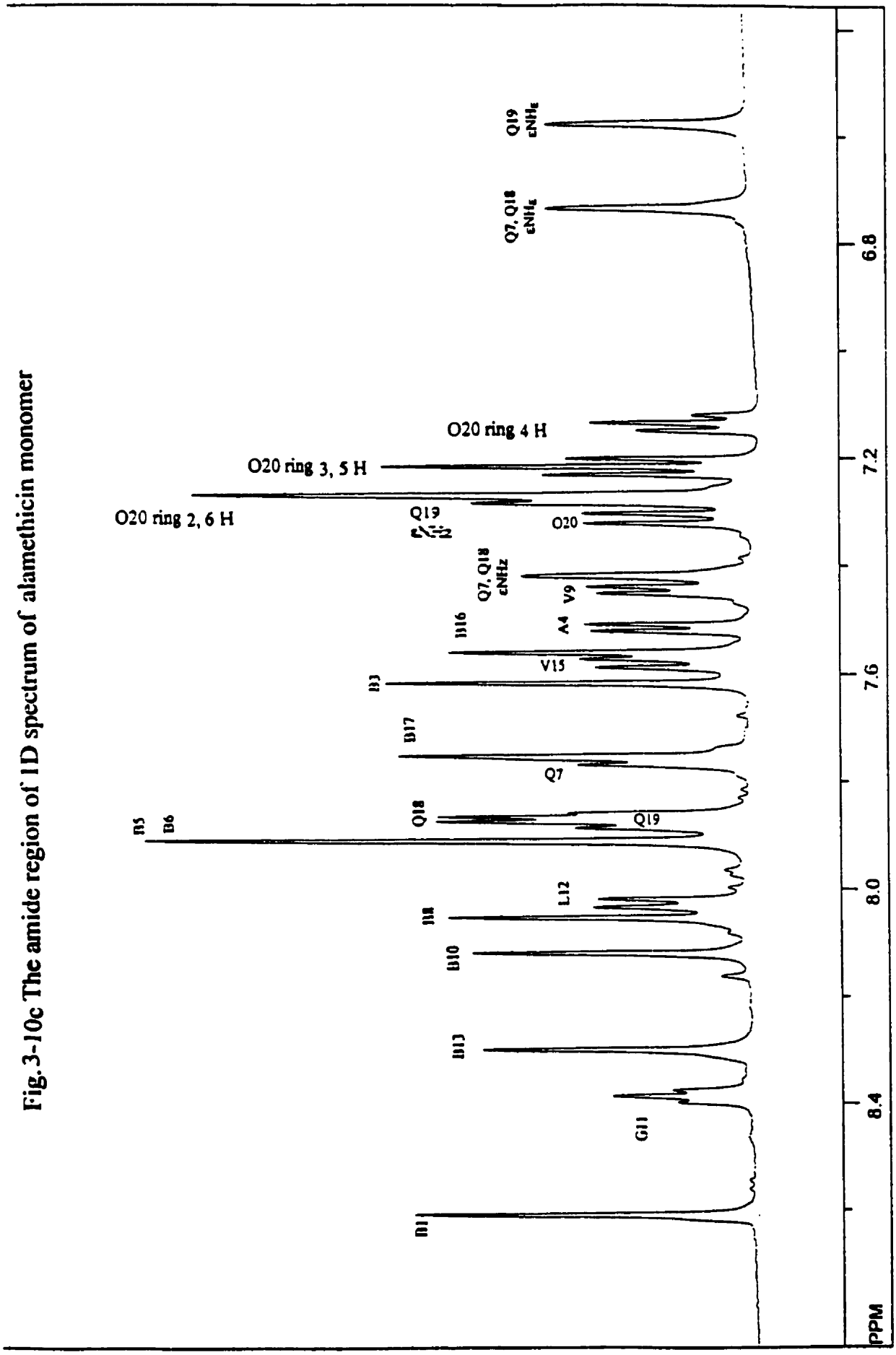

Fig. 3-10c The amide region of 1D spectrum of alamethicin monomer

Table 3-5 Assignments of ^{1}H and ^{15}N Resonances of ^{15}N Alamethicin Dimer (in ppm)

Residue		NH	αH	βH (β'', β')	γH (γ'', γ')	15N	Other
N-Acetyl							CH_3 2.05
Aib1		8.60		1.53, 1.45		139.8	
Pro2			4.24	2.37, 1.79	2.09, 1.97		δH 3.96, 3.49
Aib3		7.62		1.50		127.0	
Ala4		7.53	4.10	1.49		119.8	
Aib5		7.93		1.52, 1.48		131.2	
Aib6		7.93		1.50		126.4	
Gln7		7.78	3.90	2.24, 2.17	2.55, 2.38	118.0	εNH 7.43, 6.67. $\varepsilon^{15}N$ 109.3
Aib8		8.07		1.59, 1.50		131.2	
Val9		7.46	3.61	2.29	1.09, 0.98	116.0	
Aib10		8.12		1.54		132.8	
Gly11		8.40	3.94, 3.66			102.8	
Leu12		8.03	4.47	1.92, 1.59	1.92	120.9	δH 0.91
Aib13		8.29		1.60, 1.54		135.8	
Pro14			4.38	2.33, 1.81	2.07, 1.98		δH 3.87, 3.67
Val15	a	7.56	3.73	2.33	1.05, 0.96	117.2	
	b	7.62	3.80	2.34	1.07, 0.97	116.7	
Aib16	a	7.55		1.52		132.1	
	b	7.59		1.52		132.5	
Aib17	a	7.77		1.53		127.6	
	b	7.73		1.53		127.2	
Gln18	a	7.87	4.08	2.26	2.60, 2.37	116.6	εNH 7.43, 6.67. $\varepsilon^{15}N$ 109.3
	b	7.80	4.07	2.26	2.60, 2.37	114.8	εNH 7.43, 6.67. $\varepsilon^{15}N$ 109.3
Gln19	a	7.86	4.20	2.02	2.34, 2.22	118.3	εNH 7.32, 6.61. $\varepsilon^{15}N$ 109.1
	b	7.84	4.20	2.02	2.34, 2.22	117.5	εNH 7.32, 6.61. $\varepsilon^{15}N$ 109.1
Pho20	a	7.36	4.15	2.91, 2.76		122.0	β_2H_a 3.61; $C^{2,6}H$ 7.26; $C^{3,5}H$ 7.22; $C^{4}H$ 7.16
	b	7.42	4.35	2.92, 2.80		121.5	β_2H_b 4.17, 4.08
Linker		CH_2 2.29, 2.19, 1.58, 1.31, 0.89					

3.3.3. HSQC Spectrum of ^{15}N Alamethicin Dimer

Fig. 3-11 shows a contour plot of the ^{15}N-^{1}H heteronuclear single-quantum coherence spectrum [5] of ^{15}N dimer. Each cross peak represents a one-bond ^{15}N-^{1}H correlation. Twenty-two cross peaks (18 backbone, 4 side-chains of three glutamines) with ^{1}H and ^{15}N chemical shifts nearly identical to those observed in the monomer [3] were observed in the dimer spectrum. All residues between Aib_1 and Aib_{13} give rise to a single strong correlation. Consistent with the 1D-^{1}H spectrum, 6 new cross peaks with varying intensity were observed and were assigned to residues between Val_{15} and Pho_{20}. Thus, a total 28 cross peaks were observed in the spectrum.

Fig. 3-11. High resolution ^{1}H-^{15}N HSQC [5] spectrum of ^{15}N alamethicin dimer with presatuation at 300 K. The spectrum was recorded with ^{1}H decoupling during evolution by application of a ^{1}H 180° pulse at the midpoint of t_1 and with ^{15}N decoupling during the acquisition time (GARP). SW_2 = 2358.49Hz, TD2 = 4 k, SW_1 = 32,260Hz, TD_1 = 256, NS = 112, DS = 32, 90°(^{1}H) = 14.5 μs, 90°(^{15}N) = 26 μs, total acquisition time is about 15.5 hours. Data were zero-filled to 512 points in F_1 and a GM window function was applied in both dimensions ($LB_1 = LB_2 = -10$, $GB_1 = 0.2$ and $GB_2 = 0.03$).

Fig. 3-11 ^{1}H-^{15}N HSQC spectrum of ^{15}N alamethicin dimer at 300K

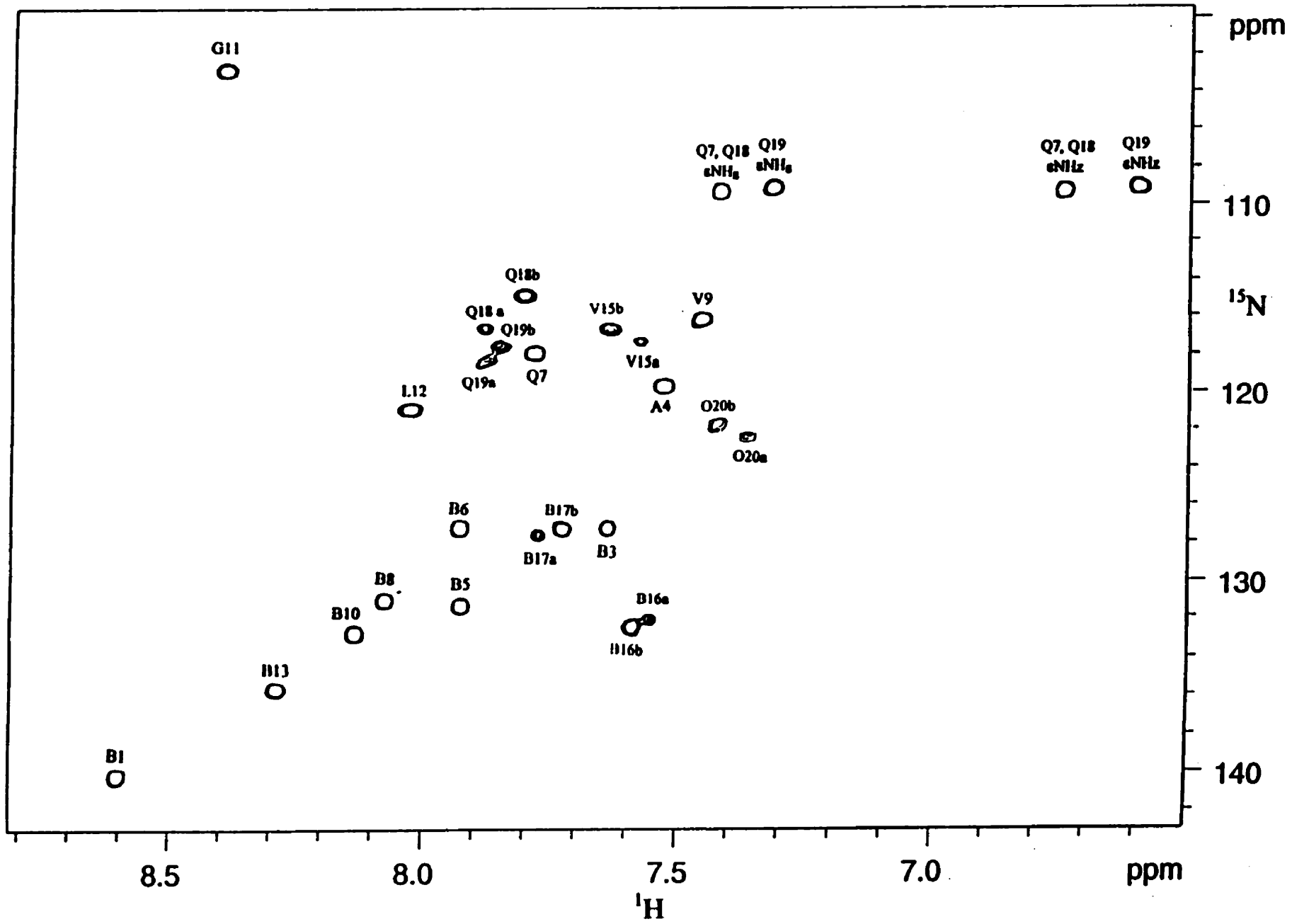

3.3.4. TOCSY Spectrum of ^{15}N Alamethicin Dimer

A ^{1}H homonuclear TOCSY spectrum [6-7] of ^{15}N alamethicin dimer is shown in Fig. 3-12. The diagonal and cross peaks in TOCSY are in the same positive phase. Each amino acid is treated as an isolated ^{1}H spin system, which is identified in the fingerprint and aliphatic regions. For sufficiently long mixing times, coherence transfer in the TOCSY experiment extends throughout the entire spin network [6]. For instance, the NH of Val_9 (resonates at 7.46 ppm) is coupled with the αH (3.61 ppm) and βH (2.29 ppm) as well as two methyl groups γ'' (1.09 ppm) and γ' (0.98 ppm) in the fingerprint region (Fig. 3-12b). The αH of Val_9 is then coupled with the βH and two γ CH_3 and the two γ CH_3 are in turn coupled with the βH in the aliphatic region. The Val_{15} spin system was similarly identified, although sequential assignment required the acquisition of a ROESY experiment. Because of the significant difference in amide ^{1}H chemical shift between Val_{15a} (7.56 ppm) and Val_{15b} (7.62 ppm), complete spin system identification was achieved through amide ^{1}H connectivities. It was noted that there is a significant difference in chemical shift between the αH resonances of Val_{15a} and Val_{15b}. However, the βHs, γ'Hs, and γ''Hs for Val_{15a} and Val_{15b} resonate a virtually identical chemical shifts. A similar situation was observed for resonances of residues 18 and 19 except that the αH resonances for the *a* and *b* spin systems are not resolved. The differences in the amide ^{1}H chemical shifts between Gln_{19a} and Gln_{19b} are so small that a single spin system is observed. The chemical shift difference between the NH resonances of Pho_{20a} and Pho_{20b} is significant as is the difference between the αH resonances. There is a very large difference in the chemical shift between the β_2H_a (3.61 ppm) and β_2H_b (4.17 ppm and 4.08 ppm) resonances and much smaller differences at the other β positions.

The Gly, Leu and Ala spin systems could be sequentially assigned using

TOCSY because of their unique cross peak patterns and also because alamethicin contains only one of each of the residues. There are of course no cross peaks for the nine Aib and two proline residues in the fingerprint region of a TOCSY spectrum and the Pro spin systems were identified in the aliphatic region.

Fig 3-12. Phase sensitive ^{1}H TOCSY (homonuclear Hartman-Hahn transfer) [6-7] spectrum of ^{15}N alamethicin dimer with presatuation (1s, 55dB) and ^{15}N decoupling during acquisition along t_2 using composite pulse decoupling (GARP). Spin lock (SL) trim pulses at the beginning and end of the mixing period were employed to capture the I_y components and dephase I_x [6]. The values of rf field strength for the SL ranged from 6-10 kHz. The spectrum was recorded using the MLEV17 sequence [7] for mixing and two power levels for excitation (4dB) and spinlock (11dB). $SW_2 = SW_1 = 5434.8$Hz, $TD_2 = 1$ k, $TD_1 = 512$, $Hz/pt_2 = Hz/pt_1 = 10.6$, NS = 96, DS = 32, preparation $90°(^{1}H) = 15.0$ μs, MLEV17 $90°(^{1}H) = 31.2$ μs, trim pulse = 2.5 ms, mixing time = 61.5 ms, receiver gain = 256, total acquisition time = 16.6 hours. The data were zero-filled to 1k in both dimensions. A squared sine-bell (Qsine) window function with a $\pi/2$ shift was applied in both dimensions. (a). Full spectrum. The lines indicate the Val_9 spin system. (b). Fingerprint region. β″ and β′ are defined as the protons attached to the β carbons whose resonances have the higher and lower chemical shift, respectively. The same definitions were applied to γ″ and γ′, and δ″ and δ′ protons.

Fig. 3-12*a* TOCSY spectrum of ^{15}N alamethicin dimer

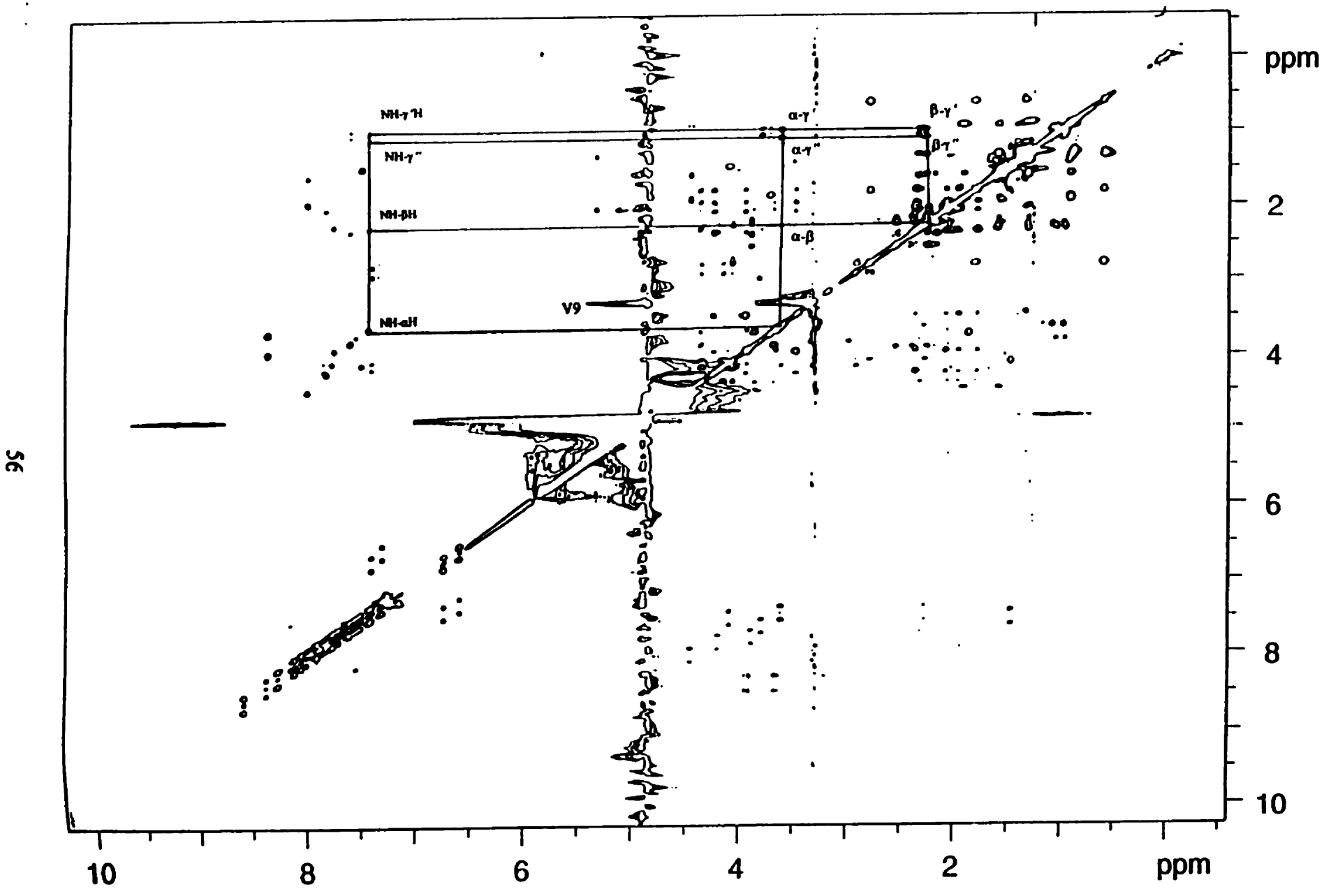

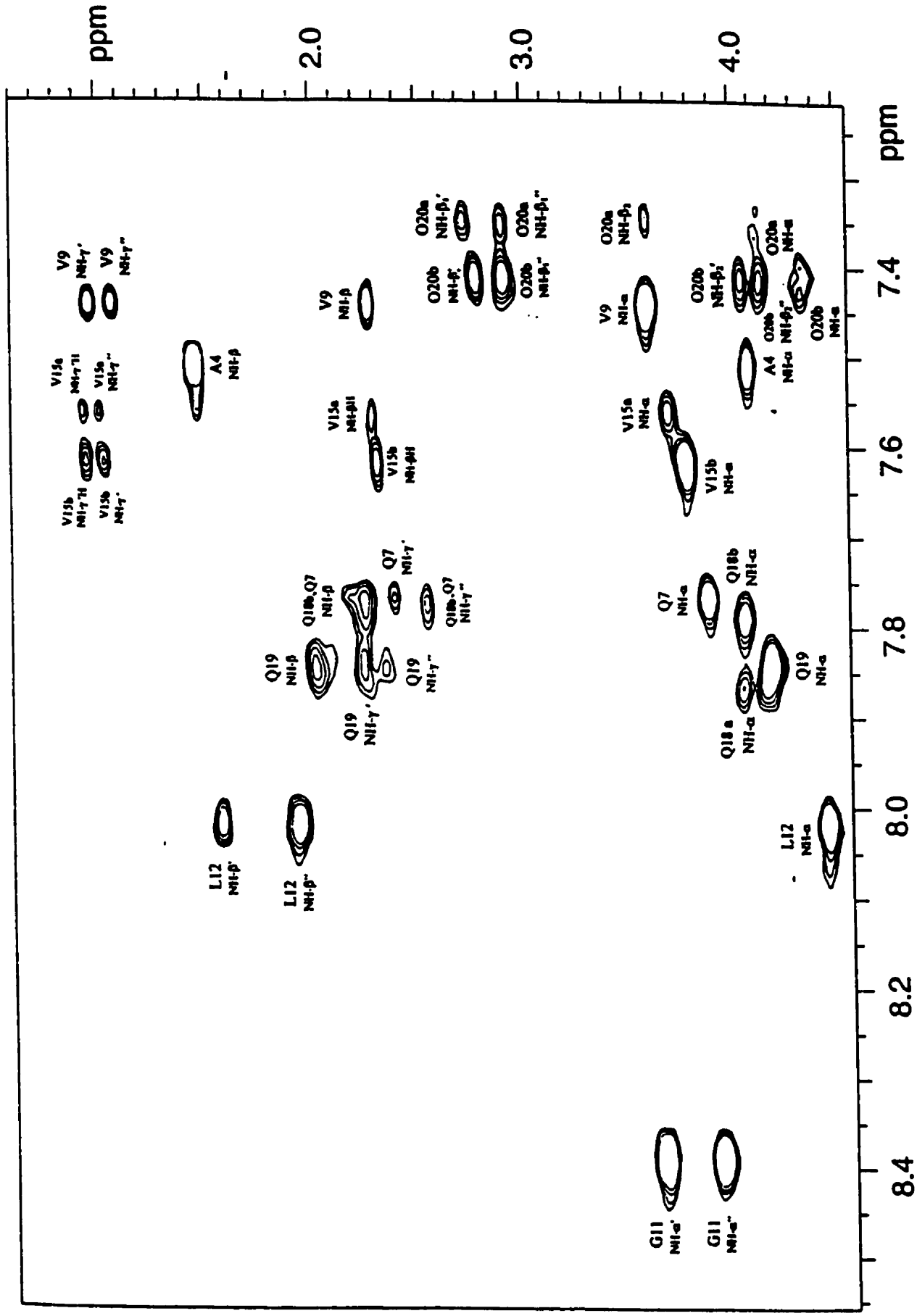

Fig. 3-12b The fingerprint region of a TOCSY spectrum of ^{15}N alamethicin dimer

3.3.5. DQF-COSY Spectrum of ^{15}N Alamethicin Dimer

The phase-sensitive DQF-COSY spectrum [8] of alamethcin dimer is shown in Fig.3-13a-b. A DQF-COSY spectrum of alamethicin monomer is shown in Fig. 3-13c for comparison. In this DQF-COSY experiment, diagonal peaks and cross peaks are in antiphase absorption mode. The antiphase fine structure in the cross peaks reflects the active and passive couplings of the spin systems. Spin systems of the non-Aib amino acids were identified in the DQF-COSY spectrum and confirmed the spin systems identified in the TOCSY spectrum (Fig. 3-12). In contrast to TOCSY, DQF-COSY shows only the cross peaks for coupled nuclei within three bonds or less. Similar to the TOCSY result, two sets of signals for the residues at the C-terminus were observed in the fingerprint region (Fig. 3-13b). Compared to the other cross peaks, an obvious loss in intensity for Gln_{18}, Gln_{19} and Pho_{20} was observed. This could be due to cancellation of cross peak components of opposite phase, especially where the $^3J_{\alpha N}$ is small, and/or due to dynamic flexibility in this part of the molecule.

The main purpose of the high digital resolution DQF-COSY in this report was to measure the spin-spin coupling constants $^3J_{N\alpha}$ for resonances which are overlapped in the 1D ^1H spectrum (Fig. 3-10). The cross-peaks along ω_2 consist of two components with the signs as +, -, +. Based on the rule 'the splitting $^3J_{N\alpha}$ is always in antiphase only once along ω_2 for one spin system' [2], the spin-spin coupling constants $^3J_{N\alpha}$ for all residues in the fingerprint region could be measured by proper selection of the cross section along the ω_2 direction. In the case of Gln_{19}, this was difficult because of the overlap of two cross peaks. An example of the cross section for Qln_7 is given inside of Fig. 3-13b, indicating how the measurement was made. The spin-spin coupling constants $^3J_{N\alpha}$ measured from the DQF-COSY and 1D spectra are summarized in Table 3-6 where they are also

compared with those values for the monomer and a random coil model. The table also indicates the range of ϕ values deduced from the $^3J_{N\alpha}$ measurements for dimer [9].

Fig.3-13. Phase Sensitive DQF-COSY spectrum of ^{15}N alamethicin dimer and monomer with presatuation (1s, 55dB) and with ^{15}N decoupling during t_1 using a 180° pulse and during acquisition using GARP. $SW_2 = SW_1 = 5434.8Hz$, $TD_2 = 4$ k, $TD_1 = 1$ k, $Hz/pt_2 = 2.65$, $Hz/pt_1 = 10.61$, NS = 96, DS = 16, 90° (^1H) = 15.7 μs. 180° (^{15}N) = 52 μs. Total acquisition time was 53 h. The digital resolution after zero-filling to 16 k in F_2 and to 2 k in F_1 is 0.33 Hz/pt_2 and 2.65 Hz/pt_1, respectively. A squared sine-bell (Qsine) window function with a phase shift of $\pi/30$ was applied in both dimensions. Positive contours are plotted with solid lines, negative contours with broken lines. (a) Expanded aliphatic region of alamethicin dimer. (b) Expanded fingerprint region of alamethicin dimer. A cross section along ω_2 at the ω_1 position of the αH of Gln_7 is shown. (c). Expanded fingerprint region of alamethicin monomer with $TD_2 = 2$ k, $TD_1 = 512$, NS = 128 and 90° (^1H) = 14.8 μs.

Fig. 3-13a The aliphatic region of the DQF-COSY spectrum of ^{15}N alamethicin dimer

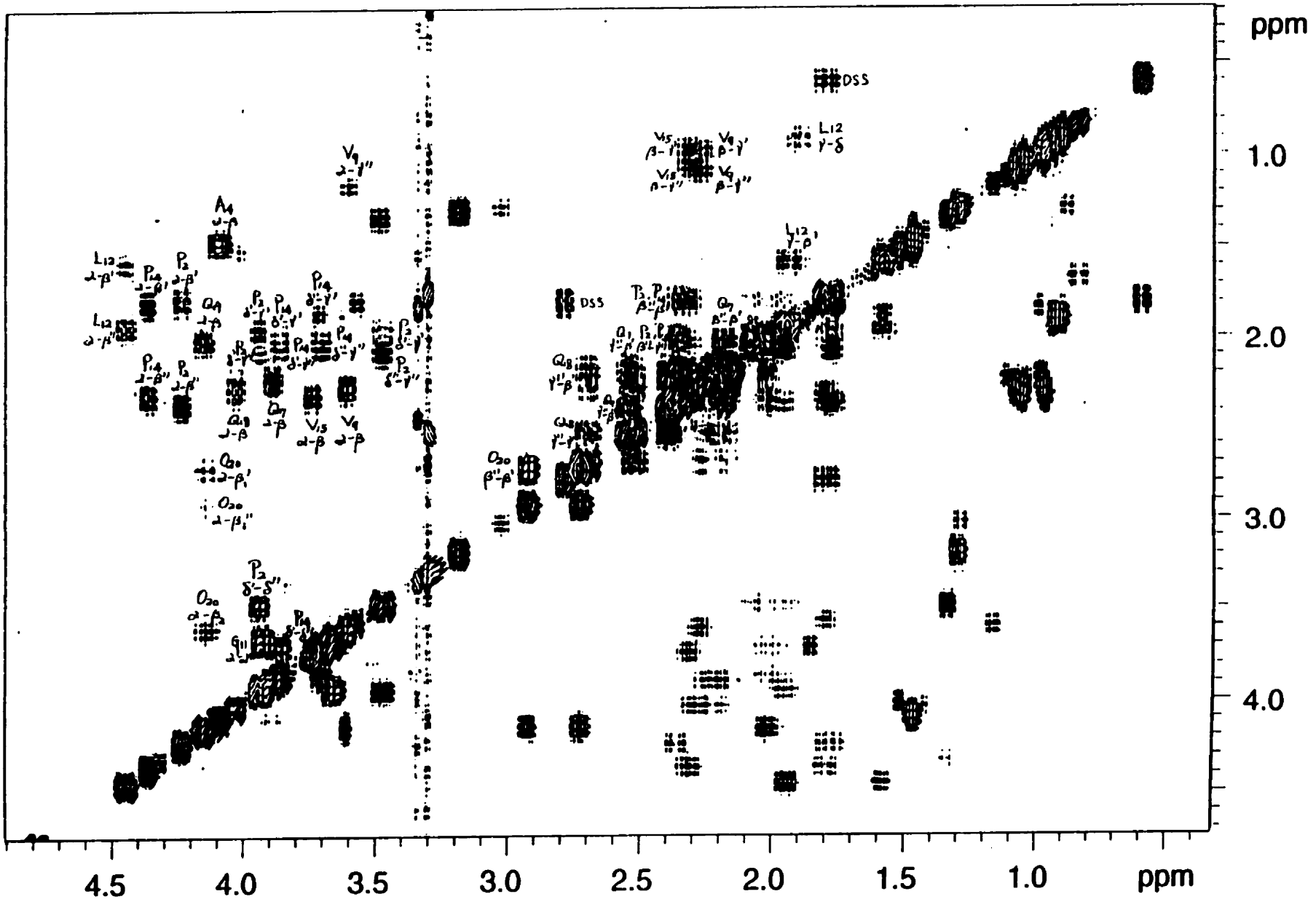

Fig. 3-13b The fingerprint region of the DQF-COSY spectrum of ^{15}N alamethicin dimer

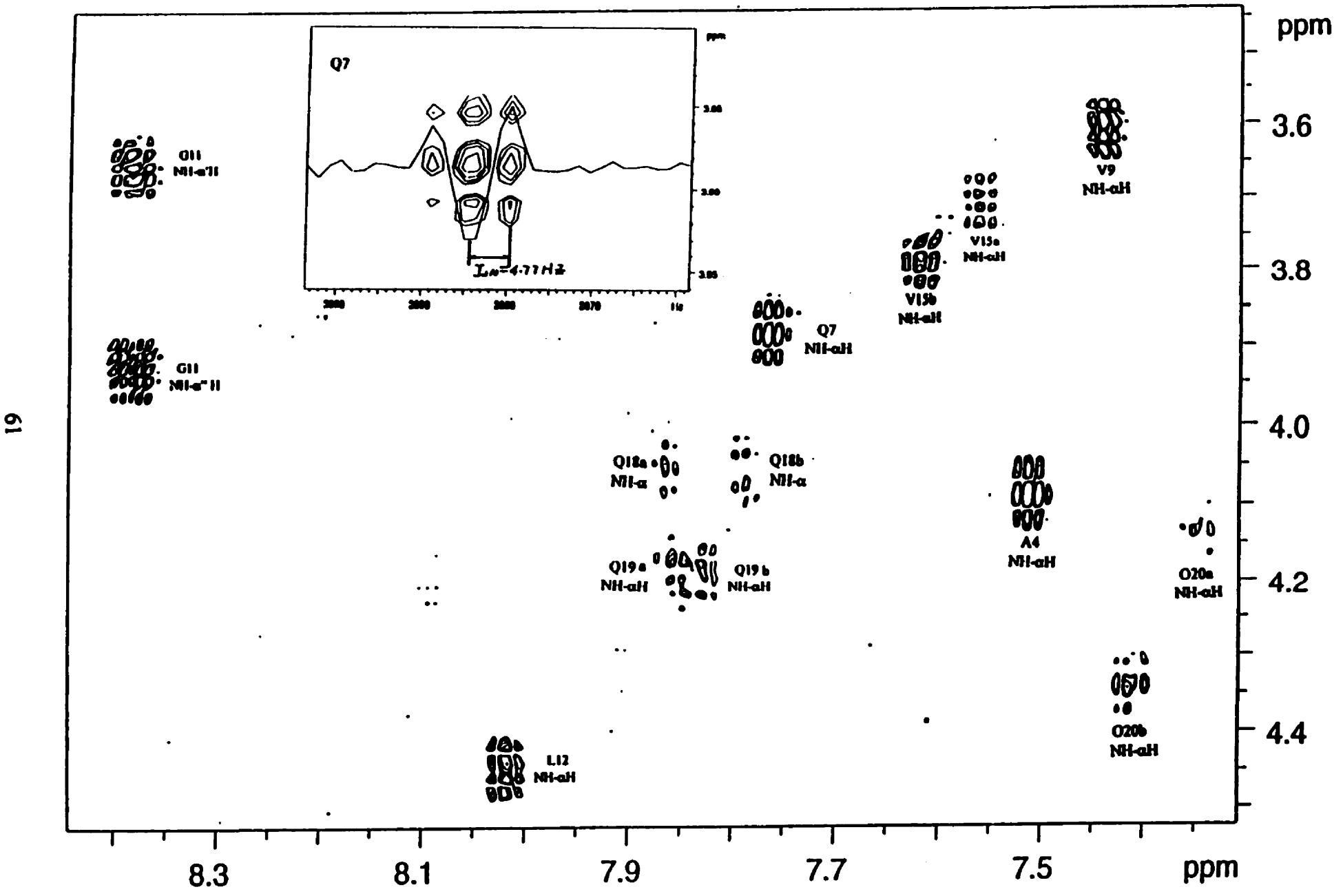

Fig. 3-13c The fingerprint region of the DQF-COSY spectrum of alamethicin monomer

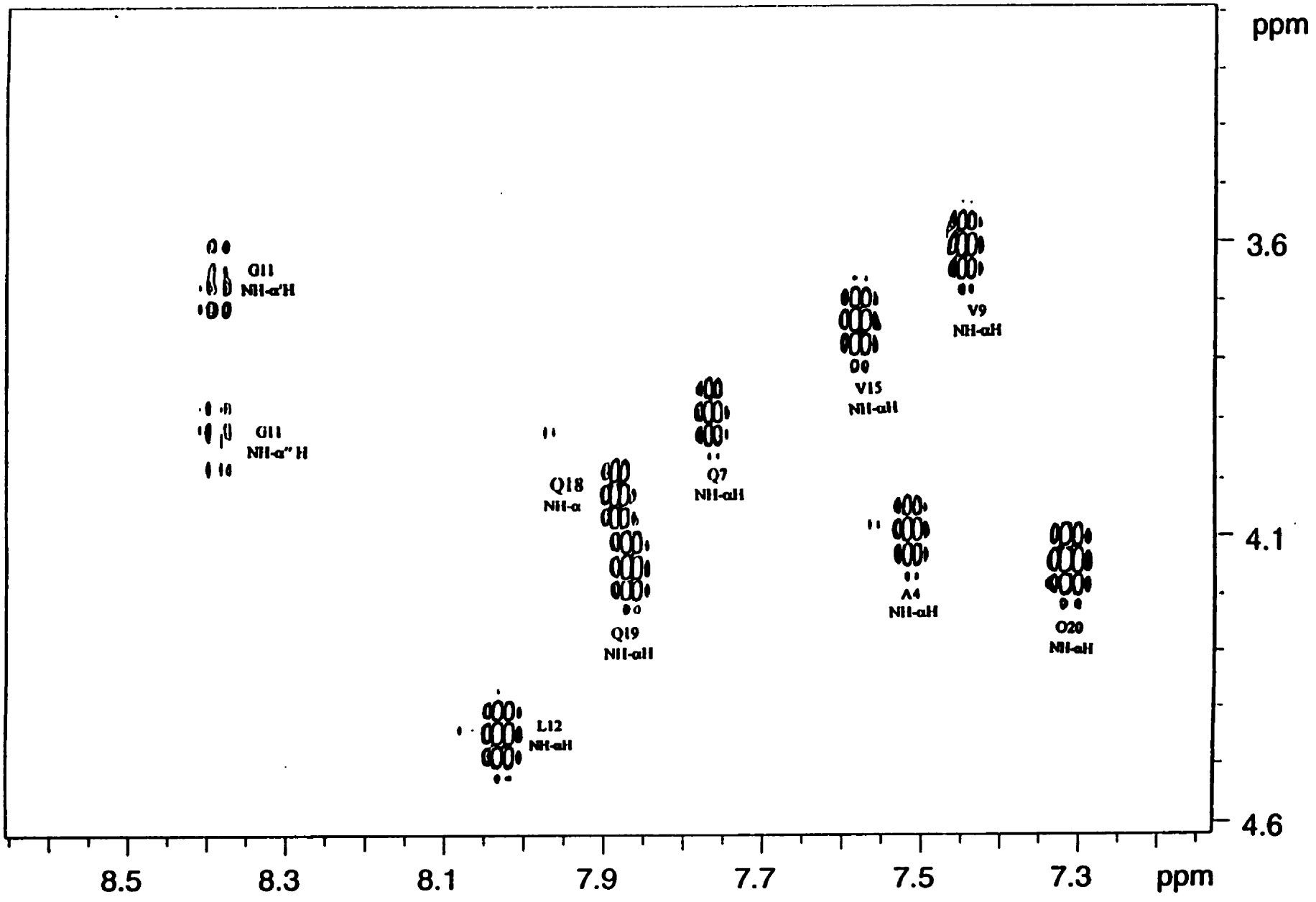

Table 3-6 Coupling Constants, $^3J_{\alpha N,}$ in ^{15}N Alamethicin Dimer in Comparison with the Values for Monomer and a Random Coil Model[a] (in Hz)

Residue	$^3J_{\alpha NH}$ of dimer		$^3J_{\alpha NH}$ of random coil	$^3J_{\alpha NH}$ of monomer	ϕ Range for dimer
	1D	DQF-COSY			
Ala4	6.10	6.16	6.1	6.14	-60° < ϕ < -90°
Qln7	4.88	4.77	7.1	5.31	-50° < ϕ < -80°
Val9	5.88	5.91	7.7	6.05	-60° < ϕ < -90°
Gly11[b]	5.27/5.68	5.31/6.02	5.9	5.56/5.43	-60° < ϕ < -90°
Leu12	7.86	7.62	7.6	7.87	-70° < ϕ < -100°
Val15a	7.41[c]	7.35	7.7	7.62	-70° < ϕ < -100°
Val15b	6.31[c]	6.46			-60° < ϕ < -90°
Qln18a	5.46[c]	5.89	7.1	5.78	-60° < ϕ < -90°
Qln18b	5.94	5.20			-60° < ϕ < -90°
Qln19a	7.36[c]	4.50	7.1	7.84	-70° < ϕ < -100°
Qln19b	7.68[c]	6.58			-80° < ϕ < -100°
Pho20a	8.80	7.97	7.5	9.19	-90° < ϕ < -120°
Pho20b	7.70[c]	7.62			-80° < ϕ < -100°

[a]The random coil values were taken from predictions based on chemical shifts of coil regions of known structures in the protein database (Smith, L. J *et al.*1996 [10]).
[b]Two $^3J_{\alpha NH}$ of Gly_{11} are caused by the proton attached to the β carbon whose resonance has the higher and lower chemical shift, respectively.
[c]Values are only approximate due to overlapping peaks.

3.3.6 ROESY Spectrum of ^{15}N Dimer

The spin systems identified in J-correlation experiments such as TOCSY and DQF-COSY can be connected sequentially and assigned via through-space NOE effects observed in ROESY [11]. The most useful region for dimer sequential assignment is the section with NH chemical shifts in F_2 (7.0-9.0 ppm) and the entire chemical shift range in F_1 (Fig.3-14 b & c).

By comparison with the TOCSY and DQF-COSY spectra, NOEs corresponding to intraresidue NH-αH and NH-βH cross-peaks could be identified and labeled in the ROESY spectrum. Since there are no cross-peaks for Aib residues in TOCSY, identification of their NOEs relied on the amide ^1H chemical shifts identified in HSQC (Fig. 3-11) and 1D-^1H (Fig. 3-10b) spectra. The weak NH-αH and NH-βH cross-peaks for Gln_{18} and Gln_{19} were noted in the TOCSY spectrum (Fig. 3-12) and in the DQF-COSY spectrum (Fig. 3-13b) and are weak in the ROESY spectrum (3-14b). After identification of intraresidue NOEs, the unlabelled NOEs which remain in the NH-NH and NH-αH (βH) regions correspond to interresidue NOEs. These are the cross peaks used to sequentially assign the spin systems.

The NH-NH region of the ROESY map (Fig. 3-14c) revealed several segments of NH_i-NH_{i+1} correlations. We used these amide connectivities for sequential assignments first, beginning at Aib_3 and following to Pho_{20}, producing four segments: Aib_3-Aib_5, Aib_6-Aib_{13}, Val_{15}-Aib_{18} and Gln_{19}-Pho_{20}. For instance, the NH of Aib_3 is dipolar coupled with the NH of Ala_4 at ω_1 = 7.53 ppm, ω_2 = 7.62 ppm. A horizontal line from this cross peak intersects the Ala_4-Aib_5 cross-peak at ω_1 = 7.53 ppm, ω_2 = 7.93 ppm. The Aib_5-Aib_6 cross peak is not observed because the NH chemical shifts of the two residues are identical. Breaks occur in the sequential contacts at the two proline residues due to the absence of amide protons. A break also occurs at Gln_{18b} -Gln_{19b} because the pairs' very similar amide proton chemical shifts. The δH protons were used for sequence-specific identification of the two proline residues. Strong and medium sequential (NH_i, δH_{i+1}) NOE contacts such as (B_{1NH}-$P_{2\delta H}$) at ω_2 = 8.60 ppm, ω_1 = 3.96 ppm, and ω_2 = 8.60 ppm, ω_1 = 3.49 ppm, along with (B_{13NH}-$P_{14\delta H}$) at ω_2 = 8.29 ppm, ω_1= 3.87 ppm, and ω_2 = 8.29 ppm, ω_1= 3.67 ppm, were observed. Furthermore, the presence of (αH_i, NH

$_{i+1}$) and (βH_i, NH_{i+1}) connectivities such as ($P_{2\alpha H}$-B_{3NH}) at ω_1=4.24 ppm, ω_2 = 7.62 ppm and ($P_{2\beta' H}$-B_{3NH}) at ω_1= 1.97 ppm, ω_2 = 7.62 ppm provided supplementary direct evidence for sequential assignments of the prolines. All possible (αH_i, NH_{i+1}) connectivities except ($P_{14\alpha H}$, V_{15NH}) and ($Q_{19\alpha H}$, O_{20NH}) were also observed. Several $d_{\beta NH(i, i+1)}$ distances show strong NOE cross-peaks, however, some of them cannot be unambiguously identified because they are overlapped with cross peaks arising from intraresidue (βH_i, NH_i) NOEs. The expected ($L_{12\beta H}$, B_{13NH}), ($Q_{18\beta H}$, Q_{19NH}) and ($Q_{19\beta H}$, O_{20NH}) connectivities are not observed in the spectrum.

Thus, a large proportion of the cross-peaks in the ROESY spectrum are attributed mostly to short intraresidue and sequential ^1H-^1H distances, with a small number of NOE cross-peaks which mostly correspond to medium-range distances. These medium-range NOE cross-peaks as well as the sequential NOE cross-peaks play an important role in the identification of specific types of secondary structure [2]. All of the medium range NOE cross-peaks in the spectrum arise from the αH, NH(i, i+3) and αH, βH(i, i+3) NOEs, indicative of helical structure. Four medium or weak cross-peaks for αH, NH(i, i+3) were observed in the segment from Pro_2 to Leu_{12} such as ($P_{2\alpha H}$, B_{5NH}) at ω_1 = 4.24 ppm, ω_2 = 7.93 ppm and ($A_{4\alpha H}$, Q_{7NH}) at ω_1= 4.10 ppm, ω_2 = 7.78 ppm. No (αH_i, NH_{i+3}) NOE effects were detected from Leu_{12} to Pho20. The P_2-B_{10} segment also contains three strong and/or medium αH, βH(i, i+3) NOEs such as ($P_{2\alpha H}$, $B_{5\beta H}$) and ($Q_{7\alpha H}$, $B_{10\beta H}$) NOEs. A putative αH, βH (i, i+3) cross peak between residues 14 and 17 at ω_2 = 4.38 ppm, ω_1 = 1.53 ppm was observed in the C-terminus, but it cannot be ruled out that this arises from αH, βH (i, i+2).

A precise identification of all the NOE cross-peaks obtained from different regions of the ROESY spectrum and their integrations are presented in Tables 3-7 ~ 11, including intraresidue, sequential and medium range connectivities. Further

information in these Tables includes the corresponding NOEs for alamethicin monomer [3] presented for comparison, and classification of the NOEs as strong (s), medium (m), or weak (w) based on the intensity of the integral. The NOEs are also classified into three distance ranges based on the integral intensities.

Fig. 3-14 Phase-sensitive ROESY spectrum of ^{15}N-alamethicin dimer with presatuation (1s, 47dB) and ^{15}N decoupling by application of a 180° ^{15}N pulse at the mid-point of t_1 along with the use of GARP decoupling during acquisition. The spectrum was collected with a cw spinlock (0.2s, 26dB) during the mixing time (τ_m = 200ms). $SW_1 = SW_2$ = 5434.8Hz, TD_2 = 2K, TD_1 = 512, Hz/pt_2 = 5.3, Hz/pt_1 = 14.2, NS = 576, DS = 64, 90°(^{1}H) = 15.5 μs, receiver gain = 1024. Total acquisition time was 88.5 hours. A squared sine-bell (Qsine) window function with a phase shift of π/2 was applied in both dimensions. Only negative contour levels are plotted. (a) The aliphatic region. (b) The fingerprint region (c) The amide (NH-NH) region.

Fig. 3-14*a* The aliphatic region of the ROESY spectrum of ^{15}N alamethicin dimer

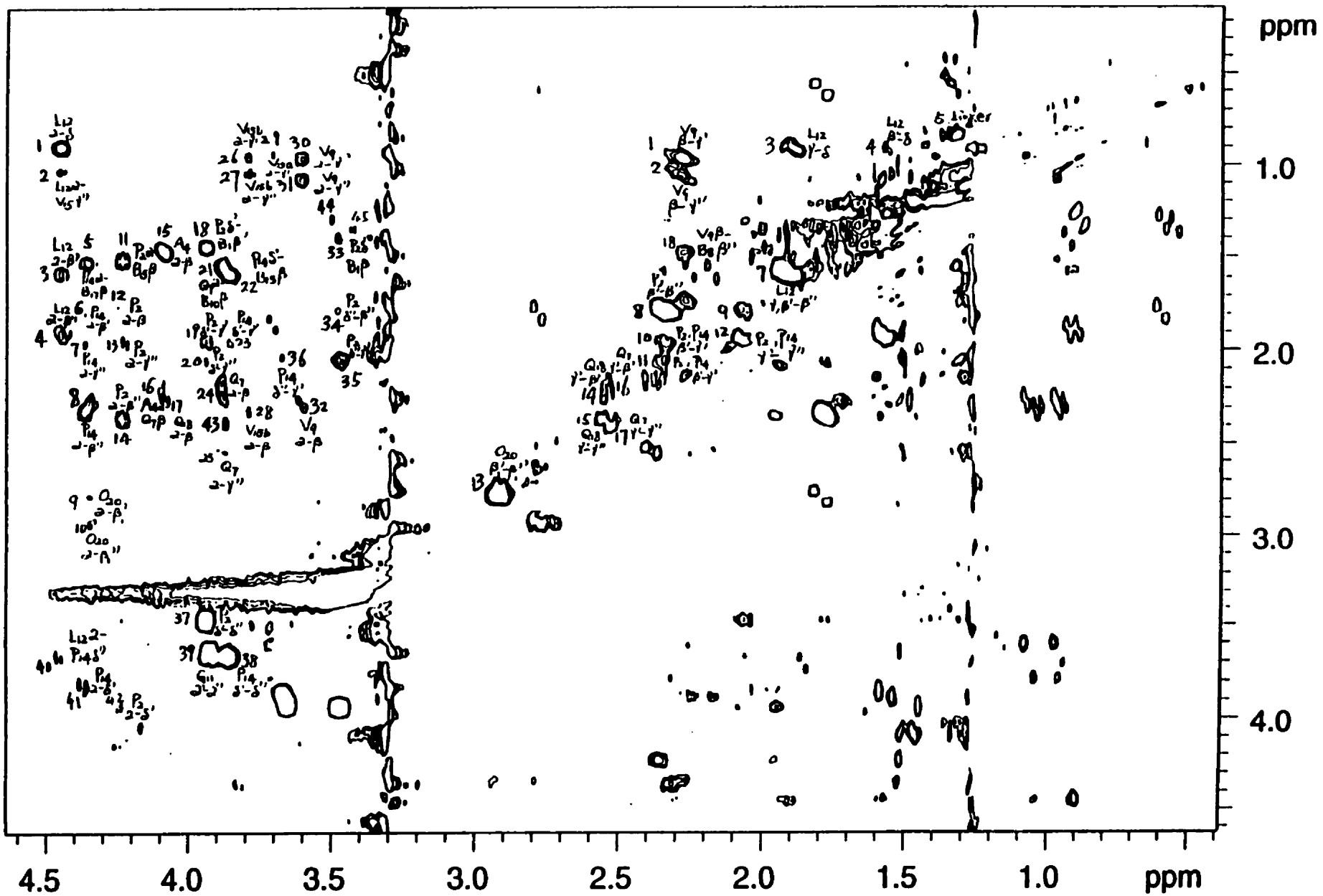

Fig. 3-14b The fingerprint region of the ROESY spectrum of ^{15}N alamethicin dimer

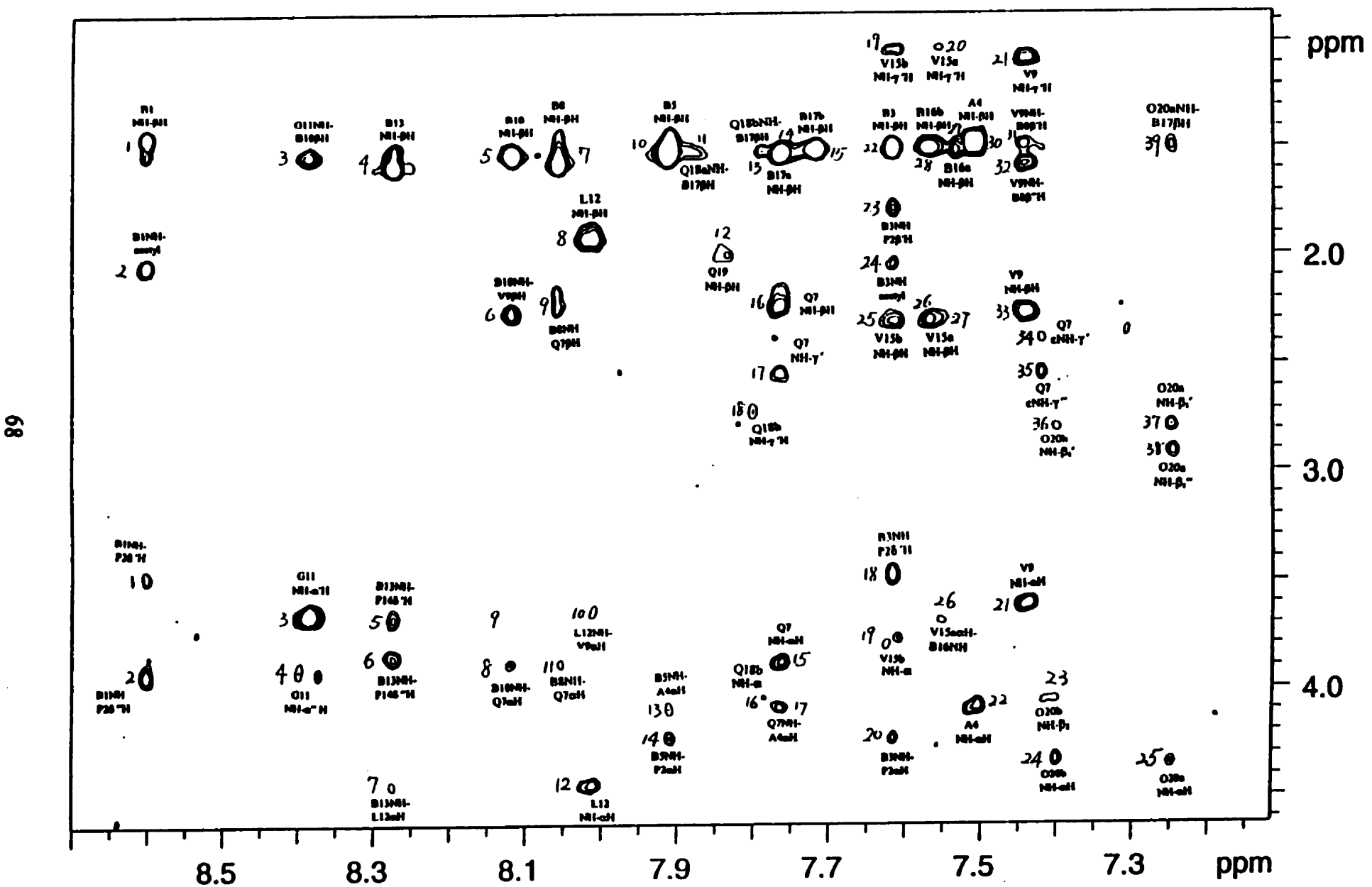

Fig. 3-14c The NH-NH region of the ROESY spectrum of ^{15}N alamethicin dimer

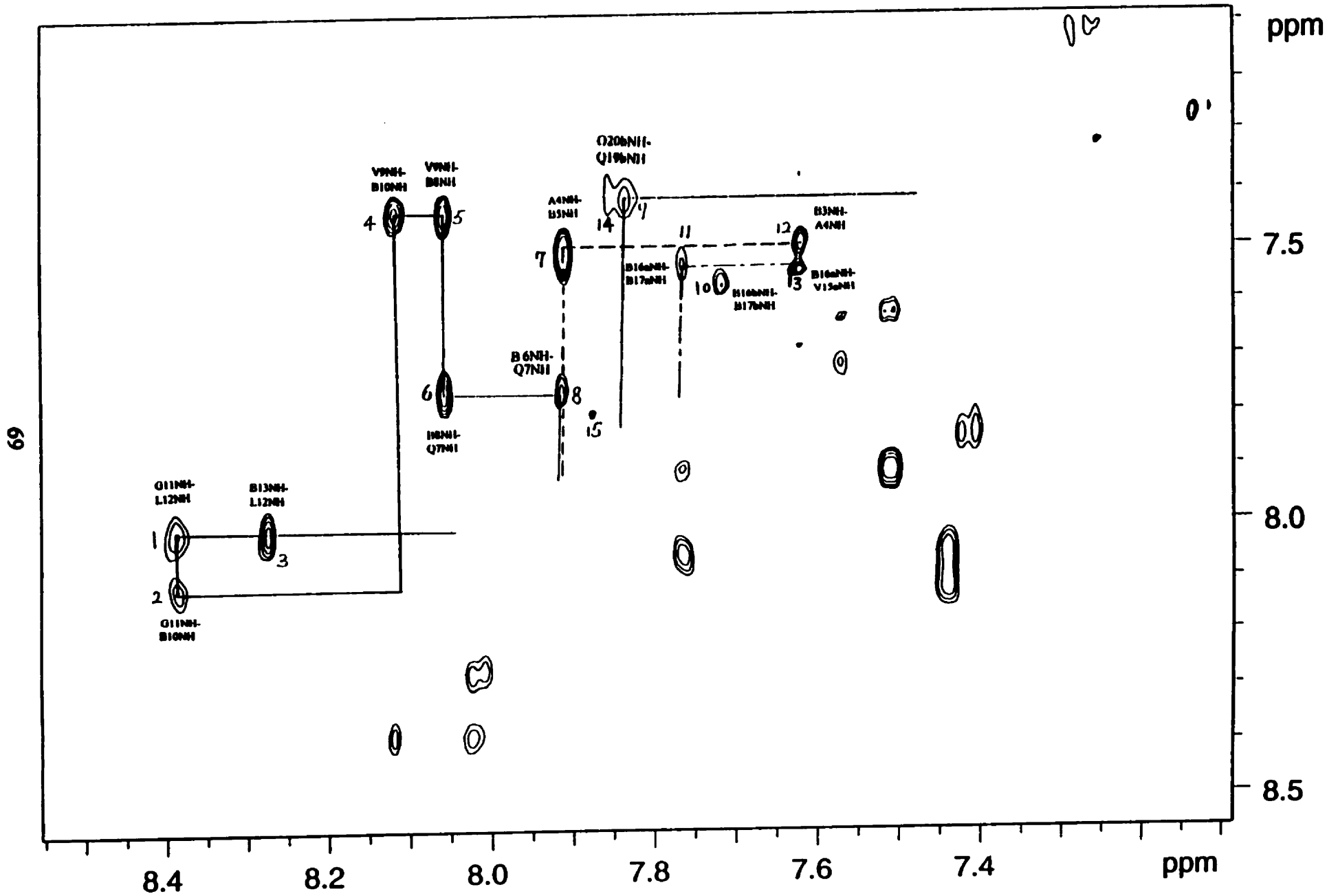

Table 3-7. NOE Cross Peaks in the β-γ-δ Region

Peak number	Assignment of cross peak	Integral (-)	Distance range Å	Classif-ication	Mono-mer
1	V9 βH-γ''H	483.5	1.8-2.8	S	S
2	V9 βH-γ'H	314.2	1.8-2.8	S	S
3	L12 γ, β'H-δH	441.0	1.8-2.8	S	S
4	L12 β''H-δH	21.9	3.5-5.0	W	W
5	Linker	256.9	1.8-2.8	S	
6	Linker	98.2	1.8-2.8	S	
7	L12 γ, β'H-β''H	905.2	1.8-2.8	S	S
8	P2, P14 β'H-β''H	1205.3	1.8-2.8	S	S
9	P2, P14 γ'H-β''H	229.9	1.8-2.8	S	M
10	P2, P14 β'H-γ''H	80.5	2.8-3.5	M	M
11	P2, P14 β'H-γ'H	78.1	2.8-3.5	M	W
12	P2, P14 γ'H-γ''H	450.7	1.8-2.8	S	S
13	O20 β1'H-β1''H	1010.4	1.8-2.8	S	S
14	Q18 γ'H-βH	82.1	2.8-3.5	M	M
15	Q18 γ'H-γ''H	200.2	1.8-2.8	S	S
16	Q7 γ'H-β''H	18.6	3.5-5.0	W	M
17	Q7 γ'H-γ''H	284.9	1.8-2.8	S	S

Table 3-8. NOE Cross Peaks in the α-β-γ-δ Region

Peak number	Assignment of cross peak	Integral (-)	Distance range Å	Classif-ication	Mono-mer
1	L12 αH-δH	288.4	1.8-2.8	S	S
2	L12 αH-V15a γ''H	46.1	2.8-3.5	M	M
3	L12 αH-β'H	121.6	1.8-2.8	S	S
4	L12 αH-β'', γH	158.0	1.8-2.8	S	S
5	P14 αH-B17 βH	112.5	1.8-2.8	S	S
6	P14 αH-β'H	13.3	3.5-5.0	W	M
7	P14 αH-γ''H	36.0	2.8-3.5	M	W

8	P14 αH-β''H	386.6	1.8-2.8	S	S
9	O20a αH-β1'H	15.2	3.5-5.0	W	S
10	O20 αH-β1''H	65.0	2.8-3.5	M	S
11	P2 αH-B5βH	246.4	1.8-2.8	S	S
12	P2 αH-β'H	19.8	3.5-5.0	W	W
13	P2 αH-γ''H	71.1	2.8-3.5	M	M
14	P2 αH-β''H	322.7	1.8-2.8	S	S
15	A4 αH-βH	374.0	1.8-2.8	S	S
16	A4 αH-Q7 β',β''H	57.0	2.8-3.5	M	M
17	Q18bαH-βH	21.1	3.5-5.0	W	S
18	P2 δ'H-B1 βH	273.4	1.8-2.8	S	S
19	P2 δ'H-γ'H	141.9	1.8-2.8	S	S
20	P2 δ'H-γ''H	30.4	2.8-3.5	M	W
21	Q7 αH-B10βH	281.2	1.8-2.8	S	M
22	P14 δ'H-B13 βH	240.7	1.8-2.8	S	S
23	P14 δ'H-γ'H	64.7	2.8-3.5	M	M
24	Q7 αH-β', β''H	287.0	1.8-2.8	S	S
25	Q7 αH-γ''H	14.8	3.5-5.0	W	M
26	V15b αH-γ'H	56.5	2.8-3.5	M	S
27	V15b αH-γ''H	61.2	2.8-3.5	M	S
28	V15b αH-βH	31.6	2.8-3.5	M	S
29	V15a αH-γ'H	21.0	3.5-5.0	W	NO
30	V9 αH-γ'H	172.1	1.8-2.8	S	S
31	V9 αH-γ''H	171.8	1.8-2.8	S	S
32	V9 αH-βH	91.1	1.8-2.8	S	S
33	P2 δ''H-B1 βH	59.3	2.8-3.5	M	NO
34	P2 δ''H-β''H	57.0	2.8-3.5	M	M
35	P2 δ''H-γ'H	239.8	1.8-2.8	S	S
36	P14 δ''H-γ'H	20.5	3.5-5.0	W	M
37	P2 δ'H-δ''H*	1335.8	1.75	S	S
38	P14 δ'H-δ''H	974.0	1.8-2.8	S	S
39	G11 α'H-α''H	1780.1	1.8-2.8	S	S
40	L12αH-P14 δ''H	65.3	2.8-3.5	M	M

41	P14 αH-δ'H	35.4	2.8-3.5	M	M
42	P2 αH-δ'H	20.3	3.5-5.0	W	M
43	unassigned	78.6	2.8-3.5	M	
44	unassigned	45.6	2.8-3.5	M	
45	unassigned	34.1	2.8-3.5	M	

Table 3-9. NOE Cross Peaks in the NH-β-γ Region

Peak number	Assignment of cross peak	Integral (-)	Distance range Å	Classif-ication	Mono-mer
1	B1 NH-βH	187.9	1.8-2.8	S	S
2	B1 NH-acetyl CH3	110.5	1.8-2.8	S	S
3	G11 NH-B10 βH	100.0	1.8-2.8	S	S
4	B13 NH-βH	329.4	1.8-2.8	S	S
5	B10 NH-βH	290.4	1.8-2.8	S	S
6	B10 NH-V9 βH	102.7	1.8-2.8	S	S
7	B8 NH-βH	340.7	1.8-2.8	S	S
8	L12 NH-β'H	249.5	1.8-2.8	S	S
9	B8 NH-Q7 β', β''H	76.7	2.8-3.5	M	M
10	B5, B6 NH-βH	881.3	1.8-2.8	S	S
11	Q18a NH-B17 βH	71.4	2.8-3.5	M	NO
12	Q19ab NH-βH	57.8	2.8-3.5	M	S
13	Q18b NH-B17 b βH	35.5	2.8-3.5	M	NO
14	B17b NH-βH	282.7	1.8-2.8	S	S
15	B17a NH-βH	301.5	1.8-2.8	S	NO
16	Q7 NH-βH	186.1	1.8-2.8	S	S
17	Q7 NH-γ'H	45.6	2.8-3.5	M	S
18	Q18b NH-γ'H	22.7	3.5-5.0	W	M
19	V15a NH-γ'H	46.6	2.8-3.5	M	S
20	V15b NH-γ'H	14.9	3.5-5.0	W	NO
21	V9 NH-γ'H	121.6	1.8-2.8	S	S
22	B3 NH-βH	302.2	1.8-2.8	S	S
23	B3 NH-P2 βH	56.9	2.8-3.5	M	M

24	B3 NH-acetyl CH3	26.0	2.8-3.5	M	M
25	V15a NH-βH	89.7	1.8-2.8	S	S
26	V15b NH-βH	114.3	1.8-2.8	S	NO
27	B16NH-V15 βH	17.3	3.5-5.0	W	S
28	B16a NH-βH	222.7	1.8-2.8	S	S
29	B16b NH-βH	76.0	2.8-3.5	M	NO
30	A4 NH-βH	341.3	1.8-2.8	S	S
31	V9 NH-B8 β''H	81.6	2.8-3.5	M	W
32	V9 NH-B8 β'H	87.9	1.8-2.8	S	S
33	V9 NH-βH	163.8	1.8-2.8	S	S
34	Q7 εNH-γ'H	10.4	3.5-5.0	W	W
35	Q7 εNH-γ''H	27.4	2.8-3.5	M	M
36	O20a NH-β1''H	11.3	3.5-5.0	W	S
37	O20b NH-β1''H	34.0	2.8-3.5	M	NO
38	O20b NH-β1'H	32.1	2.8-3.5	M	NO
39	O20 NH-B17 βH	47.0	2.8-3.5	M	M
40	Q18a NH-βH	20.1	3.5-5.0	W	NO
41	Q18b NH-βH	22.7	3.5-5.0	W	S

Table 3-10. NOE Cross Peaks in the NH-α-δ Region

Peak number	Assignment of cross peak	Integral (-)	Distance range Å	Classification	Monomer
1	B1 NH-P2 δ'H	26.9	2.8-3.5	M	M
2	B1 NH-P2 δ''H	86.5	1.8-2.8	S	S
3	G11 NH-α''H	261.6	1.8-2.8	S	S
4	G11 NH-α'H	47.9	2.8-3.5	M	M
5	B13 NH-P14 δ'H	53.3	2.8-3.5	M	M
6	B13 NH-P14 δ''H	55.9	2.8-3.5	M	M
7	B13 NH-L12 αH	15.9	3.5-5.0	W	W
8	B10 NH-Q7 αH	20.5	3.5-5.0	W	W
9	B10 NH-V9 αH	11.1	3.5-5.0	W	W
10	L12 NH-V9 αH	22.2	3.5-5.0	W	W

11	B8 NH-Q7 αH	15.7	3.5-5.0	W	W
12	L12 NH-αH	76.6	2.8-3.5	M	S
13	B5 NH-A4 αH	21.7	3.5-5.0	W	W
14	B5 NH-P2 αH	30.3	2.8-3.5	M	M
15	Q7 NH-αH	72.4	2.8-3.5	M	S
16	Q18b NH-αH	4.7	3.5-5.0	W	S
17	Q7NH- A4 αH	35.1	2.8-3.5	M	M
18	B3 NH-P2 δ'H	85.0	1.8-2.8	S	S
19	V15a NH-αH	36.3	2.8-3.5	M	S
20	B3 NH-P2 αH	23.7	2.8-3.5	M	W
21	V9 NH-αH	122.1	1.8-2.8	S	S
22	A4 NH-αH	96.4	1.8-2.8	S	S
23	O20a NH-β2''H	24.6	2.8-3.5	M	S
24	O20a NH-αH	27.9	2.8-3.5	M	S
25	O20b NH-αH	18.9	3.5-5.0	W	NO

Table 3-11. NOE Cross Peaks in the NH-NH Region

Peak number	Assignment of cross peak	Integral (-)	Distance range Å	Classif-ication	Mono-mer
1	G11 NH-L12 NH	75.8	2.8-3.5	M	S
2	G11 NH-B10 NH	52.7	2.8-3.5	M	M
3	B13 NH- L12 NH	85.2	1.8-2.8	S	S
4	V9 NH-B10 NH	84.6	1.8-2.8	S	S
5	V9 NH-B8 NH	86.0	1.8-2.8	S	S
6	B8 NH-Q7 NH	77.0	2.8-3.5	M	M
7	A4 NH-B5 NH	118.8	1.8-2.8	S	S
8	Q7 NH-B6 NH	42.5	2.8-3.5	M	M
9	Q19b NH-O20b NH	87.8	1.8-2.8	S	S
10	B16b NH-B17b NH	26.1	2.8-3.5	M	NO
11	B16a NH-B17a NH	18.1	3.5-5.0	W	NO
12	B3 NH-A4 NH	27.4	2.8-3.5	M	W
13	B16a NH-V15a NH	30.2	2.8-3.5	M	W

14	unassigned	22.7	3.5-5.0	W	NO
15	unassigned	10.8	3.5-5.0	W	NO

1. Peak numbers correspond to peaks labeled in ROESY spectra (Fig. 3-14).

2. All methyl and methylene protons are not stereospecifically assigned.

3. The interproton distances were calculated by calibration of the cross-peak intensities against the δ'-δ'' proton pair of Pro_2: $r_{ij} = 1.75\ (1335.8/\alpha_{ij})^{1/6}$, where α_{ij} is the cross-peak intensity which is shown in the tables. According to the distances, cross-peak intensities were classified into strong (s), medium (m) and weak (w) cross-peaks.

4. A few cross peaks were observed in a different the experiment (TD =256, not shown) but not observed in this experiment (TD =384).

5. Some cross peaks which were observed in the dimer spectrum but not observed in monomer were denoted as "NO".

6. The monomer cross peak intensities were obtained from [3].

3.3.6 Temperature Dependence of Amide ^1H and ^{15}N Chemical Shifts

To investigate the nature of the doubled resonances for residues Val_{15} to Pho_{20}, a series of 2D ^1H-^{15}N HSQC spectra were measured at 273K, 288K, and 318K. Spectra are depicted in Fig.3-15a-c. In general, 28 cross peaks were present in all spectra at different temperatures and with the exception of residues 4 and 16, amide ^1H chemical shifts move to higher field as the temperature is elevated. Temperature has a small effect on the ^{15}N chemical shifts. The NH chemical shifts at different temperatures and their temperature dependence ($\Delta\delta/\Delta T$) are summarized in Table 3-12. Fig. 3-16 shows the temperature dependence ($\Delta\delta/\Delta T$) of the backbone (*a*; solid bars) and side-chain (*b*; open bars) amide chemical shifts as a function of amino acid residue of alamethicin dimer in methanol measured from HSQC spectra over the range 273-318 K. The results are very similar to those observed for the monomer [12]. Except for residue Aib_{17} the *a* resonances are shifted slightly further downfield with increasing temperature than the *b*

resonances. The *b* resonance from Aib_{16} is shifted upfield with temperature. Interestingly, the *a* and *b* resonances of residues 15, 16, and 19 move closer together as the temperature is increased whereas the *a* and *b* resonances of residues 17 and 20 separate.

Fig. 3-15. ^{1}H-^{15}N HSQC spectra of the ^{15}N alamethicin dimer with presatuation (1s, 55dB) and decoupling during the evolution and acquisition time at different temperatures (a) HSQC spectrum at 273 K operated and processed using the same parameters as the experiment in Fig. 3-11 except 90°(^{1}H) = 15.8 μs. (b) HSQC spectrum at 288 K with 90°(^{1}H) = 14.7 μs. (c) HSQC at 318 K with 90°(^{1}H) = 15.7 μs.

Fig. 3-15*a* ^{1}H-^{15}N HSQC spectrum of ^{15}N alamethicin dimer at 273K

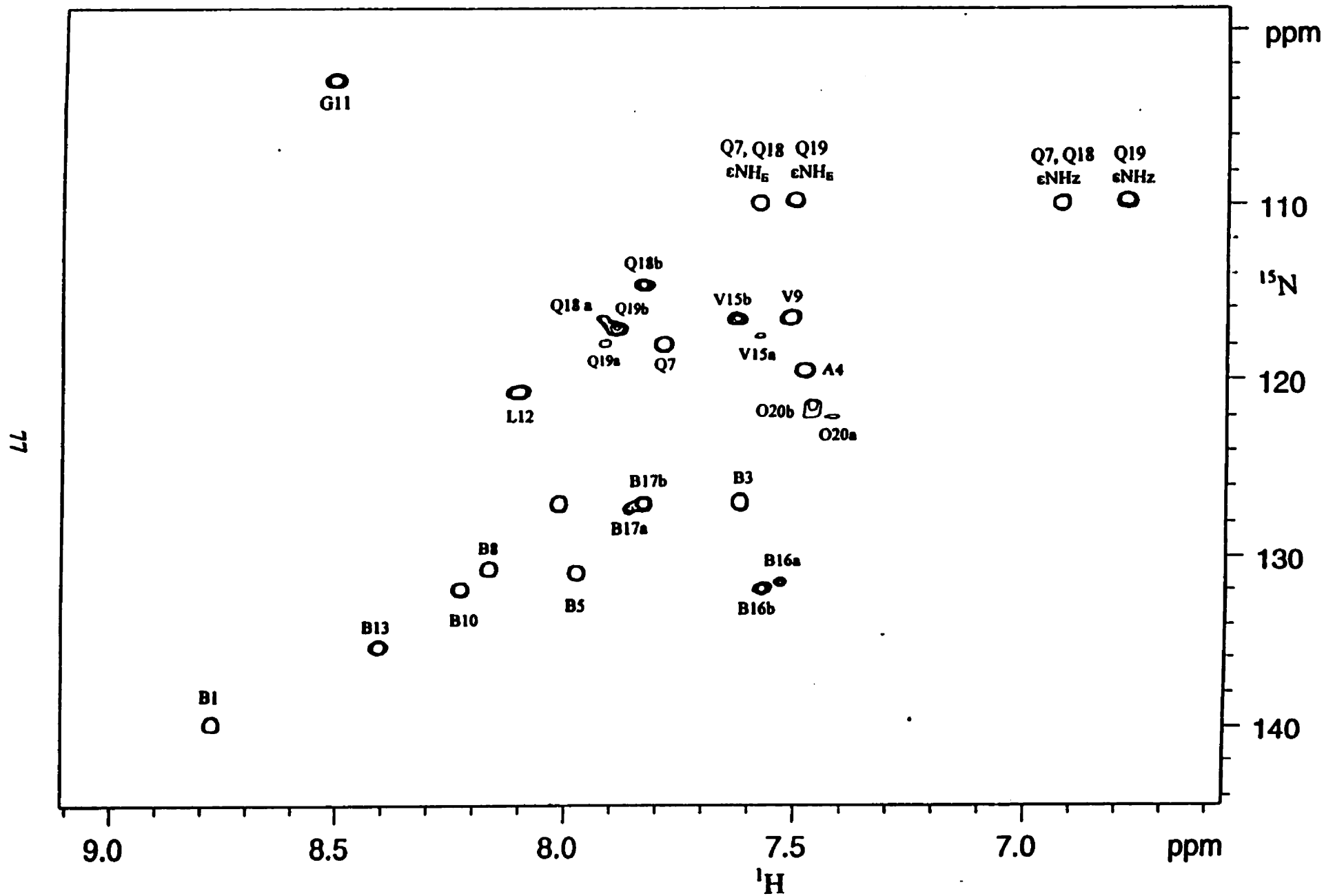

Fig. 3-15b ^{1}H-^{15}N HSQC spectrum of ^{15}N alamethicin dimer at 288K

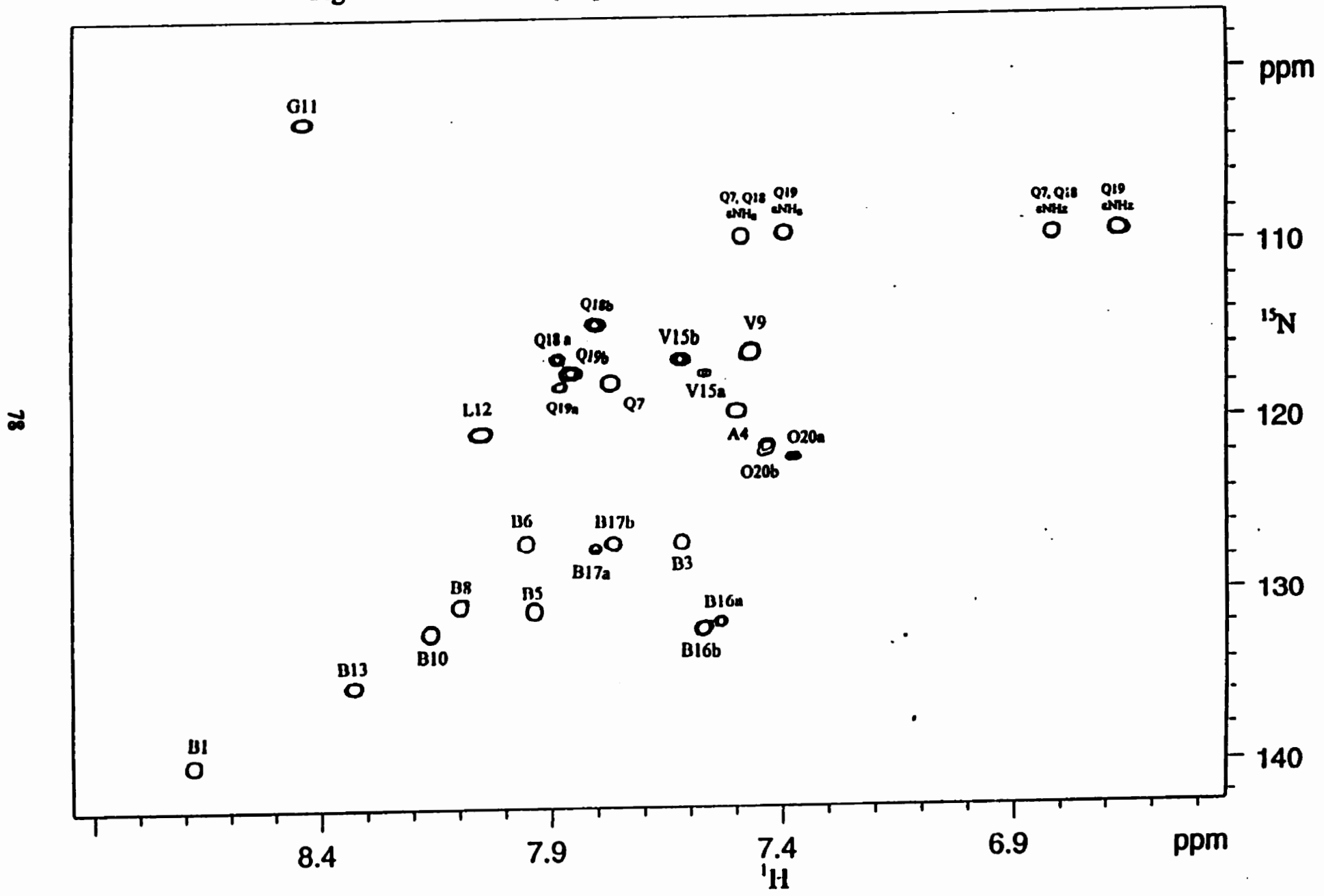

Fig. 3-15c ^{1}H-^{15}N HSQC spectrum of ^{15}N alamethicin dimer at 318K

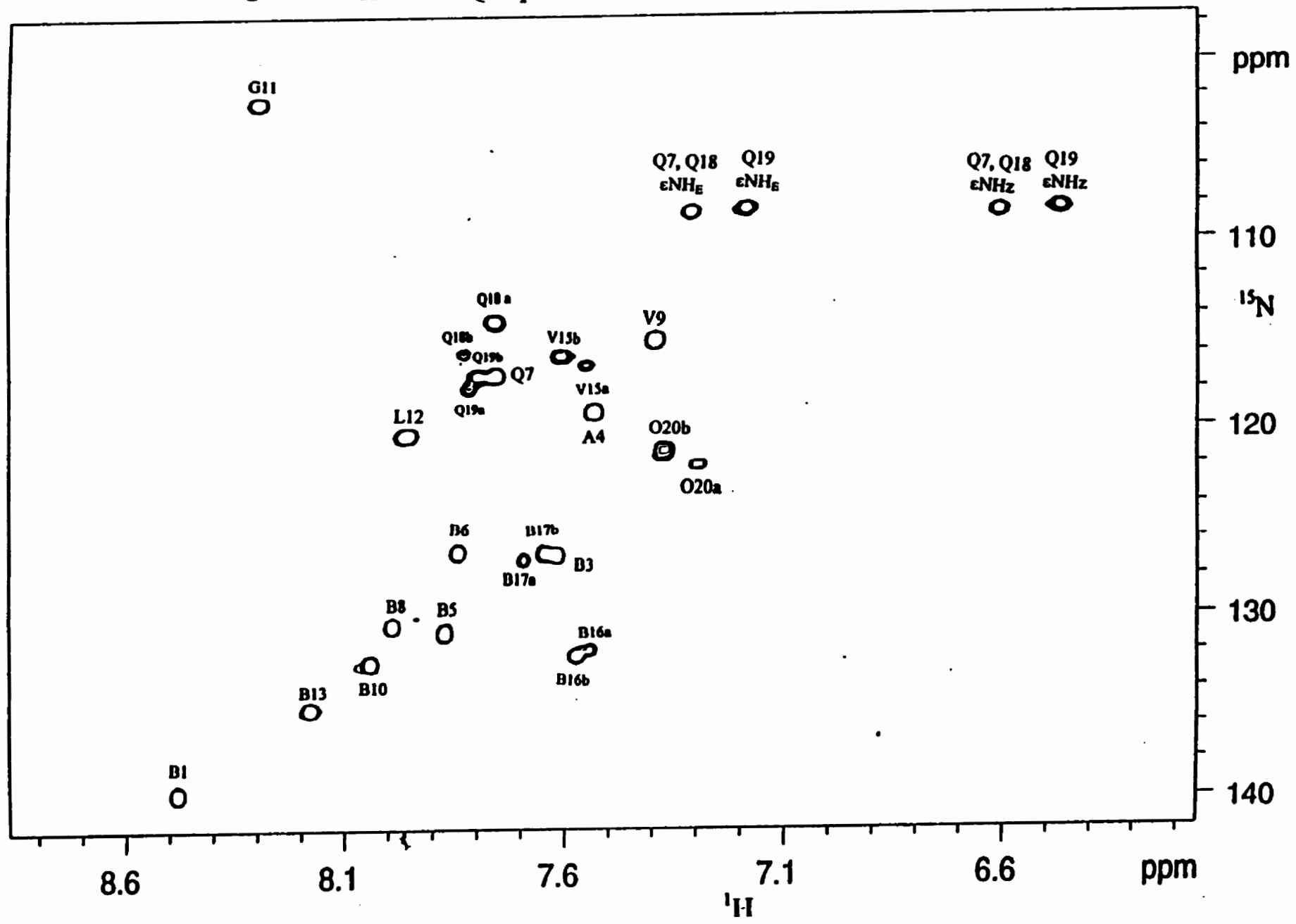

Table 3-12. The Temperature Dependence of the Backbone and Side-chain Amide Chemical Shifts of Alamethicin Dimer (ppb)

Residue		$NH_{273\,K}$	$NH_{288\,K}$	NH_{300K}	$NH_{318\,K}$	Slope $\Delta\delta/\Delta T$ (ppb/K)
Aib1		8.78	8.69	8.60	8.48	-7.5
Aib3		7.62	7.62	7.62	7.62	0.0
Ala4		7.49	7.50	7.53	7.54	1.3
Aib5		7.98	7.94	7.93	7.87	-2.7
Aib6		8.02	7.96	7.93	7.84	-4.5
Gln7		7.79	7.78	7.78	7.76	-0.8
Aib8		8.17	8.10	8.06	7.99	-4.5
Val9		7.51	7.47	7.45	7.40	-2.8
Aib10		8.23	8.17	8.12	8.04	-4.8
Gly11		8.51	8.44	8.40	8.30	-5.3
Leu12		8.11	8.06	8.03	7.96	-3.8
Aib13		8.41	8.33	8.29	8.18	-5.8
Val15	a	7.58	7.57	7.56	7.55	-0.7
	b	7.63	7.62	7.62	7.61	-0.5
Aib16	a	7.57	7.57	7.58	7.57	0.0
	b	7.53	7.53	7.55	7.54	0.2
Aib17	a	7.86	7.81	7.77	7.69	-4.2
	b	7.83	7.77	7.73	7.64	-4.7
Gln18	a	7.92	7.89	7.87	7.83	-2.2
	b	7.83	7.81	7.80	7.76	-1.7
Gln19	a	7.88	7.88	7.87	7.82	-1.6
	b	7.86	7.86	7.85	7.80	-1.5
Phol20	a	7.42	7.37	7.36	7.29	-3.2
	b	7.47	7.43	7.42	7.37	-2.5
Side-chain of Gln7 & Gln18	$\varepsilon NH_\varepsilon$	7.59	7.49	7.43	7.31	-7.0
	εNHz	6.93	6.82	6.75	6.61	-8.0
Side-chain of Gln19	$\varepsilon NH_\varepsilon$	7.51	7.40	7.32	7.19	-8.0
	εNHz	6.78	6.67	6.60	6.47	-7.8

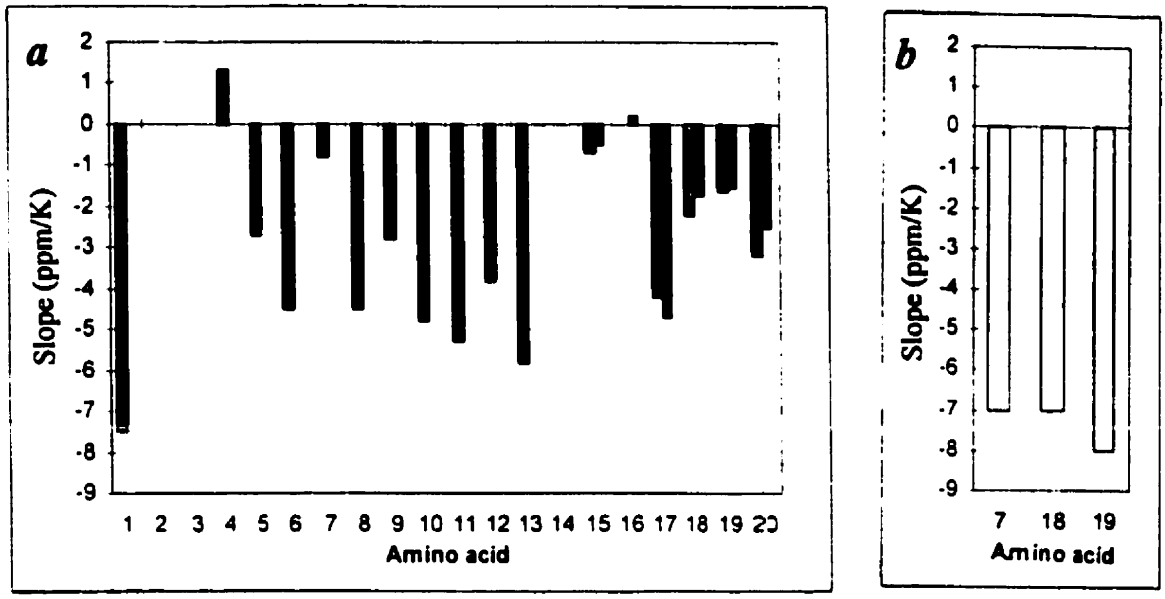

Fig. 3-16. The slopes of the amide proton chemical shifts of the ^{15}N alamethicin dimer for the backbone (a) and side-chain amides (b).

3.4. NMR Spectroscopy of an Alamethicin Dimer Mixture

As described previously, a roughly equal mixture of unlabeled Aib_6 alamethicin and Ala_6 alamethicin were used to make an alamethicin dimer. In the case of random dimerization, the mixture should produce one part Aib_6 homodimer, one part Ala_6 homodimer, and two parts Aib_6-Ala_5 heterodimer, and mass spectrometry confirmed this expectation (Fig. 3-8). As there are significant differences in the chemical shifts of the monomers, it is reasonable to expect the NMR spectra of the mixture of dimers to be complex. Assignment of the proton NMR resonances of the unlabeled dimer mixture used methods similar to those used in the assignment of the ^{15}N-alamethicin homodimer. With the help of the 1D-^1H spectra of the two monomers (Ala_6; Aib_6) and 2D spectra such as TOCSY, DQF-COSY and ROESY (not shown), ^1H NMR lines were individually assigned and listed in Table 3-13 where they are compared with the chemical shifts of the two monomers (Aib_6; Ala_6) as well as ^{15}N alamethicin dimer. For assignment, the

first step was to identify resonances in the dimer mixture identical to those of the individual monomers. These were easiest to identify for residues in the N-terminus where many residues displayed two resonances corresponding to the chemical shifts of each of the monomers. In the carboxyl terminus some monomer resonances apparently disappeared and resonances assigned to ^{15}N-Aib$_6$ homodimer were identified. All other resonances are assumed to arise either from homodimer or heterodimer.

3.4.1. 1D-^{1}H Spectrum of Unlabeled Alamethicin Dimer

Fig. 3-17 shows the amide region of a 1D-^{1}H NMR spectrum of the mixture of unlabeled alamethicin dimers. Compared with the ^{15}N alamethicin homodimer spectrum (see Fig. 3-10a), resonance identification is more difficult. In some cases, it is evident that there are two sets of NH peaks in this region. For example, two triplet peaks belonging to the NH of Gly$_{11}$ are easily identified at 8.32 and 8.40 ppm. These resonances correspond closely to the Aib$_6$ alamethicin and Ala$_6$ alamethicin monomer positions, respectively. The singlet resonances at 8.12 ppm and 8.18 ppm are easily identified as Aib resonances. The first peak corresponds exactly to the Aib$_{10}$ NH resonance of Aib$_6$ monomer, whereas the latter peak is slightly shifted to lower field of the Aib$_{10}$ NH resonance of the Ala$_6$ monomer. The Ala$_4$ doublet NH resonances of each monomer are easily identified at 7.51 ppm and 7.56 ppm. The largest difference in the NH chemical shift between the monomers is observed at Gln$_7$. The Gln$_7$ NH doublet of Ala$_6$ monomer is clearly identified at 7.98 ppm, whereas the corresponding resonance of the Aib$_6$ monomer is obscured at 7.78 ppm by overlap with other resonances.

In the carboxyl terminus, assignment of resonances was more difficult as some resonances, especially Aib$_{13}$X, Aib$_{13}$Y, Val$_{15}$Y, Aib$_{16}$Y, Gln$_{18}$Y and Gln$_{19}$Y, corresponded neither to Aib$_6$ monomer, Ala$_6$ monomer, or Aib$_6$ homodimer. The Pho$_{20}$ residues exhibit at least three NH resonances, two of which are different

from the monomer resonances. The spin-spin coupling constants $^3J_{\alpha N}$ could be measured unambiguously for residues A4X, A4Y, Q7Y, V9X, V9Y, G11X and G11Y from the 1D-^{1}H spectrum and are listed in Table 3-14. The $^3J_{\alpha N}$ measurements for other non-Aib residues are less accurate due to spectral overlap.

Fig. 3-17. The expanded amide region of the 1D ^{1}H spectrum of the unlabeled alamethicin dimer mixture with solvent presaturation (1s, 55dB). The spectrum was recorded with 32 k points, NS = 1 k, DS = 4, 90°(^{1}H) = 15.9 μs, SW = 7042 Hz, and an acquisition time of 2.327 seconds. The total acquisition time was about 1 h. An EM window function was used for processing (LB = 1). Two sets of peaks are labeled as X and Y which have chemical shifts closer to Aib_6 alamethicin monomer and Ala_6 monomer, respectively. For residues with very close X and Y chemical shifts or X and Y peaks overlapping each other, the peaks are labeled as XY.

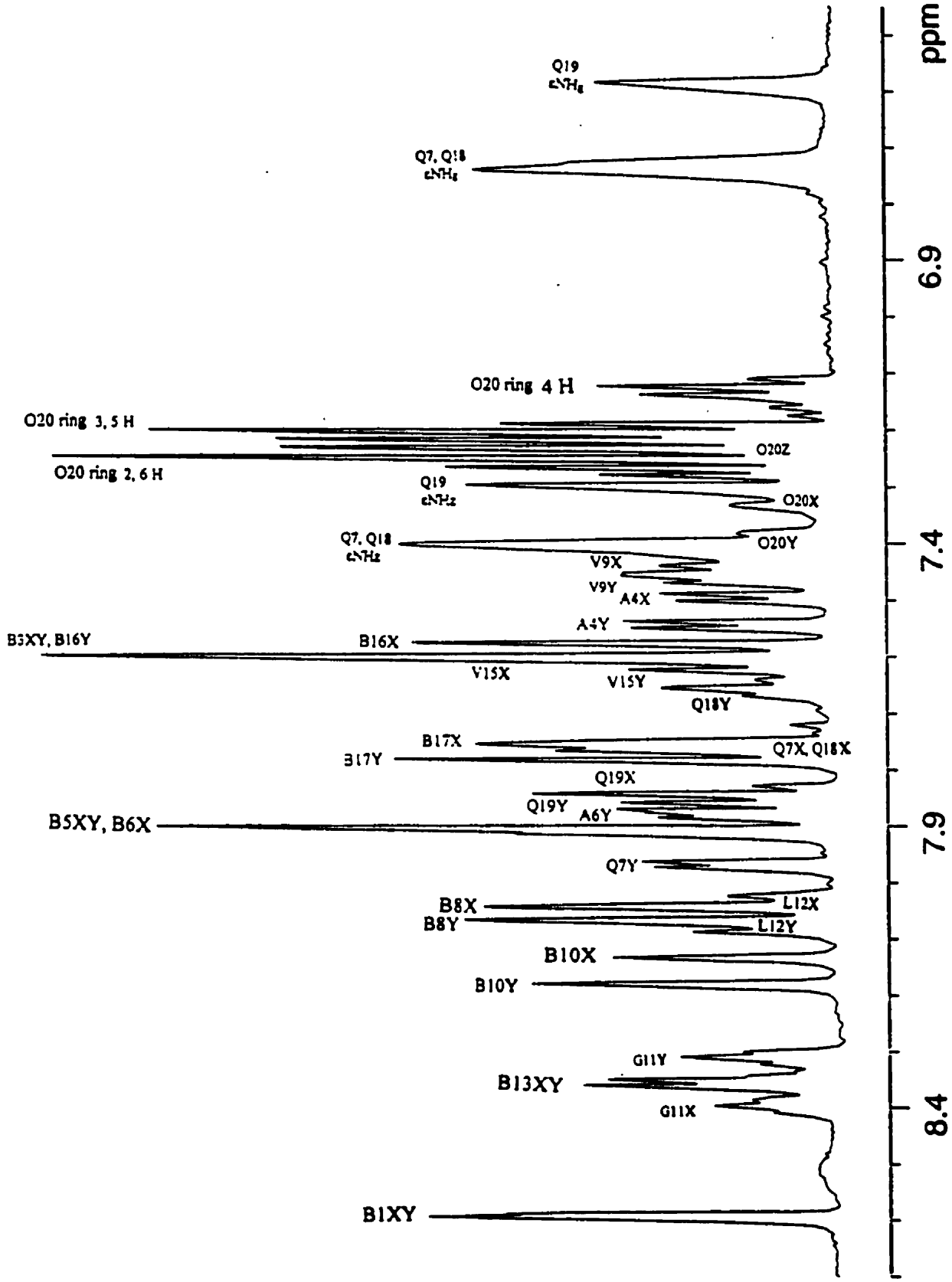

Fig. 3-17 The amide region of the 1D spectrum of ^{14}N alamethicin dimer

3.4.2. TOCSY Spectrum of Unlabeled Alamethicin Dimer

The fingerprint region of a TOCSY spectrum of the unlabeled alamethicin dimer mixture is shown in Fig. 3-18. The spin systems of all expected amino acids of the dimer give two sets of cross peaks between the NH and αH and other side-chain protons. The exception of course is the residue in position 6 since one alamethicin monomer has Aib_6 and another has Ala_6. There are no cross peaks for Aibs in a TOCSY spectrum, thus, only Ala_6 shows cross peaks at ω_1 = 4.02 ppm, ω_2 = 7.88 ppm and ω_1 = 1.52 ppm, ω_2 = 7.88 ppm for the coupling between the NH and αH and βH, respectively. For residues Val_{15}, Gln_{18} and Gln_{19}, cross peaks possibly due to the two different monomers as well as additional peaks due to dimerization in the C-terminus may be overlapped. It is impossible to distinguish these cross peaks in the TOCSY spectrum and in these cases broadened resonances appear. However, Pho_{20} appears as three sets of cross peaks, with the NH resonances at 7.24 ($Pho_{20}Z$), 7.29 ($Pho_{20}X$) and 7.40 ($Pho_{20}Y$) ppm, respectively. Because $^3J_{N\alpha}$ is large, cross peak fine structure is resolved for $Pho_{20}X$ and $Pho_{20}Y$. The $Pho_{20}Z$ NH-αH cross peak is very weak, however, the NH-β_1', NH-β_1'' and NH-β_2 cross peaks of $Pho_{20}Z$ are observed.

Fig.3-18. The expanded amide region of TOCSY spectrum of the unlabeled alamethicin dimer mixture with presatuation (1s, 55 dB). $SW_2 = SW_1$ = 5263.2 Hz; TD_2 = 2 k, Hz/pt_2 = 5.12; TD_1 = 512, Hz/pt_1 = 20.67, Mixing time = 60 ms, DS= 4, NS = 128, total acquisition time was about 23.5h; Data were zero-filled to 2048 (Hz/pt_1 = 5.12) in F_2 and 1024 points (Hz/pt_1 = 10.38) in F_1. A shifted-sine squared bell window function was applied in both dimensions with a π/2 shift.

Fig. 3-18 The fingerprint region of the TOCSY spectrum of ^{14}N alamethicin dimer

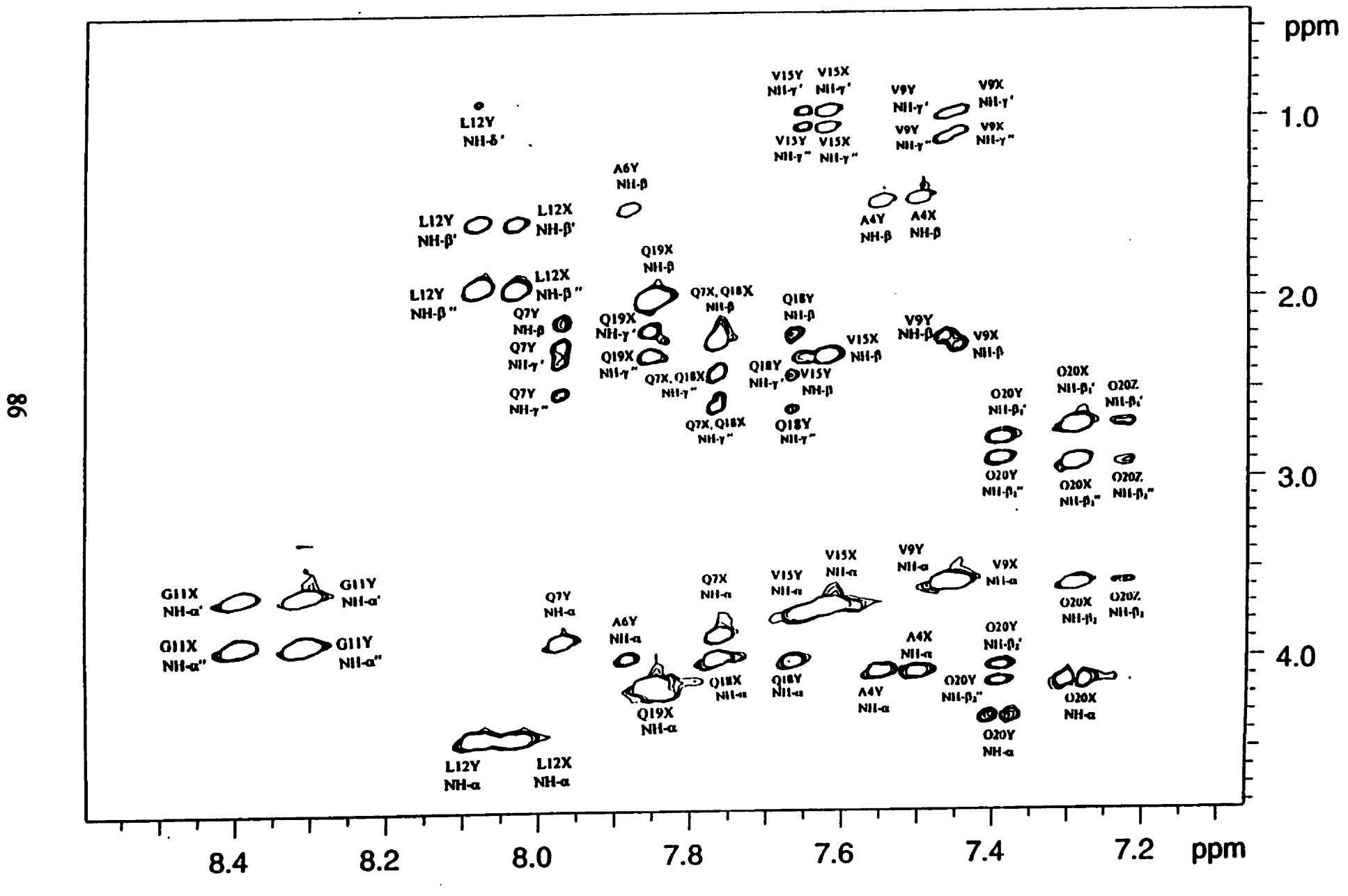

3.4.3 DQF-COSY Spectrum of Unlabeled Alamethicin Dimer Mixture

In the expanded fingerprint region of the DQF-COSY spectrum (Fig. 3-19), two sets of NH-αH cross peaks clearly show up for all expected amino acids. In the N-terminus, one set of cross peaks is consistent with Ala_6 alamethicin monomer and another corresponds to Aib_6 alamethicin monomer, supporting the assignments in the TOCSY and 1D spectra. Cross peaks are observed for residues of the C-terminus but they are more difficult to assign. The observation of the $Pho_{20}Z$ NH-αH cross peak confirmed the NH assignment of the TOCSY spectrum and provided the αH resonance assignment. The spectrum in Fig. 3-19 cannot be used for $^3J_{\alpha NH}$ coupling constant determination as it was not acquired with a sufficiently high digital resolution. Thus, the reported coupling constants $^3J_{\alpha NH}$ in Table 3-14 were measured from the 1D spectrum for the unlabeled dimer mixture.

Fig.3-19. The expanded fingerprint region of DQF-COSY spectrum of the unlabeled alamethicin dimer mixture acquired with presatuation of the water resonance (1s, 50 dB). $SW_2 = SW_1 = 5434.8$ Hz, $TD_2 =$ 1k, $TD_1 = 512$, $Hz/pt_2 = 10.58$, $Hz/pt_1 = 21.23$, NS = 128, DS = 16, 90° (^1H) = 15.7 μs. Total acquisition time was approximately 24h. Zero-filling to 2 k in F_1 and 4 k in F_2 yields a final digital resolution of 5.31 Hz/pt and 2.65 Hz/pt, respectively. Fourier transformation was performed after multiplication by a phase-shifted (π/30) sine-bell squared filter function in both dimensions. The positive and negative components of the cross peaks were plotted without distinction.

Fig. 3-19 The fingerprint region of the DQF-COSY spectrum of ^{14}N alamethicin dimer

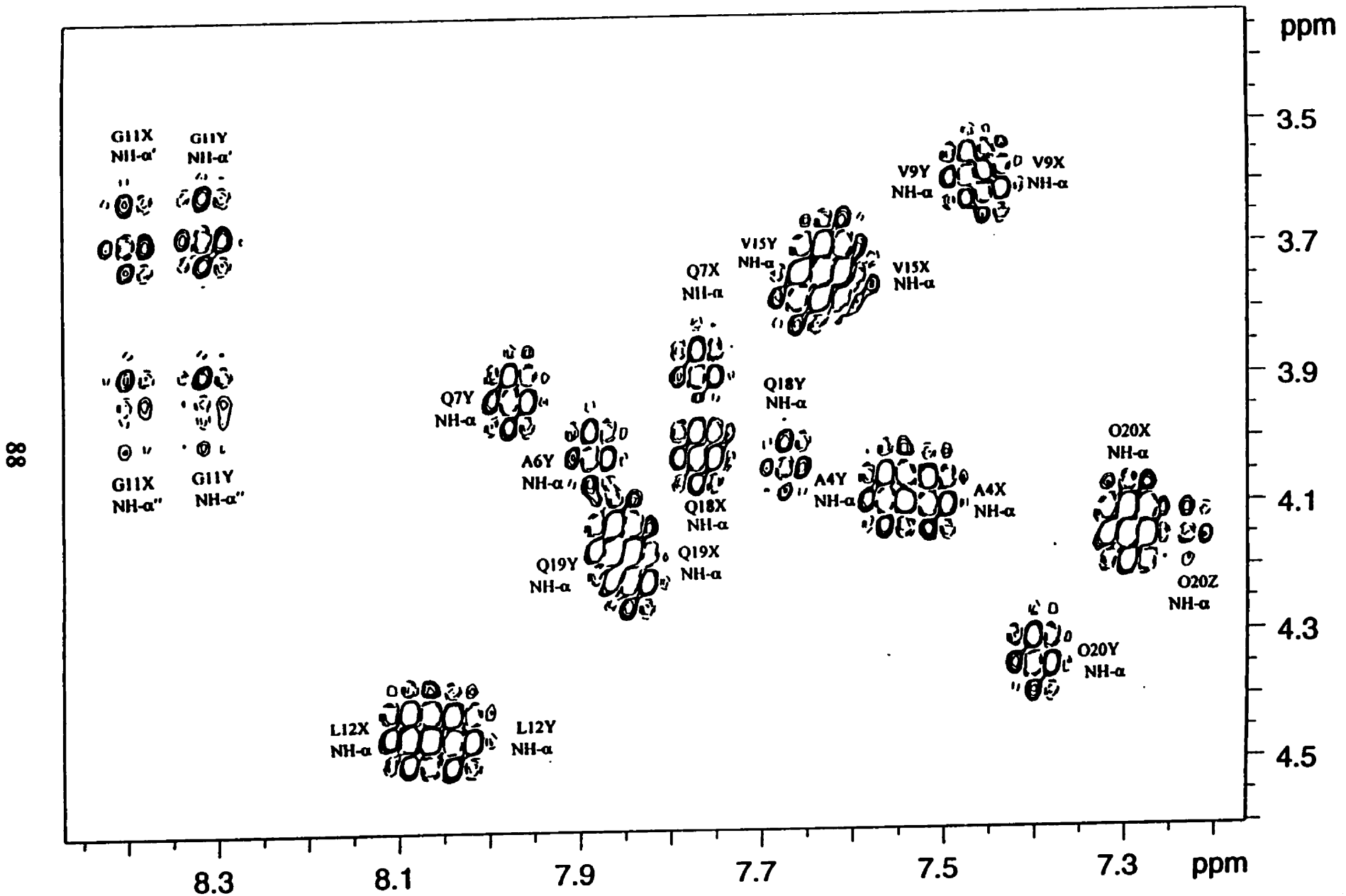

Table 3-13 ^{1}H Chemical Shifts of Unlabeled Alamethicin Dimers (in ppm)

Residue		NH	αH	βH	γH	Other	NH of Aib_6 monomer	NH of Ala_6 monomer	NH of ^{15}N dimer (Aib_6)
N-Acetyl						CH_3 2.05			
Aib1	X	8.61		1.44			8.61		8.60
	Y	8.61		1.44				8.61	
Pro2	X		4.25	2.36, 1.80	2.10, 2.00	δH 3.95, 3.50			
	Y		4.22	2.36, 1.80	2.10, 2.00	δH 3.94, 3.47			
Aib3	X	7.62		1.51			7.62		7.62
	Y	7.62		1.51				7.62	
Ala4	X	7.51	4.10	1.48			7.52		7.53
	Y	7.56	4.10	1.49				7.56	
Aib5	X	7.92		1.50			7.92		7.93
	Y	7.92		1.50				7.92	
Aib6	X	7.93		1.50			7.92		7.93
Ala6	Y	7.88	4.02	1.52				7.90	
Gln7	X	7.77	3.90	2.24, 2.22	2.60, 2.42	εNH 7.43, 6.75	7.77		7.78
	Y	7.97	3.92	2.27, 2.15	2.53, 2.35	εNH 7.43, 6.75		7.98	
Aib8	X	8.06		1.56			8.06		8.07
	Y	8.04		1.56				8.06	
Val9	X	7.45	3.60	2.26	1.10, 0.99		7.45		7.46
	Y	7.47	3.60	2.25	1.12, 1.00			7.48	
Aib10	X	8.12		1.54			8.12		8.12
	Y	8.18		1.54				8.20	
Gly11	X	8.40	3.94, 3.66				8.39		8.40
	Y	8.32	3.94, 3.66					8.33	
Leu12	X	8.03	4.44	1.94, 1.60	1.92	δH 0.93	8.03		8.03
	Y	8.08	4.44	1.94, 1.60	1.92	δH 0.93		8.09	
Aib13	X	8.36		1.55			8.30		8.29
	Y	8.37		1.55				8.38	
Pro14	X		4.37	2.34, 1.81	2.08, 1.98	δH 3.88, 3.73			
	Y		4.40	2.34, 1.81	2.08, 1.98	δH 3.86, 3.72			
Val15	X	7.62	3.73	2.33	1.06, 0.97		7.58		7.56, 7.62
	Y	7.66	3.79	2.33	1.06, 0.97			7.63	
Aib16	X	7.58		1.50			7.57		7.55, 7.59
	Y	7.61		1.50				7.59	
Aib17	X	7.76		1.51			7.75		7.77, 7.73
	Y	7.79		1.51				7.80	
Gln18	X	7.77	4.03	2.23	2.62, 2.43	εNH 7.43, 6.76	7.88		7.87, 7.80
	Y	7.67	4.02	2.23	2.62, 2.43	εNH 7.43, 6.76		7.78	
Glu19	X	7.85	4.18	2.01	2.33, 2.20	εNH 7.32, 6.60	7.86		7.86, 7.84
	Y	7.87	4.18	2.01	2.33, 2.24	εNH 7.32, 6.60		7.89	
Pho20	X	7.29	4.14	β1 3.61	β2 2.93, 2.73	$C^{2,6}H$ 7.27;	7.32		7.36, 7.42
	Y	7.40	4.35	β1 4.14, 4.07	β2 2.91, 2.80	$C^{3,5}H$ 7.23;		7.29	
	Z	7.24	4.14	β1 3.60	β2 2.93, 2.72	$C^{4}H$ 7.14			
Linker	$^{E}CH_2$ 0.89, $^{D}CH_2$ 1.30, $^{C}CH_2$ 1.61, $^{B}CH_2$ 2.04, $^{A}CH_2$ 2.25 (2.34)								

Table 3-14 Coupling Constants of Unlabeled Alamethicin Dimers Compared with those of Monomers (in Hz)

Residue		$^3J_{\alpha NH}$ of dimer	$^3J_{\alpha NH}$ of Aib_6 monomer	$^3J_{\alpha NH}$ of Ala_6 monomer
Ala4	X	6.01	6.02	
	Y	5.75		5.90
Ala6	Y	4.41		4.50
Qln7	X	*	5.34	
	Y	4.86		5.10
Val9	X	6.48	5.90	
	Y	5.50		5.50
Gly11	X	5.50	5.42	
	Y	5.55		5.80
Leu12	X	*	7.87	
	Y	*		7.90
Val15	X	7.20	7.62	
	Y	8.52		8.50
Qln18	X	*	5.72	
	Y	5.80		5.60
Qln19	X	8.39	7.84	
	Y	7.53		7.50
Phol20	X	*	9.46	
	Y	*		9.90

* Coupling constants not well-determined due to overlapping peaks.

References

1. Biemann, K. (1992) *Annu. Rev.Biochem. 61*, 977-1010.
2. Wuthrich, K. (1986) <<*NMR of Proteins and Nucleic Acids*>>, John-Wiley and Sons, Inc., New York.
3. Adelinda, A. Y. & O'Neil, J. D. J. (1992) *Biochemistry 31*, 3135-3143.
4. Shaka, A.J., Barker, P. B. & Freeman, R. (1985) *J. Magn. Reson. 64*, 547.
5. Bruhwiler, D & Wagner, G. (1986) *J. Magn. Reson. 69*, 546.
6. Davis, D. G.& Bax, A. (1985) *J. Am. Chem. Soc. 107*, 2820.
7. Bax, A. & Davis, D. G. (1985) *J. Magn. Reson. 65*, 355-360.
8. Derome, A. & williamson, M. (1990) *J. Magn. Reson. 88*, 177-185.
9. Pardi, A., Billeter, M. & Wüthrich, K. (1984) *J. Mol. Biol. 180*, 741.
10. Smith, L. J. Bolin, K. A. et, al, (1996) *J. Mol. Biol. 255*, 494-506.
11. Bax, A & Davis, D. G. (1985) *J. Magn. Reson. 63*, 207-213.
12. Adelinda, A. Y., Randal, B. & O'Neil, J. D. J. (1995) *Biopolymers 36*, 781-792.

Chapter 4

Discussion

4.1. Introduction

The purpose of this research was to synthesize an alamethicin dimer and determine its conformation by high-resolution ^{1}H and ^{15}N NMR spectroscopy. The mass spectral data presented in Chapter 3.2 provide convincing evidence that ^{15}N-labeled and unlabeled dimers were successfully prepared. The spectra also indicate the presence of several fragments presumably created during the electrospray ionization of the molecules. In the ^{15}N-labeled dimer mass spectrum, there is a fragment with m/z = 1999.7. This ion may represent unfragmented monomer, present in the dimer preparation before ionization or it may have arisen by fragmentation of the dimer. The NMR analysis presented below suggests the former. The complexity of the unlabeled dimer mixture precluded detailed analysis of its conformation by NMR spectroscopy. The NMR spectra of the ^{15}N-labeled homodimer were complicated by the observation of duplicated resonances in the C-terminus. Analysis of the NMR data suggests an explanation for this observation and provides information about the conformation of the dimer.

4.2. Chemical Shift Analysis

The differences in NH and αH chemical shifts between the observed values of the dimer and their random coil values as well as the differences from the alamethicin monomer (Aib_6) are listed in Table 4-1.

Table 4-1 Chemical Shift Differences between Alamethicin Dimer Resonances and Their Random Coil and Monomer Values at 300K (in ppm)

Residue		$\Delta\delta NH_{d-r}$ [a-b]	$\Delta\delta\alpha H_{d-r}$	$\Delta\delta^{15}N_{d-r}$	$\Delta\delta NH_{d-m}$ [c]	$\Delta\delta\alpha H_{d-m}$
Aib1		0		0	-0.01	
Pro2			-0.18			0.00
Aib3		-0.97		-12.8	0.00	
Ala4		-0.59	-0.10	-2.4	0.01	0.01
Aib5		-0.67		-8.6	0.01	
Aib6		-0.67		-13.1	0.01	
Gln7		-0.54	-0.45	-1.8	0.01	0.00
Aib8		-0.53		-8.6	0.01	
Val9		-0.57	-0.52	-3.2	0.01	-0.01
Aib10		-0.48		-8.6	0.00	
Gly11		0.06	-0.17, 0.01	-7.4	0.01	0.02, 0.00
Leu12		-0.13	0.13	-1.6	0.00	0.02
Aib13		-0.31		-4.0	-0.01	
Pro14			-0.04			0.01
Val15	a	-0.47	-0.39	-2.2	-0.02	-0.01
	b	-0.41	-0.32	-3.0	0.04	0.06
Aib16	a	-1.05		-7.7	-0.02	
	b	-1.02		-7.3	0.02	
Aib17	a	-0.83		-12.6	0.02	
	b	-0.87		-12.8	-0.02	
Gln18	a	-0.45	-0.27	-3.7	-0.01	0.05
	b	-0.52	-0.28	-5.6	-0.08	0.04
Gln19	a	-0.45	-0.15	-2.6	0.00	0.05
	b	-0.47	-0.15	-3.0	-0.02	0.05
Pho20	a	-0.94	-0.47	1.7	0.04	0.01
	b	-0.88	-0.27	1.2	0.10	0.21

[a]Values were calculated using the equation: $\Delta\delta_{d-r} = \delta_{dim}-\delta_{ran}$. The differences between the chemical shifts of Aib_1 and those of the other Aibs were calculated as $\Delta\delta H^n = \delta H_{dim}{}^n - \delta H_{dim}{}^1$.
[b]Random coil chemical shifts (at 25 °C) were taken from Wishart, *et al.* (1998) [1].
[c]Chemical shifts of alamethicin monomer (Aib_6) were measured from a 1D and 2D DQF-COSY spectrum. Chemical shift differences were calculated using the equation: $\Delta\delta_{d-m} = \delta_{dim} - \delta_{mon}$.

Tables 3-5 and 4-1 show that a single set of resonances is observed in the ^{15}N-dimer preparation for all residues between Aib_1 and Gly_{11}. A high-resolution 1D ^{1}H spectrum (Fig. 3-10) suggests that the NH resonance of Leu_{12} may be doubled. Table 4-1 also shows that all the resonances between Aib_1 and Pro_{14} differ from the chemical shift values of the monomer by 0.01 ppm or less. The slight differences between the chemical shifts of dimer and monomer suggest only minor differences in conformation between the two in this region.

Large differences in chemical shift between monomer and dimer are observed in the region between Val_{15} and Pho_{20} where all NH resonances are doubled and some $C^{\alpha}H$ and side-chain resonances are doubled as well. The largest difference in chemical shift is observed for the two β_2H_b resonances which are 0.56 ppm and 0.47 ppm downfield of the monomer resonances. This change is most likely due to the introduction of new carbonyl two bonds away from the $C^{\beta 2}$ atom. The chemical shifts of the two β_2H_a resonances (3.61 ppm) are nearly identical to those of the monomer, suggesting that the molecule which gives rise to the set of resonances denoted "*a*" is free alamethicin monomer. This hypothesis is supported by the observation that most of the *a* resonances differ from the monomer chemical shift by less than 0.02 ppm. The only exception is the Pho_{20} NH, which is 0.04 ppm downfield of the monomer resonance. We also tested the possibility that the monomer resonances *a* are in dynamic equilibrium with resonances *b* by searching for *a-b* ROESY exchange cross-peaks. None were observed suggesting that resonances *a* and *b* arise from separate molecules. We also examined the temperature dependence of resonances *a* and *b*. No coalescence was achieved over the range of temperatures 0°C-40°C and this indicates that the dimer and monomer exist in separate molecules.

What is the origin of the chemical shift differences between the C-terminal dimer resonances denoted "*b*" and the monomer chemical shifts? One possible

explanation is that the new C-terminal carbonyl oxygen in the linker may directly affect the chemical shifts of neighboring resonances and this is a likely explanation of the effect on the β_2H. This effect would depend on the relative orientations and distances between a shifted hydrogen and the carbonyl. Curiously, we observe very little perturbation of αH, βH and other side chain resonances in the vicinity of the carbonyl. On the other hand, the NH resonance of Gln_{18b} is strongly perturbed in the dimer (0.08 ppm) and even the NH of Val_{15b} is significantly shifted. Fig.4-1 shows the effect of dimerization on the NH chemical shifts in the C-terminus.

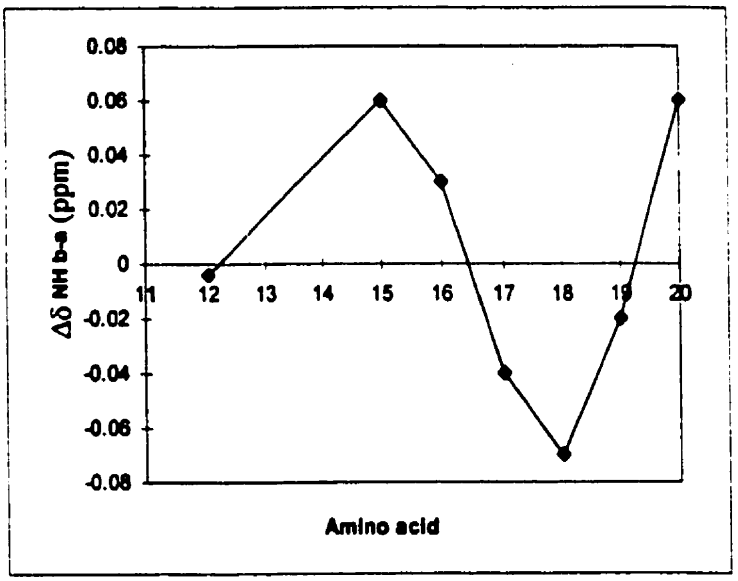

Fig. 4-1. The effect of dimerization on the NH chemical shifts in the C-terminus. $\Delta\delta NH = \delta NH_{dimer} - \delta NH_{monomer}$.

The change in the effect of dimerization on the NH chemical shift from positive to negative and back to positive is reminiscent of an effect dependent on position in a helix. So a second possibility is that dimerization affects NH chemical shift by helix association. This effect is strongest at the C-terminus and does not extend past residue 12. It is tempting to speculate that two Gln_{18} side-chains interact with each other in the folded dimer but there is no measurable effect of this

on the εNH_2 chemical shifts. Whatever the structure of the dimer, it is evident that there is a subtle change in conformation of the C-terminus manifested in the NH chemical shift. Evidently, the H-bonding strength or partners are changed in the residues 15-20.

Comparison of the NH chemical shifts in the dimer to their random coil shift, (Figure 4-2a) shows that, just as in the monomer, the NH resonances from Aib_3 to Aib_{10} are shifted upfield characteristic of a helical structure. The NH resonance of Gly_{11} is the only residue that exhibits a slight downfield shift and the NH resonances of Leu_{12} and Aib_{13} also occur close to their random coil chemical shifts, implying conformational flexibility in the region of Gly_{11}-Aib_{13}.

In the C-terminus, most of the NH resonances exhibit an upfield chemical shift characteristic of a helical structure. Fig. 4-2a also shows that NH chemical shifts of resonances *b* for residues 17, 18 and 19 are slightly upfield of those of resonances *a*, suggesting that dimerization may promote helix formation in the C-terminus with little appreciable effect on the N-terminus.

The ^{15}N chemical shift analysis shown Fig. 4-2b indicates that the ^{15}N chemical shifts for all residues except Pho_{20} are shifted upfield characteristic of a helical conformation. Several resonances, including Gly_{11}, resonate near their random coil chemical shift. The ^{15}N chemical shifts of all *b* resonances between Val_{15} and Pho_{20} are slightly upfield of the monomer *a* resonances, suggesting that this segment is more helical in the dimer than in the monomer.

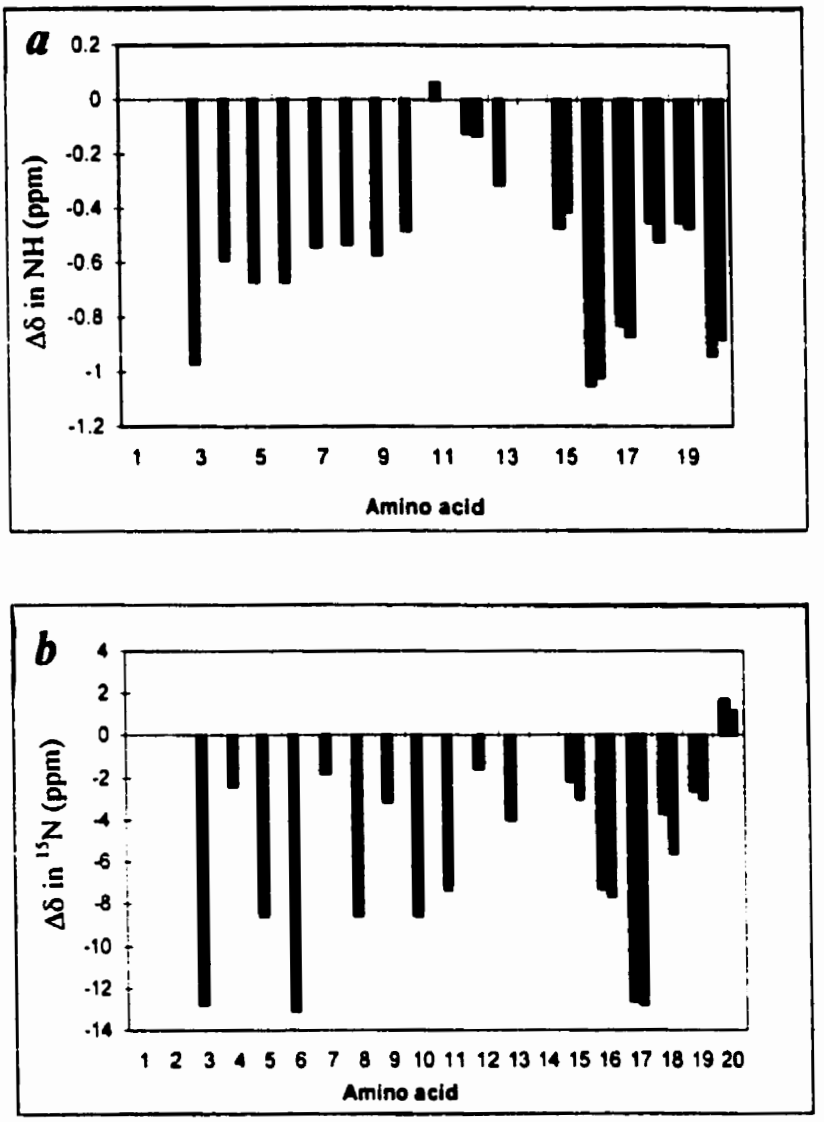

Fig. 4-2. Chemical shift analysis indicating the difference between the observed NH (a) and ^{15}N (b) chemical shift and its random coil shift. Bright shadow bars represent the "*a*" resonances and dark shadow bars represent the "*b*" resonances in the C-terminus.

4.3. Temperature Dependence of the Amide Proton Chemical Shifts

Most of the chemical shifts of the amide protons of ^{15}N alamethicin dimer (Fig. 3-16) move upfield with temperature increase, thus, their temperature coefficients ($\Delta\delta$ /ΔT) are negative. The exceptions are the values of $\Delta\delta$ /ΔT for

Ala_4 and Aib_{16} which are small and positive, i.e., the chemical shifts of their amide protons move downfield with temperature increase.

The largest negative $\Delta\delta/\Delta T$ values were observed for Aib_1 NH (-7.5 ppb/K) and the εNH_2 amide protons of $Gln_{7(18)}$ and Gln_{19} side-chains (-7.0 ~ -8.0 ppb/K), indicating that these groups are completely exposed to the solvent and not intramolecularly hydrogen bonded.

The Aib_6, Aib_8, Aib_{10}, Gly_{11}, Leu_{12}, Aib_{13}, and Aib_{17} residues (most of them are in the middle of the peptide) have relatively large negative $\Delta\delta/\Delta T$ values (in the range -3.8 ~ - 5.8 ppb/K), suggesting that the amide protons of these residues are weakly intramolecularly hydrogen bonded. Slopes between 0 and -3.2 ppb/K are observed for the amide protons of residues Aib_3, Aib_5, Gln_7, Val_9, Val_{15}, Gln_{18}, Gln_{19}, and $Phol_{20}$, and small positive $\Delta\delta/\Delta T$ values in the range 0 to 1.3 ppb/K for Ala_4 and Aib_{16} are observed, suggesting strong H-bonding for those residues. The smallest shifts with temperature occur for Aib_3, Gln_7, Val_{15} and Aib_{16}, indicating the protons of these residues are well shielded from solvent and in very stable intramolecular hydrogen bonds. The very small changes in NH chemical shift for Aib_3 and Aib_4 may be indicate the existence of the two 3_{10} interactions between the N-terminal acetyl and Aib_3 as well as between Aib_1 and Aib_4, in agreement with the report of Yee & O'Neil for monomer [2]. It is noteworthy that most of the dimer "*b*" NH resonances are less temperature sensitive than the monomer "*a*" resonances (Fig. 3-18). This effect would be expected if the C-termini of the monomers in the dimer folds to form a parallel helix bundle.

4.4. $^3J_{N\alpha}$ Coupling Constant Analysis

Coupling constants $^3J_{N\alpha}$ measured from the DQF-COSY are in reasonable agreement with the values from the 1D spectrum. Nearly all of the measured coupling constants $^3J_{N\alpha}$ for alamethicin dimer suggest that the peptide backbone is

helical (Table 3-6). It is not possible using $^3J_{N\alpha}$ to distinguish between α- and 3_{10}-helix. Gly_{11} adopts a small $^3J_{N\alpha}$ values, which is not quite in agreement with chemical shift analysis. In the C-terminal half, Leu_{12} and Pho_{20} have $^3J_{N\alpha}$ values in the 7-9 Hz range, reflecting populations in a more dynamic conformation. However, Gln_{18} has $^3J_{N\alpha}$ values characteristic of a helical structure. These observations are in accord with the NOE data. The values of $^3J_{N\alpha}$ for residues 15-20 of dimer (the "*b*" resonances) are smaller than those of free monomer, implying that the overall percentage population of a helical structure in the dimer is increased in the C-terminus compared to the monomer.

4.5. Structure Studies from NOE Measurements

The sequential and medium-range NOE data in the Tables 3-7~3-11 can be used to generate a map of ^1H-^1H connnectivities for alamethicin ^{15}N dimer, as shown in Fig. 4-3. In general, individual NOE cross peaks cannot by themselves provide conclusive evidence of conformation at specific residues. Instead, NOE patterns over several consecutive residues are taken as evidence of secondary structure. An exception is the distinction between *cis* and *trans* peptide bonds at X-Pro. We didn't observe strong sequential (α_i, α_{i+1}) and (N_i, α_{i+1}) NOEs for X-Pro dipeptide fragments (X is Aib_1 or Aib_{13}), implying Pro_2 and Pro_{14} exist as *trans* peptide bonds. No (α_i, N_{i+4}) or long-range NOEs were observed, suggesting that distances longer than 4.2 Å cannot be observed in this experiment or that the helix formed is flexible.

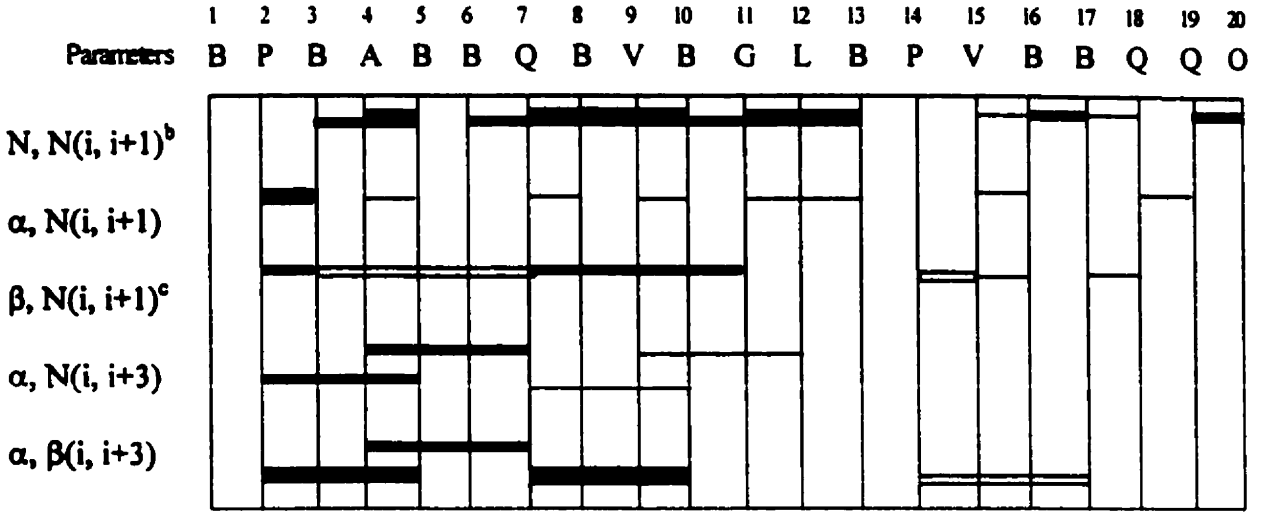

Fig. 4-3. Sequential and medium-range dimer ROEs versus the amino acid sequence[a]

[a]The ROEs are classified as strong, medium and weak as reflected by the line thickness. The numbers at the top represent the amino acid residues in the sequence.
[b]Breaks occur at B_5 and Q_{18} residues due to similar chemical shifts.
[c]Open bars represent ambiguous assignments owing to resonance overlap

The observation of strong and medium sequential (N_i, N_{i+1}) NOEs in several consecutive residues indicates that a helical secondary structure exists throughout the sequence. Fig. 4-3 shows that nearly the entire protein exists in a helical conformation. A few strong or medium (α_i, β_{i+3}) cross-peaks and some medium and weak (α_i, N_{i+3}) cross-peaks were also observed, which would support the assignment of a helical structure particularly in the N-terminal half of the peptide. Indirect evidence comes from the absence of weak (α_i, N_{i+2}) interactions and short strong (α_i, N_{i+1}) NOEs. In addition, sequential ^1H-^1H distances with proline can also provide supporting information for identification of specific secondary structures. The strong (B_{1N}-$P_{2\delta}$), medium (B_{13NH}-$P_{14\delta H}$) and weak sequential ($P_{2\alpha H}$-B_{3NH}) NOEs provided evidence of helical structure and confirmed that the helices include the two proline residues.

It is generally difficult to distinguish between 3_{10} and α-helical conformation by NOE patterns. This is especially true for the alamethicin dimer preparation

which was dilute so that the absence of (i, i+4) NOEs cannot be taken as evidence of 3_{10} structure. The relative intensities of the NOEs are however, quite informative. For example, in Fig. 3-14c, it is quite evident that a range of very weak to strong (N_i, N_{i+1}) NOEs exist. Between residues 3-10, all cross peaks are strong, suggesting a stable helix whereas the cross peaks between Aib_{10} and Gly_{11} and between Gly_{11} and Leu_{12} are weaker. This may be explained by conformational flexibility at Gly_{11} at a rate faster than the chemical shift and relaxation time scales. However, confounding this interpretation is the fact that cross peaks in ROESY spectra are diminished in intensity as they approach the diagonal [3]. Nevertheless, the Gln_7-Aib_8 cross peak is more intense than the Aib_{10}-Gly_{11} cross peak despite being the same distance from the diagonal. The Leu_{12}-Aib_{13} cross peak is more intense than the cross peaks involving Gly_{11} but is considerably closer to the diagonal.

All of the sequential (N_i, N_{i+1}) cross peaks for the segment Val_{15} to Pho_{20} are weak. For the Aib_{15}-Aib_{16}, Aib_{17}-Gln_{18}, and Gln_{18}-Gln_{19} cross peaks, this is due in part to their proximity to the diagonal. However, the Aib_{16}-Aib_{17} and Gln_{19}-Pho_{20} cross peaks are considerably weaker than cross peaks from the N-terminus equidistant to the diagonal. This strongly suggests that the segment Val_{15}-Pho_{20} is in conformationally flexible.

The weaker cross-peaks for (α_i, N_{i+1}), (β_i, N_{i+1}) and (α_i, N_{i+3}) in the C-terminal half suggest that the N-terminus (Aib_1-Gly_{11}) has more stable α-helical structure than the C-terminal half. A more extended conformation at the C-terminus may be due to local conformational dynamics. If the alamethicin dimer forms a stable parallel helix bundle it should be possible, in principle, to observe intermonomer NOEs. In practice, it is difficult to imagine any NOE, which would be present in the folded dimer but absent in the monomer. More likely is that some NOEs may be greater in intensity in the dimer than the monomer because they correspond to a

sum of intramonomer and intermonomer NOEs. Detection of such subtle effects amounts to comparison of the NOE intensities of monomer and dimer and that is the purpose of the data presented in Table 3-7~3-11. Comparison of the ROESY cross peak intensities does not reveal any clear evidence of parallel helix bundle formation.

4.6. A Model of the Dimer

Usually in peptides, when multiple conformations are adopted, there is rapid interconversion between them which is fast on the chemical shift timescale. In this case, the resonances will be averaged over the contributing conformers and a single resonance is observed [4]. For the alamethicin dimer, the NMR data show two sets of NH resonances for residues between Val_{15} and Pho_{20}. The NH of Aib_{13} is broadened and the NH of Leu_{12} also appears as a doublet in the resolution-enhanced 1D ^1H NMR spectrum (Fig. 3-10b). This pattern may be explained by calculating the effective concentrations, C_{eff}, of the residues, which depends on the distances between the residues in an idealized linear dimer (Fig. 4-4). Two Pho_{20}, situated next to the linker, have a much higher effective concentration (270.0 mM) than two B_1 at the ends of the dimer (2.2 mM), indicating that dimerization of the C-terminus is more likely than dimerization of the N-terminus. The presence of a single set of resonances for residues Aib_1-Gly_{11} also suggests that the helix is bent at Pro_{14} or that the region around Gly_{11} is dynamic and little association of the N-terminal halves of the peptide occurs. The NMR data suggest that dimerization of alamethicin increases slightly the stability of the C-terminal helix.

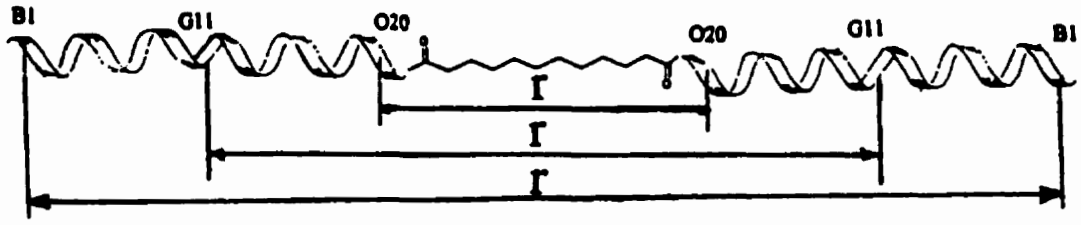

$$C_{eff} = \frac{2}{\frac{3}{4}\pi r^3 N}$$

Fig. 4-4. The effects of distance from the center of the linker on the effective concentration of the residues in the dimer. N is Avogado's number (6.022×10^{23}), r is distance shown in the model. The linker is assumed to be 11.3 Å in length and the rise/residue of the alamethicin helix is assumed to be 1.5Å. The effective concentrations for O_{20}, G_{11}, and B_1 are 270.0 mM, 9.1 mM and 2.2 mM, respectively.

4.7. The Motions of the Dimer Molecule

The motions of any molecule can be classified into the slow overall motions of the dimer molecule and the small-amplitude and relatively fast local motions. They usually cannot be separated completely. In the case of alamethicin dimer, it is possible that the C-terminal helix association/dissociation would be expected to occur in a slower timescale. NOEs and coupling constants show that the C-terminus has a less stable helical conformation, which mainly means that the C-termini have faster local conformational dynamics.

The intensities and chemical shifts of the Aib_1-Gly_{11} segment appear to be less affected by dimerization than the C-terminus. An obvious loss of cross-peak intensity for Gln_{18}, Gln_{19}, and Pho_{20} in DQF-COSY and ROESY spectra was observed, indicating differences in linewiths between N- and C- termini. This may arise from the fact that the C-terminal halves are closer to the linker, resulting in more restriction in the overall motion of the C-termini with respect to the N-termini, which in turn leads to a shorter transverse relaxation time (T_2). Because of the shorter T_2 of the signal for the residues in the C-termini, which causes the line

broadening, the cross peaks in the spectra are weaker for the C-termini than those from the N-termini. This difference in T_2 between N- and C-termini is a strong indication that the two segments have different overall motional characteristics.

4.8. Structural Studies of ^{14}N Alamethicin Dimer

1D and 2D spectra show that the amino acid residues of the ^{14}N dimer have two sets of cross peaks with significantly different chemical shifts, mainly due to the fact that the dimer consists of two different monomers (Ala_6; Aib_6). In the C-termini, residues like Pho_{20} show more than two sets of cross peaks, implying the presence of dimerization in the C-terminus. The strongest evidence of this comes from chemical shift analysis. Two sets of cross peaks in the N-termini of the dimers show very similar chemical shifts with the corresponding monomer. For example, the NH of Gln_7 in the dimer gives resonances at 7.77 and 7.98 ppm, which are identical with those of the Aib_6 monomer and Ala_6 monomer, respectively (see Table 3-13). However, starting from Val_{15} to Pho_{20}, the chemical shifts for the two sets of peaks are different from those of the two monomers. For example, the NH protons of residue Val_{15} appear at 7.62 and 7.67 ppm, whereas the NH of the related monomers resonates at 7.58 and 7.63 ppm, respectively. These differences in the NH chemical shifts are very likely due to dimerization in the C-termini, confirming the results from the ^{15}N labeled dimer. The absence of some monomer resonances in the C-terminus shows that the unlabeled dimer preparation is free of monomer contaminant.

Most of the coupling constant values measured from the 1D spectrum such as those for residues Ala_6, Gln_7, and Val_9 in the N-termini together with residues Val_{15} and Gln_{18} in the C-termini are in the range of 4.0-6.5 Hz, which are values characteristic of a helical secondary structure. On the other hand, the $^3J_{N\alpha}$ values for Gly_{11} (5.81 and 6.05 Hz) and for Leu_{12} (6.96 Hz) are close to their random coil values of 5.90 Hz and 7.10 Hz, respectively, reflecting populations in a random

structure in the middle of the peptide. Gln_{19} and Pho_{20} have relatively large $^3J_{N\alpha}$ values (7.57 and 9.96 Hz, respectively), suggesting a more flexible structure in the C-termini. Taken together, NMR data for ^{14}N alamethicin dimer suggest a similar structure as for the ^{15}N labeled dimer.

In addition, it is also interesting to observe all $^3J_{\alpha N}$ of Ala_6 monomer are significantly smaller than those of the Aib_6 monomer from Ala_4 to Val_9 in the N-terminus. The Aib_6 monomer has smaller $^3J_{\alpha N}$ in the middle of the peptide starting from Gly_{11} to Val_{15} relative to the same region of the Ala_6 monomer. The C-terminus of the Aib_6 monomer has slightly larger $^3J_{\alpha N}$ values (with the exception of Pho_{20}) than the Ala_6 monomer. These observations suggest that the replacement of Aib_6 by Ala_6 favors α-helix over 3_{10}-helix in the N- and C-terminus, in agreement with the established view that Ala is a good α-helix former, whereas Aib is 3_{10}-helix favorable [5].

4.9. Implications of the Dimer Structure

NMR data provide detailed structural and dynamic information of alamethicin dimer at the atomic level. The structural modeling of alamethicin helical dimer is a first step toward moldeling alamethicin channels in lipid bilayers. The NMR data here revealed provide a consistent structure for alamethicin dimer.

NOEs, $^3J_{\alpha N}$ values, chemical shifts of the NH and ^{15}N resonances, suggest basically that the entire alamethicin dimer is predominantly a helix with a less regular structure in the middle and a more extended structure in the C-terminus, similar to the structure of alamethicin monomer observed in the x-ray [6] and solution NMR [7, 8]. The present results reveal no significant difference between the linked and unlinked alamethicin conformation in methanol, implying that the presence of the linker won't perturb the pore structure of alamethicin dimer. NMR spectra also showed that the dimer exists in a measurably different conformational

state in the C-terminus. We propose that this state corresponds to a dynamic equilibrium between associated and dissociated C-terminal helices, as presented in Fig. 4-5.

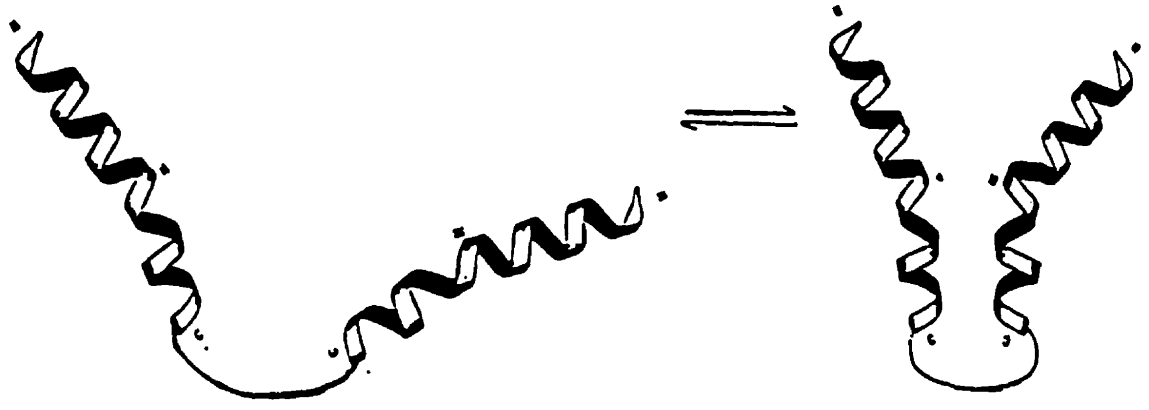

Fig. 4-5. The proposed structure of alamethicin dimer with the monomeric state and dimeric state in the equilibrium.

In the associated state, alamethicin monomers are packed with their N-terminal helical segments (Aib_1-Pro_{14}) slightly bent away from each other, due to the presence of Gly_{11} and Pro_{14} residues in the middle of the peptide which are believed to be helix-breaking residues [9]. (Gly has the smallest side-chain and Pro possess the most rigid side-chain. Both of them may play a critical role in the transmembrane insertion during the forming of the alamethicin channel). It appears that the C-termini of the dimer interact with each other, possibly through interhelix hydrogen-bonded interactions. The side-chains of three glutamines in the hydrophilic face could point toward one another. In one model, Aib_1, Aib_{13}, Gly_{11} and Aib_{10} residues are located on the hydrophilic face of the amphipathic helix, exposed to solvent, while Aib_3, Gln_7, Val_{15} and Aib_{16} residues are located on the hydrophobic face, oriented toward the interior of the channel, shielded from the solvent. Gln_7 is the only polar residue in the N-terminal half and has been proposed

to form an inter-helix hydrogen bonded ring within the channel and stabilize the open state of the channel [6, 10].

Many models for alamethicin voltage-gating were proposed previously which involve different mechanisms. Our NMR data support a gating mechanism that undergoes a voltage-dependent conformational rearrangement of the peptide with respect to the bilayer. The bent alamethicin dimer suggest that the transition from a bent to a more linear conformation is a likely gating mechanism of alamethicin dimer, i.e., the helical rotation of ϕ and φ angles occurs at Pro_{14} through to Gly_{11} during the gating of the channel formed by alamethicin dimer, similar to that suggested for the monomer [6].

During the opening of the channel, the single-channel conductance switches between a number of levels. For the helix-bundle channel model of alamethicin monomer, the previous studies have suggested that an increase or decrease in conductance level corresponds to addition or removal of an alamethicin monomer from the channel. Alamethicin dimer channels are known to exist in a smaller number of conductance states with significantly increased lifetime [11]. Our prediction for the helix-bundle formed by alamethicin dimer (2-6 dimers, i.e., 4-12 monomers in the parallel arrangement) is that the covalently-linked dimer reduces the chance of addition and leaving of alamethicin in the channel due to an even-number molecularity, thus increasing the open channel stabilities of helix bundles and decreasing the rate of switching between adjacent conductance levels. This results in significantly longer mean channel lifetimes for dimer than for monomer.

4.10. Future Work

It would be of interest to study the alamethcin dimer in methanol (or/and in a membrane or detergent solution) using circular dichroism (CD) spectroscopy [12] at different temperatures in order to estimate the amount of secondary structures in

the peptides and temperature effects on the structures. The CD spectra of the ^{15}N labeled alamethicin dimer in methanol at 25°C and 45°C have been acquired recently and are shown in Fig. 4-6. The strong negative ellipticities at 208 and 222 nm and the positive band near 190 nm indicate the presence of a helical conformation of the dimer in methanol. The results also indicate a small decrease in helicity as the temperature is elevated.

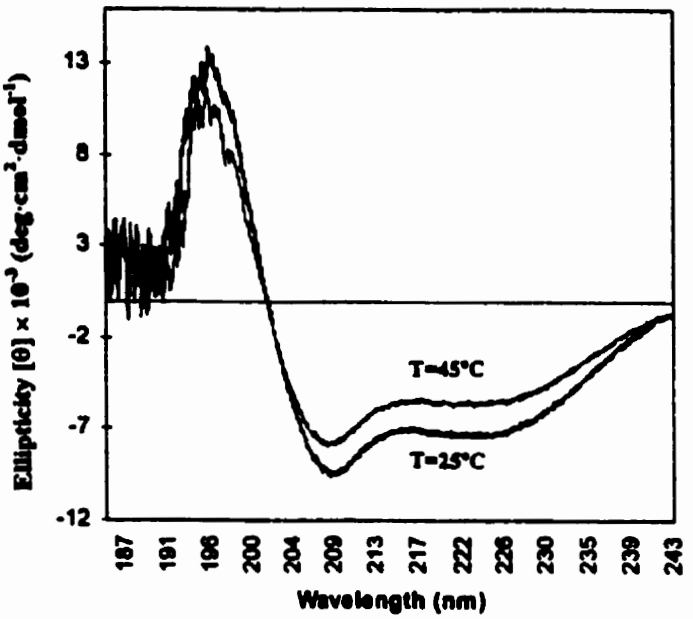

Fig. 4-6. The CD spectra of ^{15}N alamethicin dimer in methanol at 25°C and 45°C, corrected by subtraction of the baseline. CD measurements were made on a Jasco J500A spectropolarimeter over a range of 250-185 nm with a sensitivity of 5 m°/cm and a scan speed of 0.5 nm/min. The temperature of the sample in a 0.05 cm path length cell was controlled by a circulating water bath. A mean residue mass of 102.2 Da and a concentration of 0.75×10^{-3} g/ml were used for calculation of mean residue ellipticities of the dimer.

The overlapping cross peaks in the 2D spectra of dimer, e.g. ROESY (Fig. 3-14) may result in ambiguity of the assignment. Thus, three-dimensional experiments which involve using an isotopic label such as ^{15}N for indirect detection via the HSQC method in combination with ROESY are required to confirm these assignments. In addition, in order to better understand the voltage-

gated mechanism of this peptide, it would be useful to examine the structure of alamethicin dimer bound to micelles such as sodium dodecyl sulfate (SDS) using high-resolution NMR spectroscopy. A heterogeneous environment closer to that of a bilayer should provide a more defined structure of the alamethicin dimer. In the present study, it was impossible to observe the side-chain interactions at the dimer interface since the side-chains of the monomers in ^{15}N homodimer have very close chemical shifts. However, heterodimers composed of Aib_6 and Ala_6 alamethicin dimer might make it possible to observe sidechain-sidechain contacts between the helices in ROESY or NOESY spectra due to significantly different chemical shifts between the two alamethicin monomers.

The rotational correlation time for the dimer can be estimated according to the equation $\tau_c \approx 10^{-12.6}$ MW $(\eta/T)_{rel} \approx 0.25$ MW for methanol solution [13], where $(\eta/T)_{rel}$ is viscosity/T ratio relative to H_2O at 20°C. Molecular weight of the dimer is about 4091 Da, thus, τ_c is approximately 10×10^{-10} seconds in methanol in comparison with 4×10^{-10} seconds for alamethicin monomer. At 500 MHz $\omega_0 = -\gamma B \approx 3.0 \times 10^{10}$, and this gives $\omega_0\tau_c \approx 3.0$, which should induce observable negative NOE (between - 0.5 to -1) in a NOESY spectrum. It is would be of interest to run NOESY spectra for both alamethicin dimers. Furthermore, molecular models of channels formed by alamethicin dimer could be developed using simulated annealing via molecular dynamics techniques [14, 15]. Finally, single-channel current recording of channels formed by alamethicin dimers in diphytanoylphosphatidylcholine/decane under a solution of KCl (0.5 or 1 M) could be measured by applying potential of 160 mV across the membrane using techniques described by Seoh & Busath [16]. Single-channel current-voltage relationships (I-V) [17] of alamethicin dimer channel should be measured and compared with those of monomer to confirm that the linker has no major effect on the structure of the conducting channel.

References

1. Wishart, D. S & Nip, A. M. (1998) *Biochem. Cell Biol. 76*, 153-163.
2. Yee, A. A. & O'Neil, J. D. J. (1995) *Biopolymers. 36*, 781-792.
3. Neuhaus, D. & Williamson, M. (1989) <<*The Nuclear Overhauser Effect*>>, VCH Publisher, Inc., New York.
4. Smith, L. J., Mark, A. E., Dobson, C. M. & van Gunsteren, W. F. (1995) *Biochemistry* 34, 10918-10931.
5. Karle, I. L. & Balaram, P. (1990) *Biochemistry 29*, 6747-6756.
6. Fox, R. O. & Richards, F. M. (1982) *Nature 300*, 325-330.
7. Esposito, G. Carver, J. A., Boyd, J. & Campbell, I. D. (1987) *Biochemistry 26*, 1043-1050.
8. Yee, A. A. & O'Neil, J. D. J. (1992) *biochemistry* 31, 3135-3134.
9. Charles, M.D. & Li, Shen-Cheng (1995) *Biopolymer 37*, 295-318.
10. Jaiharan, D. C. J., Biggin, P. C., Wenschuh, H., Sansom, M. S. P. & Woolley, G. A. (1997) *Biochemistry 36*, 13873-13881.
11. Shaochun Y., Shuyun, P., Linda, L, Breed, J., Sansom, M. S. P. & Woolley, G. A (1996) *Biochemistry 35*, 6225-6232.
12. Johnson, W. C., Jr. (1988) *Annu. Rev. Biophys. Chem. 17*, 145-166.
13. WilliaM, R. C. & Robert, M. K.C. (1994) <<*Two-Dimensional NMR Spectroscopy*>>, VCH Publisher, Inc., New York.
14. Nilges, M., & Brunger, A. T. (1993) *Proteins 15*, 133-146.
15. Breed, J., Biggin, P.C., Kerr, I. D., Smart, O. S. & Sansom, M. S. P. (1997) *Biochim. Biophys. Acta 1325*, 235-249.
16. Seoh, S., & Busath, D. (1993) *Biophys. J. 64*, 1017-1028.
17. Sansom, M. S. P. (1993) *Eur. Biophys. J. 22*, 105-124.

Appendix A: The names of pulse programs and file number for each NMR experiment

Num.	Experiments	Pulse programs	File numbers
1	1D ^{1}H of ^{15}N dimer	zgprxdec·aay	/nmrdata/umlix0/xl-aladimern15/50
2	1D ^{1}H of ^{15}N monomer	zgprxdec·aay	/nmrdata/umlix0/xl-aladmonomer/1
3	HSQC of ^{15}N dimer at 300 K	hsqcfzor·km	/nmrdata/umlix0/xl-aladimern15/2
4	TOCSY of ^{15}N dimer	mlevprtpxd·tw	/nmrdata/umlix0/xl-aladimern15/5
5	DQF-COSY of ^{15}N dimer	cosydfprtpxd·tw	/nmrdata/umlix0/xl-aladimern15/51
6	DQF-COSY of ^{15}N monomer	cosydfprtpxd·tw	/nmrdata/umlix0/xl-aladmonomer/3
7	ROESY of ^{15}N dimer	roesyprtpxd	/nmrdata/umlix0/xl-aladimern15/45
8	HSQC of ^{15}N dimer at 273 K	hsqcfzor·km	/nmrdata/umlix0/xl-aladimern15/55
9	HSQC of ^{15}N dimer at 388 K	hsqcfzor·km	/nmrdata/umlix0/xl-aladimern15/58
10	HSQC of ^{15}N dimer at 318 K	hsqcfzor·km	/nmrdata/umlix0/xl-aladimern15/60
11	1D ^{1}H of ^{14}N dimer mixture	zgprcp2·km	/nmrdata/umlix0/xl-ala-dimer/2
12	TOCSY of ^{14}N dimer mixture	mlevprtp	/nmrdata/umlix0/xl-ala-dimer/3
13	DQF-COSY ^{14}N dimer mixture	cosydfprtpxd·tw	/nmrdata/umlix0/xl-aladimern15/9
14	ROESY of ^{14}N dimer mixture	roesyprtpxd	/nmrdata/umlix0/xl-aladimern15/16